University of Massachusetts Medical School

eScholarship@UMMS

GSBS Dissertations and Theses   Graduate School of Biomedical Sciences

Dynamics of Erythropoietic Survival Pathways In Vivo: A Dissertation

Miroslav Koulnis
University of Massachusetts Medical School

Let us know how access to this document benefits you.

Follow this and additional works at: https://escholarship.umassmed.edu/gsbs_diss

🟡 Part of the Amino Acids, Peptides, and Proteins Commons, Animal Experimentation and Research Commons, Biological Factors Commons, Cell and Developmental Biology Commons, Cells Commons, Circulatory and Respiratory Physiology Commons, Hemic and Immune Systems Commons, Hormones, Hormone Substitutes, and Hormone Antagonists Commons, and the Therapeutics Commons

DYNAMICS OF ERYTHROPOIETIC SURVIVAL PATHWAYS *IN VIVO*

A Dissertation Presented

By

MIROSLAV KOULNIS

Submitted to the Faculty of the
University of Massachusetts Graduate School of Biomedical Sciences, Worcester
in partial fulfillment of the requirements for the degree of

DOCTOR OF PHILOSOPHY

JULY 11, 2011

PROGRAM IN IMMUNOLOGY AND VIROLOGY

DYNAMICS OF ERYTHROPOIETIC SURVIVAL PATHWAYS *IN VIVO*

A Dissertation Presented
By

MIROSLAV KOULNIS

The signatures of the Dissertation Defense Committee signifies
completion and approval as to style and content of the Dissertation

Merav Socolovsky, Ph.D., MBBS, Thesis Advisor

Peter Newburger, M.D., Member of Committee

Madelyn Schmidt, Ph.D., Member of Committee

Robert F. Paulson, Ph.D., Member of Committee

The signature of the Chair of the Committee signifies that the written dissertation meets
the requirements of the Dissertation Committee

Leslie J. Berg, Ph.D., Chair of Committee

The signature of the Dean of the Graduate School of Biomedical Sciences signifies
that the student has met all graduation requirements of the school.

Anthony Carruthers, Ph.D,
Dean of the Graduate School of Biomedical Sciences

Immunology and Virology Program

July 11, 2011

ACKNOWLEDGEMENTS

I would like to sincerely thank the following people:

My thesis mentor, Merav Socolovsky, for her outstanding support and guidance in one of the most interesting and unique areas of biology I have come across. You taught me how to think critically and independently as a scientist, and showed me just how interrelated the diverse areas of science can be.

My previous mentors, Mercedes Rincón, Ph.D, Gustavo Pedraza-Alva, Ph.D, and George Long, Ph.D, for their patience and for giving me an amazing opportunity to experience molecular biology first-hand during my high school and undergraduate years at the University of Vermont.

My friends in the laboratory (in no particular order): Ramona Pop, Alberto and Ermelinda Porpiglia, Kelly Hallstrom, Jeffrey Shearstone, Qichang Shen, Daniel Hidalgo and Ying Liu. You have put up with a lot, and you were all awesome!

David P., Sergei P., Alexander A., Vladimir and Svetlana G., and the rest of my friends and mentors. Each of you affected me in some important way.

My committee members Leslie Berg, Madelyn Schmidt, and Peter Newburger. Your faith in me was instrumental to my success. I would also like to thank my external examiner Robert Paulson, Karl Simin and the rest of the Cancer Biology Department, and many others in the Immunology and Virology Program at UMASS.

Most of all, I would like to thank Julia Powell and my family for all their love and support throughout the many years of graduate school.

ABSTRACT

Erythropoiesis maintains stable tissue oxygenation in the basal state, while accelerating red cell production in anemia, blood loss or high altitude. The principal regulator of erythropoiesis is the hormone erythropoietin (Epo). In response to hypoxic stress, Epo can increase a 1000-fold, driving erythropoietic rate by up to 10-fold. It's been suggested that survival pathways activated by the Epo receptor (EpoR) underlie its regulation of erythropoietic rate. A number of apparently redundant EpoR survival pathways were identified *in vitro*, raising the possibility of their functional specialization *in vivo*.

Here I assessed the roles of three survival pathways activated by EpoR in erythroblasts *in-vivo*: the suppression of cell-surface Fas and FasL, the suppression of the pro-apoptotic regulator Bim, and the induction of the anti-apoptotic regulator Bcl-x_L. I used the novel CD71/Ter119 flow-cytometric method of identifying erythroblast maturation stages *in vivo* to measure these apoptotic pathways in fetal liver and adult erythropoietic tissues. I found that these pathways differ markedly in their regulation of erythropoietic rate.

Using mouse genetic models, I found that apoptosis mediated by interaction between erythroblasts that co-express cell-surface Fas and FasL plays a key autoregulatory role in stabilizing the size of the erythroblast pool in the basal state. Further, mice mutant for Fas or FasL showed a delayed erythropoietic response to hypoxia or high Epo. This suggests that Fas and FasL accelerate the stress response by providing an apoptotic 'cell reserve' that can be rescued by Epo in stress.

I also examined the *in-vivo* behavior of two cell-intrinsic apoptotic regulators, Bcl-x_L and Bim, previously unexamined in stress. The induction of Bcl-x_L was rapid but transient, whilst the suppression of Bim was slower but persistent. My data suggest that Bcl-x_L is a key mediator of EpoR's anti-apoptotic signal very early in the stress response, before Bim and Fas are suppressed. Bcl-x_L adaptation to high Epo occurs through inhibition of Stat5 activation, and resets it for the next acute stress.

My findings suggest that *in vivo*, Epo regulates erythropoietic rate through erythroblast apoptosis, and that various apoptotic regulators play distinct and unique roles in this process. My work provides new molecular insights into erythropoiesis that are relevant to cytokine biology and to clinical approaches of disease treatment.

TABLE OF CONTENTS

LIST OF FIGURES

LIST OF TABLES

Chapter I Attributions and Copyright information

INTRODUCTION

All sections of this chapter were written by me.

Figure 1.1C and Figure 1.4 represent my original art work.

Figure 1.2B was modified from Chapter III.

Figure 1.3 was used with permission from owner.

CHAPTER I

INTRODUCTION

1.   Erythropoietin-dependent feedback loop in erythropoiesis

Erythropoiesis is the process of hematopoietic progenitor differentiation into red blood cells. In mice, definitive erythropoiesis takes place in the fetal liver during embryogenesis, and in the bone marrow and spleen microenvironments in the adult. In the basal state, erythropoietic rate is low, allowing only for the continued replacement of senescent erythrocytes in the periphery. Insufficient pO_2 supply in tissues occurs during blood loss, malignant disease, high growth rate in embryogenesis, and during ascents to high altitude. These situations lead to an increase in the erythropoietic rate, a process termed stress erythropoiesis (Figure 1.1A-B). The principal regulator of both basal and stress erythropoiesis is hormone erythropoietin (Epo), produced in the adult kidney in response to hypoxia. This gives rise to a negative feedback loop (Figure 1.1A), whereby hypoxia-induced Epo can increase the rate of erythropoiesis up to 10-fold. In turn, generated erythrocytes correct tissue hypoxia and lower Epo level to normal. It is not clear how Epo regulates basal and stress erythropoiesis *in vivo* (Figure 1.1C). In my thesis work, I used novel flow-cytometric methods and various mouse models of erythropoietic stress to address this important question.

2.   Molecular basis of serum erythropoietin increase in hypoxic stress

Epo is essential to erythropoiesis, and Epo^{-/-} or Epo receptor (EpoR)[-/-] mice are embryonic lethal due to failure to produce nucleated red cells [1]. Epo is a 34 kDa glycoprotein with a high degree of sequence homology between humans and mice [2,3]. It is produced in the fetal liver during embryogenesis, while in adulthood, the kidney peritubular fibroblast-like cells are the primary source of Epo [4]. Epo gene transcription is activated by basic helix-loop-helix hypoxia-inducible transcription factors (HIF-2α and HIF-β) at the hypoxia-response element (HRE) sites in the 3' enhancer of Epo [5]. While HIF-β is constitutively expressed and localizes to the nucleus, HIF-2α stability is regulated post-translationally. Under normal oxygen conditions, HIF-2α is hydroxylated by the prolyl hydroxylase domain enzymes (PHDs), polyubiquitinated by the von Hippel-Lindau (VHL) E3 ubiquitin ligase protein, and subsequently degraded by the proteasome. Low oxygen results in a reduced hydroxylation of HIF-2α, and leads to its stabilization and nuclear translocation to markedly induce Epo transcription [6,7]. HIF-2α conditional-knockout mice develop anemia after post-natal ablation [8]. Conversely, mice with targeted inactivation of the VHL gene have increased Epo and over-abundance of erythrocytes (polycythemia) [9,10]. Serum Epo increases with decreasing hematocrit (red cell fraction of total blood volume), reaching up to 10,000 mU/mL in severe anemia compared to basal levels of about 10 mU/mL [4,11]. Epo induction can be detected within the first two hours of hypoxic stress. It peaks by 12 to 48 hours, and then tails off as corrective mechanisms are activated [12,13]. Conversely, polycythemia suppresses endogenous Epo production to prevent any additional erythropoiesis until balance is restored [14]. Hematopoietic

progenitors committed to the erythroid lineage express EpoR and become Epo-dependent for their survival and the subsequent differentiation.

3. Acute and chronic erythropoietic stress

Abnormally low erythropoietic rate results in anemia, while higher-than-needed erythropoiesis results in erythrocytosis, sluggish blood flow and clotting. In mice, the bone marrow, with its limited physical space, serves as the primary site for basal erythropoiesis, while the spleen contains stress-responsive progenitors [15-17]. Acute tissue hypoxia occurs when blood oxygen tension is sharply reduced. It results from blood loss, upon acute exposure to low atmospheric oxygen, or from acute carbon monoxide poisoning. Mammals have multiple and complex mechanisms to correct tissue hypoxia. For example, acclimatization to low oxygen at high altitude includes changes in ventilatory and cardiovascular function [18], plasma volume [19], blood acid-base balance, and systemic and cellular metabolic changes [20]. Importantly, tissue hypoxia also leads to an increase in erythropoietic rate, which is a slower, but often more permanent corrective function [20]. Epo and many other stress-induced factors, such as stem cell factor (SCF), glucocorticoids, and bone morphogenetic protein 4 (BMP4) regulate stress erythropoiesis *in vivo* [17,21-23]. Of those, Epo is the principal regulator of erythropoietic rate.

Although Epo peaks in a matter of hours, erythropoiesis is increased for many days until homeostasis is re-established [24]. Acute tissue hypoxia, if not corrected, becomes chronic hypoxic stress where the stimulus for increased erythropoietic rate persists. Of note, the term chronic erythropoietic stress describes the persistence of

erythropoietic stimulus with or without hypoxic stress (e.g. polycythemia). Chronic erythropoietic stress where tissue hypoxia is present often results from long-term physiological and pathological conditions. Pregnancy is a physiological chronic stress due to continued fetal demand for oxygen. Other causes include chronic obstructive pulmonary disease, thalassemias and sickle cell disease, and renal failure. Chronic stress is also present in myelodysplasia (MDS) and cancer patients with ineffective bone marrow erythropoiesis due to inflammatory response or chemotherapy.

Polycythemia results from over-active erythropoiesis in pathology, and also in physiological settings, such as upon a descent from high altitude [25,26]. Physiological polycythemia resolves naturally via suppressed erythropoietic activity. In contrast, pathological polycythemia results from defects in hematopoietic progenitors, such as mutations in the EpoR or Jak2 [27,28], or due to mutations in the Epo production pathway [9,29,30]. Understanding how Epo regulates the erythroid molecular pathways will allow us to develop new and effective treatments for anemia present in various human disorders.

4.   Classical stages of erythroid differentiation

Definitive erythropoiesis is Epo-dependent and begins in the fetal liver on day ~E11 of gestation, eventually moving to the bone marrow by birth. Starting with the hematopoietic stem cell (HSC) and its progeny, the common myeloid progenitor (CMP), cells are restricted to the megakaryocytic-erythrocytic progenitor stage (MEP) via the cross-antagonism between erythroid transcriptional factor GATA-1 and myeloid/lymphoid transcriptional factor PU.1 (Figures 1.1 and 1.2) [31,32]. MEP

compartment contains "Burst-forming unit-erythroid" (BFU-e) progenitors and the "Colony-forming unit-erythroid" (CFU-e) progenitors, identifiable by colony-forming potential in semi-solid culture medium. BFU-e progenitor gives rise to ~500 cells in 6 to 10 days in response to Epo and a burst promoting factor, such as interleukin-3 (IL-3) or SCF [33,34]. In response to Epo only, CFU-e progenitor gives rise to colonies containing 8 to 32 hemoglobinized cells after 2 to 3 days of *in vitro* culture [35]. Starting with the CFU-e, terminal differentiation is achieved in 3 to 4 cell cycles, with cells progressing through the pro-erythroblast, basophilic, polychromatic and orthochromatic erythroblast stages, as identified morphologically (Figure 1.2 and 1.3). Pro-erythroblasts and basophilic erythroblasts are large cells. They have a large nucleus and appear blue with H&E stain. As cells differentiate, they condense their nuclei, reduce in size, and accumulate hemoglobin [2,36]. Orthochromatic cells are small and stain light brown. They expel their nuclei to become reticulocytes and are released into the bloodstream. Reticulocytes complete hemoglobin synthesis and mature into erythrocytes whose number and quality in the circulation determine tissue oxygen levels.

5.   Erythroblastic islands: critical niches for erythropoiesis *in vivo*

Erythroblasts possess cell-autonomous differentiation properties. However, *in vivo*, efficient erythropoiesis also relies on cell-cell interactions that occur in specialized developmental niches, called erythroblastic islands (Figure 1.3) [22,37]. Present in the erythropoietic tissue, each island consists of a central macrophage surrounded by up to 30 developing erythroblasts of various maturation status. Major functions of erythroblastic

island macrophages are numerous and include: iron supply for heme biosynthesis; phagocytosis of expelled nuclei upon differentiation; and improved erythroblast proliferation and survival (via cell-cell interactions through adhesion factors, or via secreted cytokines). These functions lead to an amplified erythroblast frequency and faster reticulocyte release, both essential for stress response [22]. Erythroblastic islands also provide an opportunity for erythroblasts to interact and regulate each other (for example, through Fas/FasL co-expression by early erythroblasts).

6.   Flow-cytometric detection of primary erythroblasts *in vivo*

The drawback of previous studies of Epo action in erythropoiesis was the use of leukemic erythroid cell lines, indirect detection of progenitors via colony assays, and the lack of reliable flow-cytometric markers for *in vivo* detection of erythroid cells. Our lab pioneered a new flow-cytometric method to study erythroblast development stages *in vivo* using two markers, CD71 and Ter119, and the cell size parameter (FSC, forward scatter) (Figure 1.2A). CD71 is a transferrin receptor that is highly expressed in early erythroblasts for iron acquisition [38,39]. Ter119 is an erythroid-specific cell surface antigen [40]. This method allows us to quickly and easily identify different stages of erythroid development, similar to those seen by morphological examination, directly in freshly harvested hematopoietic tissues [41,42]. In the adult, $Ter119^{mid}/CD71^{high}$ cells have pro-erythroblast morphology and are termed ProE. Total $Ter119^{high}$ cells further resolve into three subpopulations: EryA ($Ter119^{high}/CD71^{high}/FSC^{high}$), EryB ($Ter119^{high}/CD71^{high}/FSC^{low}$), and EryC ($Ter119^{high}/CD71^{low}/FSC^{low}$). In cytospin

preparations, EryA, B and C subsets morphologically correlate to the basophilic, polychromatic and orthochromatic stages, respectively (Figure 1.2A) [42,43]. A similar staging method based on CD71 and Ter119 markers is applied to the fetal liver (Figure 1.2C) [44-46]. Recently, other groups have used similar flow-cytometric methods to visualize erythroid precursors *in vivo* [47,48]. In my thesis work, I used our flow-cytometric method to test the *in vivo* roles of erythroid survival pathways in the mouse stress response.

7.   Epo-responsive erythroid progenitors

In the basal state, the onset of Epo dependence occurs at the CFU-e stage [2,46,]. Pro-erythroblasts (ProE) and basophilic erythroblasts (EryA) are Epo-responsive because they also express EpoR [49,50]. Late erythroblasts are Epo-independent. Epo appears to act on a broader spectrum of progenitors during stress, when BFU-e and CFU-e subsets rapidly expand [15,51,52]. Recently, stress response was shown to depend on a specialized spleen BFU-e progenitor [17,53,54]. This self-renewing subset responds to BMP4, SCF, hypoxia and Epo by giving rise to stress BFU-e. In turn, stress BFU-e cells rapidly divide to form large colonies *in vitro* in response to only Epo [17]. Proliferating stress BFU-e are characterized by their unique expression of both immature (CD34 and cKit) and mature (CD71 and Ter119) markers, similar to the putative human stress progenitor (CD34$^+$Kit$^+$GlyA$^+$) isolated from patients with sickle cell anemia [55]. In addition to CFU-e, ProE and EryA cells rapidly increase in frequency and absolute number, most notably in the spleen during stress response (Figure 1.2B). This early increase is disproportionate

compared to the frequency of later erythroblasts, and is concomitant with a decrease in erythroblast apoptosis [42]. The molecular mechanisms of how Epo regulates this cell expansion *in vivo* are not clear.

8.   Epo Receptor structure and function in erythropoiesis

EpoR is a homodimeric type I receptor expressed at a low density on the surface of hematopoietic progenitors [2,56,57,58,59]. EpoR is 82% homologous between humans and mice [2]. It does not possess intrinsic kinase activity, but is pre-associated with Janus tyrosine kinases 2 (Jak2) required for receptor activation [60,61]. Similar to EpoR$^{-/-}$ embryonic-lethal phenotype, Jak2$^{-/-}$ embryos die on day E12.5 due to severe anemia [62]. In contrast, V617F mutation in the Jak2 leads to hyper-activation of signaling and myeloproliferative disease [27,63]. Upon Epo binding, activated Jak2 phosphorylates eight conserved tyrosines in the cytoplasmic tail of EpoR to recruit signaling partners via their Src Homology 2 (SH2) domains [64,65]. EpoR can activate various signaling pathways leading to cell proliferation, survival and differentiation. They include signal transducer and activator of transcription 5 (Stat5), phosphoinositide-3-kinase/AKT, phospholipase Cγ, Grb2/Shc, Ras, and MAPK [65,66]. In addition to positive signaling that facilitates erythropoiesis, EpoR recruits negative regulators including CIS, SOCS1 and SOCS3, Shp1 and 2, and SHIP1 to prevent its over-activation [65,67]. Truncations of the EpoR distal domain, where negative regulators of signaling are normally recruited, lead to polycythemia in humans and mice [28,68]. Because signaling studies were performed using

in vitro culture, the precise *in vivo* stages of development at which they are activated, and their functional outcomes, are still not understood.

Interestingly, signaling pathways activated by the EpoR are common to other cytokine receptors [69]. EpoR carries no instructive signal for erythroid differentiation [1,66,70]. Instead, EpoR is thought to play a permissive role by providing an essential survival signal to erythroblasts starting with the CFU-e stage, the onset of Epo-dependence [46,71-73]. Pro-erythroblasts and basophilic erythroblasts (ProE and EryA) are also the targets of EpoR signaling. Past the basophilic stage, EpoR expression diminishes and is not required to complete differentiation [2,36,49,50].

EpoR signaling requirements are more stringent during stress where Epo can increase a 1000-fold. EpoR-haploinsufficient mice have normal steady-state erythropoiesis, but fail to achieve normal stress response [74]. Similarly, mice with truncated EpoR lacking all tyrosines (known as EpoR-HM) respond poorly to stress [67,75]. One important function of EpoR is activation of transcriptional factor Stat5, implicated in the stress response *in vivo* [43,76,77]. Stat5-null mice die perinatally from anemia [77]. In contrast, Stat5-deficient mice lack only the first exon of Stat5a and Stat5b, but still express variable levels of N-terminally truncated Stat5 that is constitutively activated [78]. These mice are viable but suffer from embryonic anemia and a deficient stress response as adults [43,77]. Stat5 in erythropoiesis participates in the induction of pro-survival protein Bcl-x_L and the transferrin receptor, both important functions still unexamined during stress response *in vivo* [43,76,79,80]. An additional EpoR-activated pathway, implicated in stress response, is the PI3K/AKT which inhibits forkhead transcriptional factors and

death receptor expression [81-84]. To date, few studies have directly addressed how EpoR survival signals regulate basal and stress erythropoiesis *in vivo*.

9.   Hypothesis: Epo regulates erythropoietic rate *in vivo* via progenitor apoptosis

One well-established molecular consequence of EpoR signaling *in vitro* is erythroblast survival [2,36,51,73,85-87]. Therefore, EpoR has been suggested to regulate erythropoietic rate *in vivo* by activating progenitor survival pathways [73]. A mechanistic model has been proposed where the majority of continuously generated erythroblasts undergo apoptosis in the basal state. Only cells least sensitive to apoptosis become erythrocytes. During stress, the greater the concentration of Epo, the greater the number of total cells rescued from cell death (Figure 1.4). This hypothesis is based on the observations that *in vitro*, CFU-e-like cells undergo apoptosis when deprived of Epo. Increasing Epo concentration in culture results in the increased rescue from apoptosis, while the cell-cycle is unaffected [36,51,73,85-87]. This model contains two implicit requirements, untested *in vivo*: the strength of anti-apoptotic signal delivered by EpoR increases with more Epo; and that progenitors vary in sensitivity to Epo via unknown mechanisms. To date, multiple pathways have been implicated in erythroblast survival *in vitro*. They include pro-survival protein Bcl-x_L, pro-apoptotic proteins Bim and Nix, death receptor Fas and its ligand, FasL, Trail-R, anamorsin, oncostatin M, Serpina-3G, Pim1, Trb3 and FoxO3a [42,43,88-93]. However, the precise nature of the EpoR survival signal *in vivo* remains unclear. To test the hypothesis that Epo regulates erythropoietic

rate through erythroblast apoptosis *in vivo*, I focused on three survival/apoptosis pathways: Fas, Bim and Bcl-x$_L$. My specific aims were to investigate their *in vivo* behavior in different erythropoietic tissues, and to compare and contrast their potentially unique roles in basal and stress erythropoiesis.

10.   Extrinsic and intrinsic apoptotic pathways

Apoptosis is a programmed cell death triggered for many reasons, including development, growth factor withdrawal, DNA damage, and death receptor ligand binding [94]. Apoptosis is characterized by a coordinated process of cell and nuclear shrinkage, cleavage of intracellular proteins and DNA, and the formation of apoptotic bodies for phagocytosis. The proteolytic activation of cysteine-rich aspartate proteases (caspases) initiates apoptosis in the cell. Two main apoptotic pathways exist in the cell: the intrinsic pathway initiated at the mitochondria, and the extrinsic pathway activated by death receptors of the tumor necrosis factor superfamily (for example, Fas and Trail-R) [94].

Growth factor withdrawal or DNA damage initiate the intrinsic pathway. In this pathway, B-cell lymphoma 2 (Bcl-2) family of pro-survival and pro-apoptotic proteins regulate the mitochondrial permeability to cytochrome c and other proteins [95]. Upon release from the mitochondria, these factors activate caspases in the cytosol or cleave DNA directly. The extrinsic pathway is activated upon death receptor ligand binding. This event leads to the recruitment of adaptor proteins to form death-inducing signaling complex (DISC), proteolytic cleavage of initiator caspases (e.g. caspase-8) and the activation of executioner caspases (e.g. caspase-3). The intrinsic and extrinsic apoptotic

pathways are linked through the caspase-8-mediated cleavage of pro-apoptotic protein Bid that leads to mitochondrial permeability downstream of the death receptor activation. My thesis work describes how Epo modulates the intrinsic and extrinsic apoptotic pathways in erythroblasts *in vivo*.

11.   Pro-survival protein Bcl-x$_L$

Bcl-x$_L$ is a pro-survival Bcl-2 family protein that forms heterodimers with pro-apoptotic proteins Bax and Bak, preventing cytochrome c release from mitochondria and caspase activation [95]. Previous work has shown that Bcl-x$_L$ is essential to prevent erythroblast apoptosis *in vitro* and in the basal state *in vivo* [43,76,96-99]. Bcl-x$_L$$^{-/-}$ mice die *in utero* of anemia [100]. Bcl-x$_L$ is synergistically induced by EpoR-Stat5 signaling and GATA-1 transcriptional factor. It accumulates with erythroid differentiation, reaching its highest levels in the most mature erythroblasts [101]. Most, but not all, studies suggest that Bcl-x$_L$ is a major mediator of the anti-apoptotic effect of Epo in erythroblasts [102]. Recent *in vitro* studies using bone marrow erythroid progenitors pre-expanded in culture showed no clear Bcl-x$_L$ induction with Epo, while spleen, the stress reserve organ, was unexamined [67]. In contrast, *in vivo* studies utilizing 5-fluorouracil-induced anemia showed a clear induction in the Bcl-x$_L$ protein in total bone marrow during the recovery [103]. Prior to my thesis work, it was unknown whether EpoR-Stat5-mediated Bcl-x$_L$ induction enhances early erythroblast survival, an essential feature of the stress response *in vivo*.

12.   Pro-apoptotic protein Bim

Pro-apoptotic BH3-only member of the Bcl-2 family, Bim, regulates lymphocyte homeostasis and has been implicated in erythroid apoptosis [90,104-106]. Bim expression in hematopoiesis is regulated by FOXO transcriptional factors [107]. At the protein level, Bim is regulated by ERK-dependent phosphorylation and degradation, as well as sequestration by the microtubular dynein motor complex [107-110]. In response to cytokine withdrawal, Bim can induce apoptosis by binding and neutralizing the pro-survival Bcl-2 proteins. In erythropoiesis, EpoR-Jak2 signaling in cultured bone marrow erythroid progenitors repressed Bim transcription, whereas in erythroid cell lines, ERK repressed Bim protein via phosphorylation and degradation [89,90]. Additional evidence suggests that GATA-1, via transcriptional factor LRF, suppresses Bim-mediated erythroblast apoptosis [106]. Bim-depleted erythroid cells are more resistant to apoptosis *in vitro*. However, $Bim^{-/-}$ mice suffer from an autoimmune syndrome making it difficult to understand the role of Bim in erythropoiesis *in vivo* [89]. To date, the pattern of Bim expression in erythroblasts during differentiation in the basal stress and during stress is unknown, nor is it known if *in vivo*, Epo suppresses Bim to enhance erythroblast survival during stress.

13.   Death receptor Fas and its ligand, FasL

Pro-apoptotic death receptor Fas (CD95) and its ligand, FasL have been proposed to regulate erythropoietic rate *in vivo*. Fas belongs to the tumor necrosis factor receptor superfamily. Upon FasL crosslinking, it activates the extrinsic and intrinsic apoptotic pathways. Fas and FasL are known to regulate the lymphoid compartment and non-

lymphoid tissue homeostasis [111-116]. Evidence also suggests that Fas apoptosis contributes to anemia in myelodysplastic syndromes and multiple myeloma [117-122]. Fas and FasL were found to be expressed on human erythroid progenitors *in vitro*. These studies proposed FasL could negatively regulate erythroid output by inducing apoptosis in Fas-bearing erythroblasts [92,123,124]. However, mice mutant in Fas or FasL suffer from an autoimmune syndrome precluding the study of Fas role in erythropoiesis *in vivo* [125].

Previous publications from our lab provided the first *in vivo* evidence for the apoptotic regulation of erythropoietic rate [42,44]. Spleen ProE and EryA were found to continually undergo high rates of cell death, an unusual finding for a healthy tissue. A proportion of primary spleen ProE and EryA erythroblasts were also found to co-express Fas and FasL, resulting in apoptosis of the Fas-bearing cells. In stress, total erythroblast apoptosis and Fas-positive erythroblast frequency decreased in an Epo-dose- and time-dependent manner [42]. Similarly, we found that Fas and FasL negatively regulate the rapid erythroblast expansion in the fetal liver [44]. These correlative data suggest that *in vivo*, Fas and FasL continually mediate apoptosis locally at the erythroblastic islands, where progenitors interact with each other (Figure 1.3). This cell-to-cell autoregulatory apoptosis may help prevent wasteful fluctuations in progenitor number for a stable basal erythropoietic rate, which is a homeostatic function. Another possible *in vivo* Fas function is to maintain an apoptotic reserve of cells which can be immediately rescued by Epo from cell death during stress (Figure 1.4). In my thesis work, I tested these proposed Fas functions in erythropoiesis using Fas- and FasL-mutant mice bred onto an immune-deficient background to rescue their autoimmune disease [125].

14. Principal questions addressed in this thesis

In Chapter III, I address the role of Fas and FasL in basal and stress erythropoiesis *in vivo*, using mutant mouse models. In Chapter IV, I examine the expression patterns of Bcl-x_L and Bim in basal and stress erythropoiesis, and the manner in which they are regulated by EpoR signaling. Chapter V summarizes the flow-cytometric methodologies developed by our laboratory. The last chapter discusses the principal results and proposes future directions.

Figure 1.1
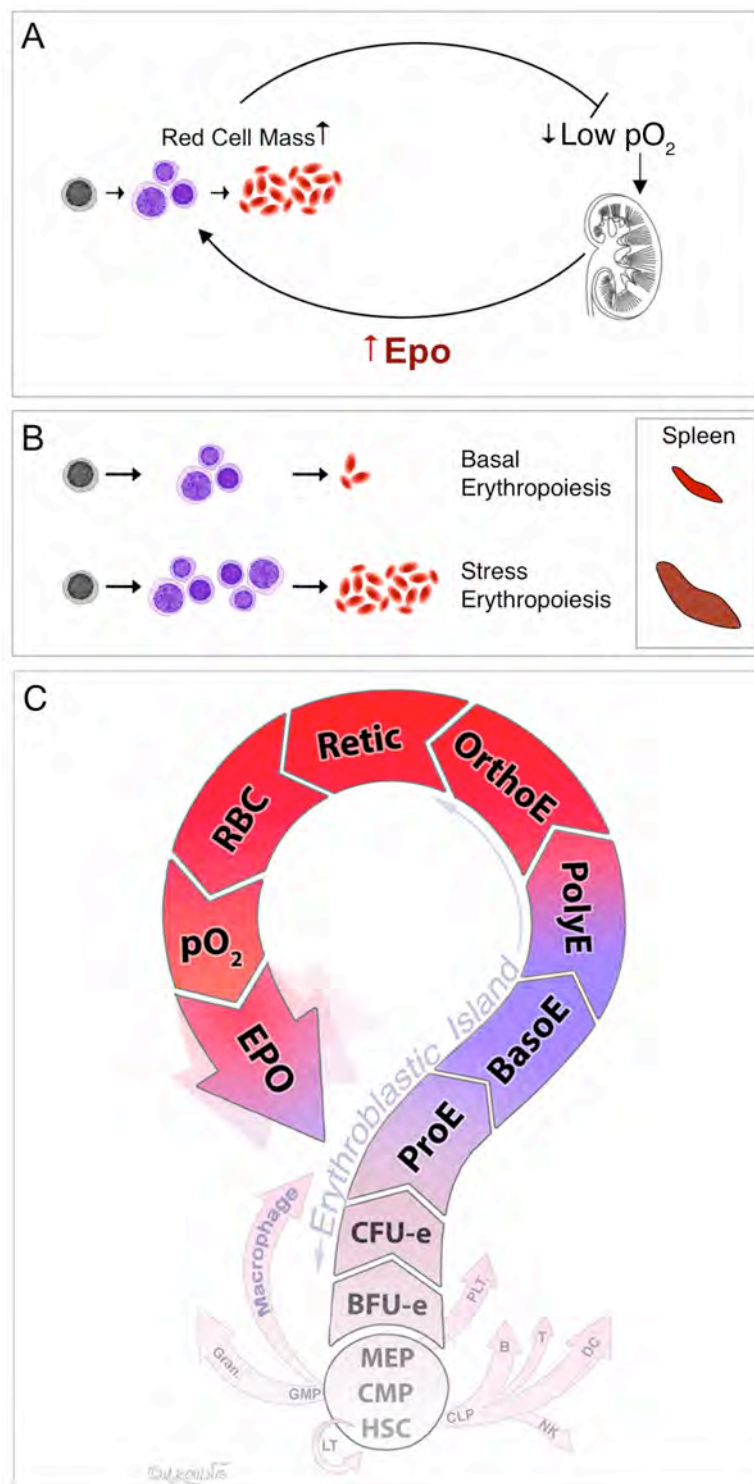
Figure 1.1 Epo-mediated negative feedback loop regulates both basal and stress erythropoiesis to maintain normal tissue oxygen.

(A)   To re-establish pO_2 homeostasis during tissue hypoxia, kidneys increase the production of erythropoietin (Epo) which increases the rate of erythropoiesis. Epo levels increase with the degree of hypoxia, reaching a 1000-fold induction in the most severe hypoxic stress.

(B)   Basal erythropoiesis in an adult occurs primarily in the bone-marrow to replace aging erythrocytes. Stress erythropoiesis is the increase in the rate of red cell production to re-establish normal tissue oxygen. In mice, spleen is an erythropoietic reserve organ (inset). In humans, bone-marrow is the primary site for both basal and stress erythropoiesis.

(C)   The path of hematopoietic and erythroid development is illustrated. <u>H</u>ematopoietic <u>s</u>tem <u>c</u>ells (HSC) give rise to multiple lineages. Downstream of the HSC, <u>c</u>ommon <u>m</u>yeloid <u>p</u>rogenitors (CMP) cells produce macrophages and the <u>m</u>egakaryocytic-<u>e</u>rythrocytic <u>p</u>rogenitors (MEP). Erythroid differentiation proceeds from the <u>b</u>urst-<u>f</u>orming-<u>u</u>nit <u>e</u>rythroid (BFU-e) stage onward. Macrophages and erythroblasts constitute a developmental niche called erythroblastic island (described in Figure 1.3). Generated red cells regulate tissue pO_2. My thesis work addresses the question of how Epo regulates erythropoietic rate.

Figure 1.2
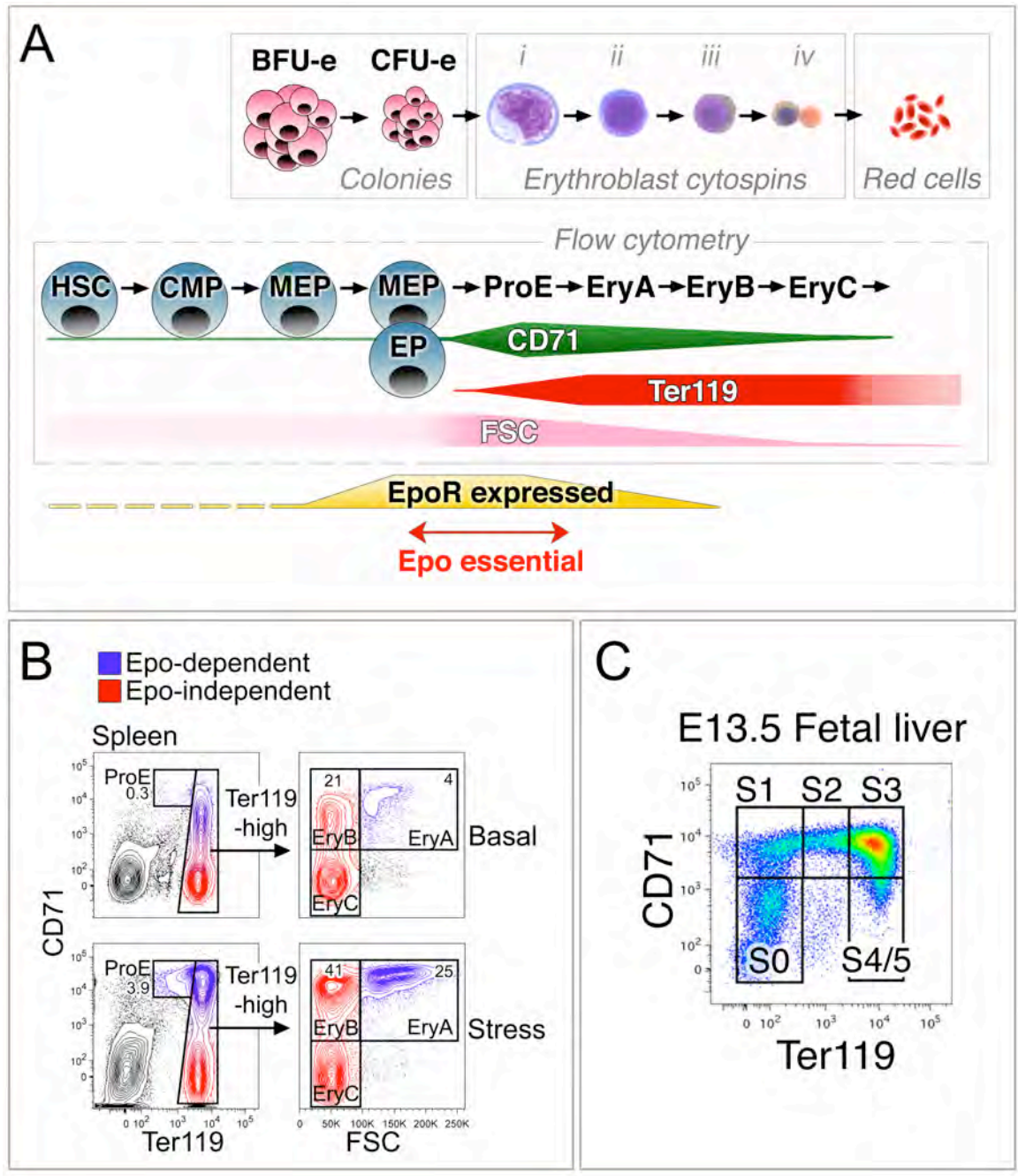
Figure 1.2 **Identification of erythroid progenitors in primary mouse tissue.**

(A) Early erythroid progenitors (BFU-e and CFU-e), found in the MEP progenitor pool, are defined by their ability to form erythroid colonies in response to Epo in culture. Later erythroid stages (labeled with roman numerals *i* through *iv*) are traditionally identified based on morphological staining criteria (top). Similar erythroblast stages can be identified directly in hematopoietic tissue using cell surface markers CD71, Ter119, and forward scatter, a measure of cell size (corresponding stages are directly below erythroblast cytospins). EpoR expression extends to earlier compartments (yellow box with dashed line), but becomes essential for the formation of ProE cells from the closely-preceding CFU-e progenitors (red arrow). ProE and EryA stages are Epo-dependent, and their frequency varies with the level of stress. Figure was created by me.

(B) Representative flow-cytometric plots of freshly-isolated splenocytes from mice injected with saline (basal) or a dose of Epo (stress). Animals were sacrificed two days post-injection. Cells were stained with CD71 and Ter119 markers. Dead cells were excluded using DAPI viability dye. Ter119^{high} gate is subdivided further based on CD71 and forward scatter (FSC). ProE (Ter119^{med}CD71^{high}FSC^{high}) and EryA (Ter119^{high}CD71^{high}FSC^{high}) subsets are Epo-dependent (blue) and greatly increase in frequency during stress. EryB (Ter119^{high}CD71^{high}FSC^{low}) and EryC (Ter119^{high}CD71^{low}FSC^{low}) erythroid progenitors (red) arise from the EryA pool, and are Epo-independent [42]. Modified from Figure 3.1B.

(C) Representative flow-cytometric plot of freshly-harvested E13.5 fetal liver stained with CD71 and Ter119 markers, and a viability dye. Erythroblast development in fetal

liver begins with the S0 subset that contains total hematopoietic progenitors [HSC through MEP, as shown in (A)]. S1 through S5 subsets contain fetal erythroblasts of increasing maturation status. Fetal liver staining method published in [46].

Figure 1.3
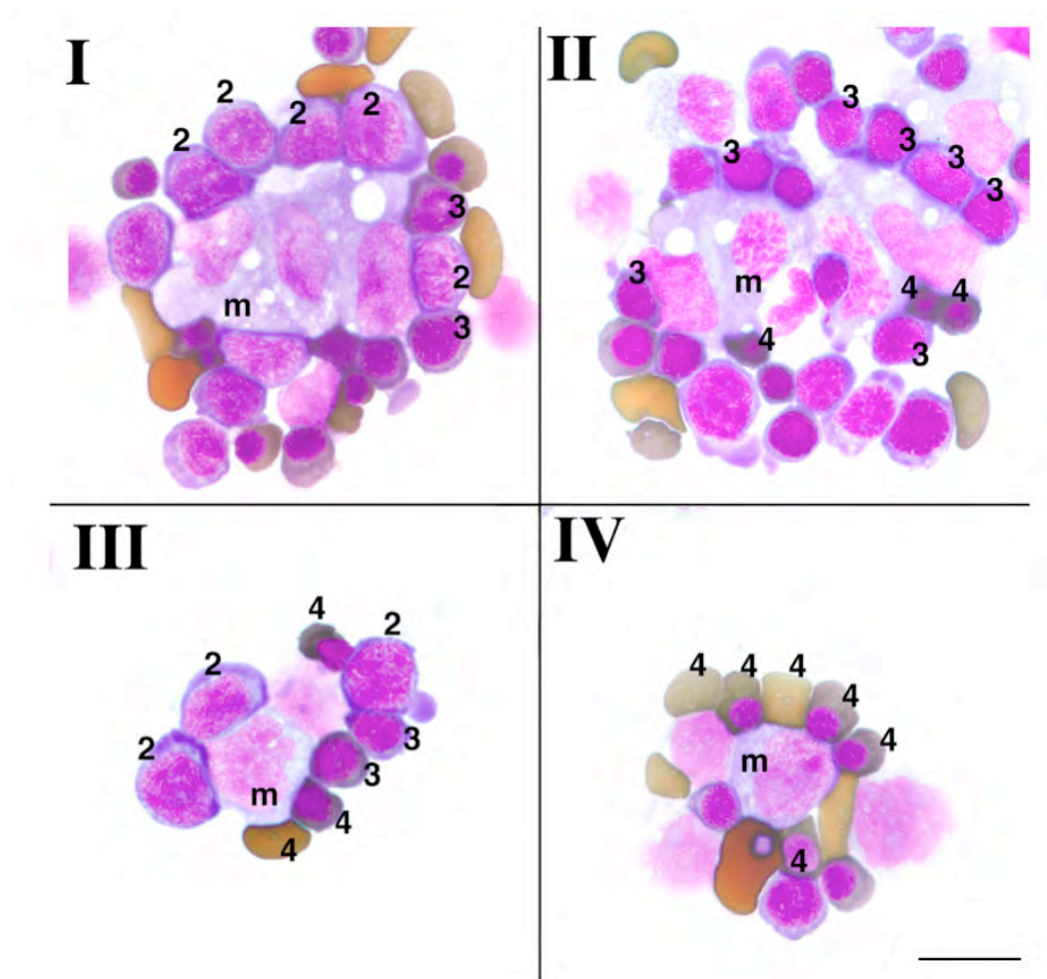
Figure 1.3   Erythroblastic islands: critical niches for basal and stress erythropoiesis *in vivo.*

(I-IV)   Erythroblastic islands isolated from E15.5 fetal liver. Erythroblasts develop around a central macrophage (m), with most of the cells in a similar developmental stage. Island IV contains more mature erythroblasts. Arabic numerals indicate the likely developmental stage of erythroblasts (2 =most immature, 4 =most mature). Scale Bar: 20μ. (Image used with permission from author Merav Socolovsky).

Figure 1.4
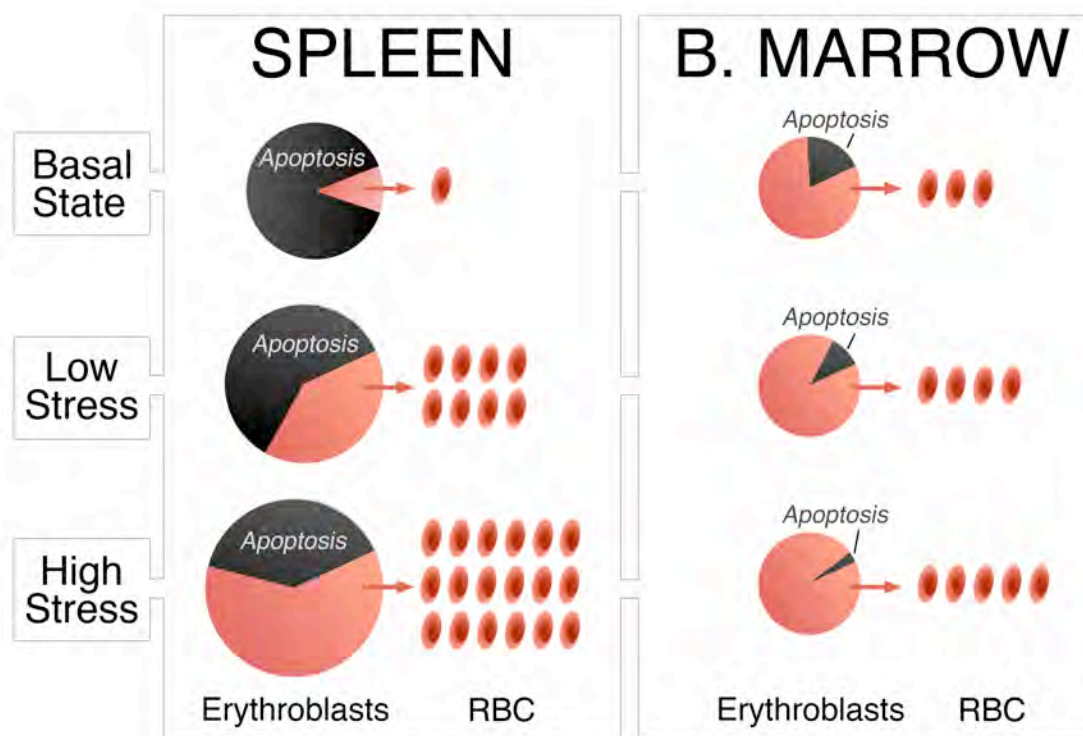
Figure 1.4 Proposed model: Epo regulates erythropoietic rate by rescuing progenitors from apoptosis.

Spleen (left), the reserve organ in mice, contains stress-responsive progenitors, which in the basal state undergo high rates of cell death [42]. This portion of dying cells forms a 'reserve' population (black fraction) to be rescued from apoptosis when needed. In contrast, bone marrow (right) replaces senescent erythrocytes (RBC) during the steady state, but it has a lower apoptotic reserve and smaller physical space capacity for stress erythropoiesis. *In vitro* studies suggested a model where increasingly greater Epo (stress) leads to a graded rescue of erythroblasts from apoptosis (indicated by a decreasing apoptotic fraction). Spleen can increase its absolute erythroblast number because, unlike the bone marrow, it can physically enlarge in size (indicated by the increasing size of the circles). My thesis work tested the survival pathways activated by the EpoR in spleen and bone marrow erythroid progenitors during stress erythropoiesis *in vivo*. Figure was designed and created by me.

Chapter II Attributions and Copyright information

MATERIALS AND METHODS

All sections of this chapter were written by me. Materials and Methods discussed in this chapter are applicable to the subsequent Chapters III and IV.

CHAPTER II

MATERIALS AND METHODS

Mice

Balb/C mice were purchased from Taconic, C57BL/6J strains were purchased from the Jackson Laboratories (Bar Harbor, ME). MyD88$^{-/-}$ mice were kindly provided to us by Dr. Egil Lien (University of Massachusetts Medical School, Worcester, MA). B6.MRL-Fas^{lpr}/J (Jackson Laboratories stock #000482) were crossed with B6.129.S7-Rag1^{tm1Mom}/J (Jackson Laboratories stock #002216) to obtain homozygous double-mutant *lpr*-Rag1$^{-/-}$ mice (C57BL/6J background). The homozygous double mutant *gld*-Rag1$^{-/-}$ mice (Balb/C background) were obtained by crossing CPt.C3-Fasl^{gld}/J (Jackson Laboratories, stock #002932) with C.129.S7(B6)-Rag1^{tm1Mom}/J (Jackson Laboratories stock #003145). Genotyping was performed by PCR according to Jackson Laboratories protocols. In all experiments, *lpr*-Rag1$^{-/-}$ and *gld*-Rag1$^{-/-}$ mice were compared to their respective Rag1$^{-/-}$ controls. Mice were used at 10 to 14 weeks of age.

Stat5$^{-/-}$ mice were obtained from Dr. Lothar Hennighausen, (NIDDK, Bethesda, MD). β-thalassemia mice and the ts-VHL$^{-/-}$ mice were described previously [42]. Bim$^{-/-}$ mice, B6.129S1-Bcl2l11$^{tm1.1Ast}$/J (stock #004525), were purchased from Jackson Laboratories. EpoR-H and EpoR-HM mice were obtained from Dr. James Ihle, St. Jude Children's Research Hospital, Memphis, TN [75]. In all experiments, mice were matched for the same background strain, gender, and age. For low oxygen chamber experiments, Balb/C male littermates of 6 to 11 weeks of age were used. All experiments with mice

were conducted in accordance with an animal protocol approved by the University of Massachusetts Medical School IACUC committee.

Erythropoietic stress

Recombinant human erythropoietin (Epoetin alfa, Amgen, Thousand Oaks, CA) was injected at the indicated doses subcutaneously in a total volume of 150 µl in sterile isotonic saline. Human purified Fas:Fc chimeric fusion protein (BD Biosciences, San Diego, CA) was injected at 100 µg per mouse, intraperitoneally. Reduced atmospheric oxygen treatment was conducted using the BioSpherix A-chamber (BioSpherix, Lacona, NY) for the indicated time periods. Hypoxia was achieved by displacing oxygen with nitrogen at normal atmospheric pressure. Temperature, humidity and carbon dioxide readings were monitored.

Live cell surface-staining for flow cytometry

Antibody staining and flow cytometry were performed as described (Chapter V and [42,44]). Cells from freshly isolated tissues were gently strained through 40-µm strainer in the presence of cold phosphate-buffered saline and 5% fetal calf serum (1xPBS/5% FCS) or 0.2% bovine-serum albumin (BSA).

The following antibodies and reagents were used: PE- or FITC-rat anti-mouse CD71 (C2 clone), PE- or APC-rat anti-mouse Ter119, biotin-hamster anti-mouse Fas (Jo2 clone) or FasL (MFL3 clone) (BD Biosciences). DAPI (Roche, Indianapolis, IN) or 7-AAD (BD Biosciences) viability dyes were used.

Cells were immunostained for 20-45 minutes on ice in the presence of blocking rabbit or mouse immunoglobulin (Jackson ImmunoResearch, West Grove, PA), 2.5 µg/mL fluorochrome-conjugated anti-Ter119 (BD Biosciences, San Diego, CA), and 2.5 µg/mL fluorochrome-conjugated anti-CD71 (BD Biosciences).

Staining for Fas or FasL was done along with anti-CD71/Ter119 for 1 hour on ice with 5 µg/mL biotin-conjugated anti-Fas (Jo2 clone, BD Biosciences) or 5 µg/mL biotin-conjugated anti-FasL (MFL3 clone, BD Biosciences). APC-conjugated streptavidin (Invitrogen, Carlsbad, CA) was used to amplify the biotin signal after washing the cells. Following all the staining steps, cells were washed twice and resuspended in the viability dye-containing buffer until analysis. Proper washing of cells is essential to specific signal detection. Alexa Fluor 350-Annexin V (Invitrogen) staining was performed according to the manufacturer's instructions (1 hour on ice in Annexin V-specific buffer; Annexin V buffer was also used for subsequent washes and viability dye staining).

Intracellular protein staining

To detect intracellular Bcl-x_L and Bim, cells were first stained with LIVE/DEAD fixable viability stain (Invitrogen), followed by surface-labeling for Ter119 and CD71 in the presence of blocking IgG. Next, cells were fixed with PBS solution containing 3% paraformaldehyde and 2% sucrose, and frozen in 90%FBS/10%DMSO at -80°C. On day 2, samples were thawed, washed with 1xPBS/0.2%BSA buffer, and permeabilized with BD Cytofix/Cytoperm™ Perm/Wash reagent. Cells were then stained in the Perm/Wash solution with anti-Ter119 (to maintain Ter119 signal in fixed cells) and with anti-Bcl-x_L

antiserum (BD Biosciences 556361) or anti-Bim antibody (Cell Signaling, #2819), or isotype control. Isotype control for Bcl-x$_L$ was Normal Rabbit Serum (Jackson Immunoresearch). Isotype control for Bim was Rabbit IgG (Jackson Immunoresearch). Primary Bcl-x$_L$ or Bim staining was detected using secondary antibody (anti-Rabbit-APC, Invitrogen A-10931). Proper washing of cells is essential to specific signal detection. Biological sample used for determining the isotype control's background fluorescence consisted of a cell mix pooled from all mouse samples in a given experiment (isotype signal was similar across individual biological samples regardless of genotype or treatment).

Phospho-Stat5 staining

Cells were first stained with LIVE/DEAD viability dye, then resuspended in phosphowash (1xPBS, 1 mM sodium orthovanadate, 1 mM β-glycerol phosphate, 1 µg/mL microcystin), fixed in 1.6% paraformaldehyde, permeabilized in 80% acetone and stored at -80°C. Thawed cells were stained in 1xPBS/3% milk with AF647-conjugated anti-phospho-Stat5 antibody (BD Biosciences 612599) and for Ter119 and CD71 as described previously.

Reticulocyte detection

Reticulocytes were detected as a DNA-negative, RNA-positive cell population in blood, as described [48]. 1-2 µl of EDTA-preserved whole blood were stained at room temperature for 30 minutes in 1xPBS with RNA/DNA dye Thiazole Orange (Sigma-

Aldrich, St. Louis, MO; used at ~1:1000 dilution of fresh 1 mg/mL stock solution in methanol), followed by addition of DNA dye DRAQ5 (BioStatus, Shepshed, United Kingdom; used at 1:2500 of 5 mM stock solution) for 5 minutes at 37°C. Cells must be kept in original Thiazole Orange/DRAQ5 staining solution until analysis. Data were collected using the 488nm and the 633nm lasers [FITC and APC (670/40 filter) channels, respectively] on LSRII (BD Biosciences) flow cytometer.

For all flow cytometry experiments, stained cells were analyzed on LSRII flow cytometer (BD Biosciences). Cell sorting was done at the Umass Flow Cytometry Core Facility on a DakoCytomation MoFlo (Fort Collins, CO).

Flow cytometry data analysis

Data were analyzed with FlowJo software (Tree Star, Ashland, OR), as described in more detail in Chapter V [42,46.] Singlets and live cells (based on DAPI, 7-AAD, or LIVE/DEAD stains) were selected, and subsets were gated based on Ter119, CD71 expression and forward scatter (FSC). Gating strategy for fetal liver and adult erythroblasts was performed as described in Chapter V. For Fas surface stain, Fas-positive gate was drawn based on secondary antibody-only control, as described above. For Annexin V, positive gate was drawn based on the sample where Annexin V stain was omitted. For each subset in each biological sample, non-specific isotype control's median fluorescent intensity (MFI) signal was subtracted from the MFI of Bcl-x$_L$ or Bim signal prior to plotting the data.

Peripheral blood analysis

Hematocrit was determined using the CritSpin Microhematocrit centrifuge kit (Iris Sample Processing, Westwood, MA). For Complete Blood Count (CBC), whole blood was collected by cardiac puncture of euthanized animal into EDTA collection tubes and processed on Heska Hematology Analyzer (Heska, Loveland, CO) at the Umass Animal Facility.

CFU-e colony assay

Freshly isolated fetal liver, spleen and bone-marrow cells were manually counted, and cells were plated for tissue culture in M3231 Methocult® methylcellulose media (StemCell Technologies, Vancouver, Canada) supplemented with 2 U/mL rh-Epo (Amgen). On day 3, plates were stained with 3,3'-Diaminobenzidine (Sigma-Aldrich) and scored for erythroid colonies. Results are expressed as total CFU-e colonies per 10^6 live plated cells.

Erythropoietin ELISA

Enzyme Linked Immunosorbent Assay (ELISA) for mouse Epo was performed according to the manufacturer's instructions (Quantikine ELISA, R&D Systems, Minneapolis, MN). EnVision 2102 Multilabel Reader (Perkin Elmer, Waltham, MA) was used to quantify fluorescence. Data were converted into mU/mL by multiplying pg/mL value by 129,000 IU/mg (International Standard for fully glycosylated Epo protein [4,126]).

Statistical analyses and data presentation

Statistical analysis of basal state Fas and FasL-mutant mouse data in Chapter III was performed using PASW (SPSS, Chicago, IL) and SAS (SAS, Cary, NC) statistical software. Specifically, data were log-transformed and residuals were tested for normality by Kolmogorov-Smirnov test (performed in PASW). Log-transformed data were then analyzed by general linear mixed model ANOVA with gender and genotype as fixed effects, and with experiment as the random effect (performed in SAS). Unadjusted p-values ($p<0.05$ considered significant) were reported in Chapter III figures for each gender-genotype group.

F probability distribution test (F test) in Chapter III was performed on residuals derived from untransformed data: First, experiment, gender and genotype were taken into account for deriving the residuals (performed in PASW). Residuals were next compared using F test in Microsoft Excel software (Redmond, WA). Similar, or even more significant, p-values were obtained via F test on raw pooled data directly within Microsoft Excel.

For all other statistical tests, Microsoft Excel or GraphPad Prism software (La Jolla, CA) were used. For presentation in the figures, all data were plotted using Microsoft Excel or GraphPad Prism software, and adjusted in Adobe Photoshop and Illustrator Software.

Quantitative real-time PCR

Total RNA was prepared from freshly sorted erythroblasts using the AllPrep DNA/RNA Micro Kit (Qiagen) with on-column DNase treatment. Reverse-transcription was conducted using Superscript II (Invitrogen) with random hexamer primers. The ABI 7300 sequence detection system, TaqMan reagents and TaqMan MGB probes (Applied Biosystems) were used, and several dilutions of each template were used to ensure detection in the linear range of the assay. A 'no template' and 'no reverse-transcriptase' controls were included. The threshold cycle (Ct) for housekeeping genes GAPDH or β-actin were subtracted from the Ct for genes of interest to yield a relative expression value. Where indicated, the relative expression for each gene of interest in each sample was then normalized to its expression in the S0 fetal liver subset or saline-injected bone-marrow EryA adult subset (Chapter IV).

QRT-PCR TaqMan probes used: GAPDH (Mm99999915_g1), β-actin (Mm02619580_g1), β-globin (Mm01611268_g1). Bcl-x$_L$ primers were CTGGGACACTTTTGTGGATCTCT and GAAGCGCTCCTGGCCTTT. Bim$_{EL}$ primers were TCTTTTGACACAGACAGGAGC and AATCATTTGCAAACACCCTCC. Bim$_L$ primers detected both Bim$_{EL}$ and Bim$_L$ isoforms, and were CTCAGTGCAATGGCTTCCATA and AATCATTTGCAAACACCCTCC.

Chapter III Attributions and Copyright information

The material in this chapter has been published in PloS One Journal in a modified format. This chapter represents original work by the authors.

Negative Autoregulation by Fas Stabilizes Adult Erythropoiesis and Accelerates its Stress Response

Miroslav Koulnis[1], Ying Liu[1], Kelly Hallstrom[1] and Merav Socolovsky[1]

[1]Department of Pediatrics and Department of Cancer Biology, University of Massachusetts Medical School, Worcester MA USA

Authorship Contributions:

MK designed and performed research, analyzed and interpreted data, created figures and wrote the manuscript. YL conducted the cross-breeding of *lpr* and *gld* mice onto immune-deficient Rag1^{-/-} background. KH helped MK with performing some of the experiments. MS designed research, analyzed and interpreted data, wrote the manuscript, and wrote Text 3.1.

Disclosure of Conflicts of Interest:

None of the authors have any conflicts of interest to declare.

CHAPTER III

NEGATIVE AUTOREGULATION BY FAS STABILIZES ADULT ERYTHROPOIESIS AND ACCELERATES ITS STRESS RESPONSE

ABSTRACT

Erythropoiesis maintains a stable hematocrit and tissue oxygenation in the basal state, while mounting a stress response that accelerates red cell production in anemia, blood loss or high altitude. Thus, tissue hypoxia increases secretion of the hormone erythropoietin (Epo), stimulating an increase in erythroid progenitors and erythropoietic rate. Several cell divisions must elapse, however, before Epo-responsive progenitors mature into red cells. This inherent delay is expected to reduce the stability of erythropoiesis and to slow its response to stress. Here we identify a mechanism that helps to offset these effects. We recently showed that splenic early erythroblasts, 'EryA', negatively regulate their own survival by co-expressing the death receptor Fas, and its ligand, FasL. Here we studied mice mutant for either Fas or FasL, bred onto an immune-deficient background, in order to avoid an autoimmune syndrome associated with Fas deficiency. Mutant mice had a higher hematocrit, lower serum Epo, and an increased number of splenic erythroid progenitors, suggesting that Fas negatively regulates erythropoiesis at the level of the whole animal. In addition, Fas-mediated autoregulation stabilizes the size of the splenic early erythroblast pool, since mutant mice had a significantly more variable EryA pool than matched control mice. Unexpectedly, in spite of the loss of a negative regulator, the expansion of EryA and ProE progenitors in

response to high Epo *in vivo*, as well as the increase in erythropoietic rate in mice injected with Epo or placed in a hypoxic environment, lagged significantly in the mutant mice. This suggests that Fas-mediated autoregulation accelerates the erythropoietic response to stress. Therefore, Fas-mediated negative autoregulation within splenic erythropoietic tissue optimizes key dynamic features in the operation of the erythropoietic network as a whole, helping to maintain erythroid homeostasis in the basal state, while accelerating the stress response.

INTRODUCTION

The production of red blood cells (erythropoiesis) is continuous throughout life, maintaining an optimal number of circulating red cells and tissue oxygen tension (pO_2). A decrease in tissue pO_2, as may occur in anemia, bleeding, high altitude or respiratory disease, drives erythropoiesis up to 10-fold its basal rate. This response is regulated through a negative feedback loop in which decreasing tissue pO_2 increases synthesis of the hormone Epo (Figure 3.1A) [7,24,127]. Epo-mediated activation of its receptor, EpoR [56], on erythroid progenitors increases their number and consequently, erythropoietic rate and tissue pO_2. During accelerated rates of erythropoiesis, Epo cooperates with additional factors, notably glucocorticoid hormones and stem cell factor [15,21,128,129].

Epo controls an early cellular compartment within the 'erythroblastic island', the developmental niche on the surface of a macrophage that supports erythroid maturation [130] (Figure 3.1A). Three to five cell divisions must elapse before cells in this early compartment mature into red blood cells. This inherent delay in the pO_2/Epo-regulated

feedback loop is likely to compromise the stability and rapid stress response of the erythropoietic system. Additional control mechanisms may therefore exist to compensate for this inherent delay.

The earliest Epo-dependent progenitor is the 'Colony-forming Unit-erythroid' or CFU-e, giving rise to colonies of at least 8 red cells within 48-72 hours *in vitro* [35]. Its erythroblast progeny are classified by their morphology [131]. We previously developed a flow-cytometric approach to identify erythroblasts directly in freshly-harvested mouse hematopoietic tissue, using cell surface markers CD71, Ter119 and cell size, measured by flow-cytometric forward scatter (FSC). We classify increasingly mature erythroid precursors subsets as 'ProE' ($CD71^{high}$ $Ter119^{med}$), 'EryA' ($CD71^{high}Ter119^{high}FSC^{high}$), 'EryB' ($CD71^{high}Ter119^{high}FSC^{low}$) and 'EryC' ($CD71^{low}Ter119^{high}FSC^{low}$) [42] (Figure 3.1A-B). We found that, in addition to the well documented increase in CFU-e [52,132], the early erythroblast subsets ProE and EryA are responsive to EpoR signaling *in vivo* [42].

Epo promotes erythroblast survival *in vitro* [73], suggesting this mechanism may underlie its regulation of erythropoietic rate. Our recent experiments *in vivo* [42] confirm this hypothesis. During basal erythropoiesis, the majority of ProE and EryA undergo apoptosis, particularly in spleen, the murine organ of erythropoietic reserve [133]. During stress, high Epo decreases their apoptosis, increasing ProE and EryA number [42]. The reasons for this apparently wasteful mechanism of erythropoietic rate regulation have not been addressed experimentally.

EpoR activates several survival pathways, including Stat5-mediated induction of $Bcl-x_L$ [76,99,134,135], other Stat5 targets [67,90,136,137] and the EpoR-activated phosphoinositide

3-kinase (PI3K)-AKT pathway [81,82]. The death receptor Fas, and its ligand, FasL, were first proposed to contribute to erythroid homeostasis based on their expression in human bone marrow [92]. We found that, *in vivo* in the mouse, splenic ProE and EryA, but not their bone marrow counterparts, co-express Fas and FasL. During stress, high Epo suppresses their Fas expression, strongly correlating with their decreased apoptosis [42]. These findings suggested the hypothesis that, in the basal state, splenic ProE and EryA negatively regulate their own survival through Fas and FasL-mediated inter-cellular interactions; and that Epo-mediated Fas suppression is a key mechanism regulating erythropoietic expansion during stress (Figure 3.1A) [42].

Negative autoregulation through co-expression of Fas and FasL was previously implicated in terminating the clonal expansion of activated T cells [138-140]. Similarly, we recently found that Fas and FasL co-expression in fetal liver erythroid progenitors terminates their initial wave of expansion at the onset of fetal erythropoiesis [44]. Here we set out to assess the contribution of Fas and FasL to erythropoiesis in the adult. We bred *lpr* or *gld* mice, mutant in Fas and FasL respectively, onto the Rag1^{-/-} immune-deficient background, in order to avoid an autoimmune syndrome that may impact erythropoiesis. Our findings in both the *lpr*-Rag1^{-/-} and *gld*-Rag1^{-/-} mice were similar, showing that Fas-mediated autoregulation in spleen negatively regulates erythropoiesis at the whole animal level. Strikingly, these experiments also revealed that Fas-mediated autoregulation imparted key dynamic properties to the erythropoietic system. We found that it is responsible for stabilizing the basal precursor pool, enhancing their resistance to random perturbations. Further, it also accelerated the erythropoietic response to high Epo, an

unexpected effect for a negative regulator. Therefore, the dynamic properties of the Fas-mediated autoregulation offset the dynamic deficits of the slower, pO_2/Epo-regulated feedback. Of interest, negative autoregulatory loops, in the context of simple transcriptional networks, were shown to accelerate the response to a stimulus, and to enhance network stability [141-144]. Our findings here suggest that these loops, which are abundant in biological systems, similarly improve the homeostasis and dynamic responses of lineage-specific progenitors *in vivo*.

RESULTS

Hypoxia and return to normoxia alter Fas expression and survival of early erythroblasts

Erythropoietic stress results in suppression of Fas expression and reduced apoptosis in splenic ProE and EryA [42]. These findings suggested the model illustrated in Figure 3.1A, in which Fas-mediated cell death is a result of intercellular interactions between Fas and FasL-co-expressing cells within the spleen early erythroblast compartment; these interactions are blocked by high Epo during stress (Figure 3.1B).

Here we investigated this model further by housing mice in a hypoxic environment of 11% oxygen for 8 days, followed by a return to normoxia (21% oxygen). Hypoxia caused a sharp increase in plasma Epo (Figure 3.1C, lower left panel), suppressing Fas expression in EryA and enhancing their survival (Figure 3.1C, upper panel: example of flow-cytometric measurements of Fas expression and Annexin V binding; middle panels: summary of data from 2 to 9 mice per time point). Decreased

apoptosis and Fas expression were associated with increased spleen EryA (Figure 3.1C, lower right panel). A return to 21% oxygen resulted in a rapid reversal, with Epo and EryA declining below their starting levels, and both Fas expression and apoptosis rising well above their starting basal levels. These results suggest that modulation of Fas-mediated apoptosis by Epo plays a role in both the expansion of the EryA pool in response to hypoxia, and in its rapid contraction with the return to normoxia.

Effect of reducing Fas-mediated apoptosis with Fas:Fc *in vivo*

To examine the effect of Fas on EryA survival directly, we administered MyD88^{-/-} mice with the purified chimeric molecule, Fas:Fc [145], which acts as a decoy receptor, binding FasL on the surface of EryA and blocking its ability to activate Fas. Control MyD88^{-/-} mice were injected intraperitoneally with an equal volume of saline. The MyD88^{-/-} strain was used in order to avoid potential reaction to contaminating bacterial Lipopolysaccharide (LPS) in the Fas:Fc preparation [146]. A single administration of Fas:Fc (100 μg) resulted in a ~20% reduction in unoccupied surface FasL in both splenic ProE and EryA, measured by binding of the Fas-blocking monoclonal antibody MFL3, directed against FasL (Figure 3.10D) [147]. This procedure decreased the number of Annexin V[+] EryA from 70% in control to 50% in Fas:Fc-injected mice by 48 hours. There was an associated increase in EryA, and a doubling in blood reticulocytes (Figure 3.10). Reticulocytes, identified by their RNA content, mature within 24 hours [148]; a doubling of reticulocytes suggests a doubling of erythropoietic rate over the most recent 24 hours. These results support a causal relationship between Fas expression, EryA

survival and erythropoietic rate.

The dose/response characteristics of Epo-mediated Fas suppression and EryA expansion

To assess the quantitative relationship between Epo, Fas suppression and EryA numbers we injected mice (n=38) with varying doses of Epo, of between 1 and 300 Units /25 g body weight. We measured the Fas response on day 3, previously found to correspond to the lowest Fas expression level attained following acute Epo injection [42]. We found that EryA frequency in Ter119$^+$ spleen cells was inversely related to the fraction of EryA cells that expressed Fas (Figure 3.2A, left panel). Half maximal suppression of Fas expression was seen in mice injected with 10 U /25 g (Figure 3.2A, right panel), corresponding to a doubling of EryA frequency. Complete suppression of Fas expression was seen at 30U /25g, and resulted in a 6-fold increase in EryA frequency.

The frequency of EryA is inversely related to their Fas expression

The relationship between EryA frequency, and the fraction of EryA that express Fas, may be fitted by a model in which EryA undergo Fas-mediated negative autoregulation (Figure 3.2B). We considered the frequency of EryA within the erythroblastic island, '*A*', to be the result of three principal factors: first, a continuous input from earlier progenitors, '*β*'; second, a continuous output, proportional to *A*, '*αA*', into more differentiated progenitor subsets; and last, Fas-dependent cell death. We assumed that Fas-mediated cell loss would result when two EryA cells, expressing Fas

and FasL respectively, interact within the erythroid compartment. The probability of such an encounter is proportional to the product of the frequencies of Fas^+ and $FasL^+$ EryA cells. This product is approximately equal to A^2F, where 'F' denote the fraction of EryA cells that express Fas (Figure 3.2B; the fraction of EryA that express FasL in adult spleen is high enough that it can be approximated to 1; see Text 3.1: 'Regulation of the EryA progenitor pool by Fas'). These considerations allow the steady-state level of EryA, at any given level of Fas, to be found by solving a quadratic equation. The inverse relationship between EryA and Fas in Figure 3.2A is fitted well by a hyperbolic curve that represents the (positive) steady-state solutions for EryA ('A') in this equation, at different steady-state levels of Fas ('F') (R^2=0.89, Text 3.1). This goodness of fit supports the model's key assumption, that Fas-mediated cell loss is a result of negative autoregulation within the EryA pool, and is proportional to the square of the frequency of EryA within the erythroblastic island. Further, it suggests that Epo concentration, which sets the desired steady-state EryA pool size, does so in part by regulating the level of Fas expression in the EryA population (Figure 3.1A).

Of note, using a different modeling approach, we found a similar relationship in fetal liver, where Fas-mediated loss of early erythroblasts was proportional to the square of the frequency of early erythroblasts in the tissue [44].

Generation of Fas and FasL-deficient mice on an immune-deficient background

We made use of the *lpr* and *gld* mouse strains that carry naturally-occurring loss-of-function mutations of Fas and FasL, respectively [125]. The *lpr* mutation consists of an

insertion of an early transposable element, carrying a polyadenylation signal, in the second intron of the Fas gene. This causes premature termination of the transcript and a drastic decrease in Fas transcription, though it does not fully eliminate it. In the *gld* strain, there is a point mutation at the C-terminus of FasL that abolishes its ability to bind Fas. Both the *lpr* and *gld* mice develop a lymphoid proliferative autoimmune syndrome [149]. In order to avoid this complication, we bred these mouse strains onto an immune-deficient, Rag1$^{-/-}$ background that lacks T and B cells [150]. Erythroid parameters, such as basal hemoglobin concentration, though consistent within a given inbred strain, differ somewhat between mice of different genetic backgrounds, likely reflecting quantitative differences in the control of erythropoiesis [151]. We therefore chose to generate two distinct genetic background strains. The *gld*-Rag1$^{-/-}$ mice were bred on the Balb/C background, and the *lpr*-Rag1$^{-/-}$ mice on the C57BL/6 background. As controls, we used age and strain-matched Rag1$^{-/-}$ mice, which on either the Balb/C or the C57BL/6 backgrounds, have normal erythropoietic parameters when compared with wild-type mice of the same background strain. Further, the double homozygous mutant strains, *gld*-Rag1$^{-/-}$ and *lpr*-Rag1$^{-/-}$, showed no sign of autoimmunity, as evident from their small spleen size, absence of immune cells from the blood and spleen, and lack of anemia (Table 3.1).

Basal Erythropoiesis in *lpr*-Rag1$^{-/-}$ and *gld*-Rag1$^{-/-}$ mice

The chronic absence of an erythropoietic regulator may not be apparent from simple inspection of the hematocrit in the steady state [76]. This is due to a vast erythropoietic reserve, coupled with the pO$_2$/Epo negative feedback loop which

automatically adjusts Epo levels and erythropoietic rate so as to maintain a near- normal tissue pO_2. Therefore, to assess how the loss of a regulator affects steady state erythropoiesis requires analysis at all levels of the pO_2/Epo negative feedback loop, including Epo concentration and the erythroid progenitor and precursor pools. We first examined the hematocrit (the fraction of all blood volume that is attributable to red blood cells), blood reticulocytes and plasma Epo. *lpr*-Rag1^{-/-} mice on the C57BL/6 background had a normal reticulocyte count and normal hematocrit (Figure 3.3A, top left panel, Table 3.1). However, plasma Epo was significantly lower, by 35%, than in control mice (p=0.001; Epo= 9.0±0.8 mU/mL, mean ±SEM, in *lpr*-Rag1^{-/-}, and 13.7±1.0 for Rag1^{-/-} controls; Figure 3.3A, bottom left panel, and Figure 3.3B). Therefore, *lpr*-Rag1^{-/-} mice compensate for the chronic absence of a negative regulator through the pO_2/Epo negative feedback loop, decreasing Epo concentration so as to avoid an unnecessary increase in hematocrit.

By contrast, the *gld*-Rag1^{-/-} mice, on the Balb/C background, had a significantly elevated hematocrit (p<0.00001; hematocrit= 52.0 ±0.3% *vs*. 49.8 ±0.4% for *gld*-Rag1^{-/-} *vs*. Rag1^{-/-} respectively, mean ±SEM, Figure 3.3A; a similar difference was found in a second group of mice assayed using a Coulter counter, Table 3.1). Reticulocyte count was also more than double that of controls (p<0.0001; Reticulocyte count= 1.40 ±0.14% *vs*. 0.59 ±0.04% for *gld*-Rag1^{-/-} *vs*. Rag1^{-/-} respectively, Figure 3.3C-D), and hemoglobin concentration was also significantly elevated in 2 independent experiments (Table 3.1). As comparison, mice we housed for 3 weeks in 12% oxygen, equivalent to an altitude of 14,000 feet, increased their hematocrit from 51.6 ±0.2 to 57.8 ±0.5%, an increase of 6%.

Therefore, the 2.2% increase in hematocrit in the *gld*-Rag1$^{-/-}$ mice represents approximately a third of the erythropoietic output in high altitude hypoxia. Unlike the *lpr*-Rag1$^{-/-}$, plasma Epo in the *gld*-Rag1$^{-/-}$ mice was not significantly different to that of controls (Figure 3.3A), possibly because of the already low basal Epo in control Balb/C mice which was ~40% lower than in control mice on the C57BL/6 background (Figure 3.3A, lower panels, black symbols).

Of note, responses by both *gld*-Rag1$^{-/-}$ (Balb/C background) and the *lpr*-Rag1$^{-/-}$ (C57BL/6 background) mice have in common a higher erythropoietic rate per unit plasma Epo than in matched control mice, consistent with the absence of a negative regulator of erythropoiesis.

Increased splenic CFU-e, ProE and EryA in *gld*-Rag1$^{-/-}$ and *lpr*-Rag1$^{-/-}$ mice

A representative flow-cytometric histogram in Figure 3.4A shows that the frequency of the ProE and EryA subsets within *gld*-Rag1$^{-/-}$ spleen erythropoietic tissue (Ter119^{+} cells) was increased. A similar analysis in 11 to 40 mice per strain/sex combination is summarized in Figures 3.4B and 3.4D. An increase in subset frequency does not necessarily reflect a corresponding increase in cell number, since it may also arise as a result of decreased cell number in other subsets. We therefore also examined the absolute number of cells in each of the erythroid precursor subsets, computed by multiplying the subset frequency data by the fraction of Ter119^{+} cells per spleen and the spleen weight, for each individual mouse (Figure 3.5A).

These data show significant increases, ranging from 1.5- to 4-fold, depending on

genotype and sex, in both the frequency and absolute number of spleen CFU-e, ProE, EryA and EryB, in *gld*-Rag1$^{-/-}$ and *lpr*-Rag1$^{-/-}$ mice (Figures 3.4A-C and 3.5A). Specifically, all the splenic ProE, EryA and EryB subsets showed increased frequency within the Ter119^{high} compartment in both *gld*-Rag1$^{-/-}$ and *lpr*-Rag1$^{-/-}$ mice relative to matched controls, with this increase reaching statistical significance in ten of the twelve comparisons made, namely ProE ($p<0.02$), EryA ($p<0.002$) and EryB ($p<0.002$) in female *lpr*-Rag1$^{-/-}$ mice, ProE ($p<0.002$), EryA ($p<0.002$) and EryB ($p<0.02$) in male *lpr*-Rag1$^{-/-}$ mice, ProE ($p<0.02$), EryA ($p<0.02$) and EryB ($p<0.02$) in female *gld*-Rag1$^{-/-}$ mice, and EryB ($p<0.02$) in male *gld*-Rag1$^{-/-}$ mice. The frequency of ProE and EryA in male *gld*-Rag1$^{-/-}$ mice was also increased relative to controls but did not reach statistical significance. Similarly, the absolute number of cells in each of these erythroid subsets increased in both *gld*-Rag1$^{-/-}$ and *lpr*-Rag1$^{-/-}$ mice, reaching significance in nine of the twelve comparisons made, namely, ProE ($p<0.005$), EryA ($p<0.0005$) and EryB ($p<0.0005$) in female *lpr*-Rag1$^{-/-}$ mice, ProE ($p<0.0005$), EryA ($p<0.0005$) and EryB ($p<0.05$) in male *lpr*-Rag1$^{-/-}$ mice, and ProE ($p<0.05$), EryA ($p<0.005$) and EryB ($p<0.05$) in female *gld*-Rag1$^{-/-}$ mice. The number of ProE, EryA and EryB in male *gld*-Rag1$^{-/-}$ mice also increased but the differences did not reach statistical significance (Figure 3.5A). The number of *gld*-Rag1$^{-/-}$ mice available for analysis was smaller than that of the other sex/strain combinations (Figures 3.4B and 3.5A), possibly accounting for the failure of the change in their erythroblast subsets to reach statistical significance.

Of note, there was no significant change in any of the equivalent subsets in bone marrow (Figure 3.4D) for any sex/strain combination. These results are consistent with

the pattern of erythroid Fas and FasL co-expression, which is largely restricted to spleen [42]. The largest increases were observed in ProE and EryA, in agreement with their higher Fas and FasL expression [42].

Variability in basal erythropoietic rate and in the size of splenic erythroid subsets in *gld*-Rag1$^{-/-}$ and *lpr*-Rag1$^{-/-}$ mice

Whilst the mean size of the ProE and EryA pools increased in *gld*-Rag1$^{-/-}$ and *lpr*-Rag1$^{-/-}$ mouse populations, their actual size in individual mice was highly variable. Using an F-test we found significantly higher variance in both the frequency and absolute number of nearly all erythroblast subsets in the *gld*-Rag1$^{-/-}$ and *lpr*-Rag1$^{-/-}$ mice, and in *gld*-Rag1$^{-/-}$ reticulocytes, compared with matched Rag1$^{-/-}$ controls (significantly different variance is marked with an '*f*'; Figures 3.3D, 3.4B-C, 3.5A). The EryA frequency distributions (Figures 3.5B and 3.11) show the larger spread of EryA pool size in the mutant mice. We also found increased coefficient of variation (CV) for EryA and ProE in male, but less so in female, *gld*-Rag1$^{-/-}$ and *lpr*-Rag1$^{-/-}$ mice (Figures 3.5B and 3.11). The coefficient of variation measures variability independently of the population mean. Overall, CV values for all splenic erythroblast subsets and for peripheral blood reticulocytes in both *gld*-Rag1$^{-/-}$ and *lpr*-Rag1$^{-/-}$ male and female mice, are significantly increased (p=0.017, Figure 3.11B). These findings indicate that a key function of Fas-mediated negative autoregulation is to suppress variability in the steady-state precursor pool and in erythropoietic rate, thus stabilizing the basal state.

A delayed response to Epo-driven erythropoietic stress in *gld*-Rag1^{-/-} and *lpr*-Rag1^{-/-} mice

We took two approaches to assess the stress response of the *gld*-Rag1^{-/-} and *lpr*-Rag1^{-/-} mice. First, we injected mice with a single high dose of Epo (300 U /25 g body weight), and followed the resulting increase in erythropoietic rate for 6 days (Figure 3.6A-D). Initially, on days 1 and/or 2, hematocrit was higher in both *gld*-Rag1^{-/-} and *lpr*-Rag1^{-/-} mice compared with controls, by 1-2%, possibly reflecting the larger basal erythroblast pool in these mice. However, between days 2 and 3, there was a significantly faster increase in hematocrit in control mice, which rose by over 4% in the space of 24 hours, overtaking the hematocrit of *gld*-Rag1^{-/-} and *lpr*-Rag1^{-/-} mice (Figure 3.6A, 3.6D). There was no equivalent rapid increase in hematocrit in the *gld*-Rag1^{-/-} and *lpr*-Rag1^{-/-} mice. By subtracting the mean hematocrit on day 2 from the mean hematocrit on day 3, in 5 independent comparisons between independent experiments on those days, we found that the rate of change in the hematocrit was significantly higher in control mice ($p<0.005$, Figure 3.6D). The slower increase in hematocrit in both *gld*-Rag1^{-/-} and *lpr*-Rag1^{-/-} mice at this time was due to a slower expansion of EryA precursors, in spite of their larger basal EryA pools (Figure 3.6B, 3.6C). The difference in EryA expansion was largest on days 2 (*lpr*-Rag1^{-/-} mice) and 3 *(gld*-Rag1^{-/-} mice) (Figure 3.6C), corresponding to the time when Epo-mediated Fas suppression in wild-type mice reaches its peak [42].

Of note, EryA expansion in control mice was a massive, 30- to 60-fold increase over the basal EryA pool. The shortfall in EryA on day 2 in the *lpr*-Rag1^{-/-} mice was equivalent to 10 times the size of the basal EryA pool, or 30% of the total expansion in

control mice on that day (Figure 3.6B,C, p<0.05; the size of the basal EryA pool is marked Figure 3.6C as a black bar). A similar delay in EryA expansion was seen in *gld*-Rag1$^{-/-}$ mice (Figure 3.6B,C). Further, injection of a much lower Epo dose (10U /25 g body weight) in *lpr*-Rag1$^{-/-}$ mice again resulted in delayed hematocrit and ProE responses (Figure 3.12). Therefore, the presence of Fas-mediated negative autoregulation accelerates the erythropoietic response over a wide Epo stress range.

Analysis of changes in the ProE population showed similar results. In spite of its larger size in the basal state, expansion of the ProE pool in both *gld*-Rag1$^{-/-}$ and *lpr*-Rag1$^{-/-}$ mice was slower between days 1 and 3, the differences in the absolute size of the pools reaching significance on days 1 (*gld*-Rag1$^{-/-}$ mice) and 3 (*lpr*-Rag1$^{-/-}$ mice) (Figure 3.7A). Furthermore, the rate of increase in ProE in response to Epo peaked in all mice between days 1 and 2, attaining a significantly lower level in *gld*-Rag1$^{-/-}$ and *lpr*-Rag1$^{-/-}$ mice compared with matched controls (p=0.00004, Figure 3.7B,C).

A delayed erythropoietic stress response to reduced atmospheric oxygen in *gld*-Rag1$^{-/-}$ mice

In a second approach, we examined the response of the *gld*-Rag1$^{-/-}$ mice to an acute reduction of atmospheric oxygen to 11% (Figure 3.8). The response to reduced atmospheric oxygen is complex since, in addition to elevating serum Epo, it stimulates additional cytokines as well as changes in ventilation and plasma volume that may indirectly alter erythropoietic responses [18,19,21]. Furthermore, the actual increase in serum Epo in response to lower atmospheric oxygen is determined not only by the initial

hypoxic stimulus, but also by the ensuing erythropoietic response, which determines the duration of tissue hypoxia (Figure 3.1A). We chose to examine *gld*-Rag1$^{-/-}$ mice, since, unlike the *lpr*-Rag1$^{-/-}$ strain, their starting baseline Epo levels are very similar to those of their matched controls (Figure 3.3B). We found that in spite of their higher starting hematocrit and reticulocyte count, the increase in erythropoietic rate in *gld*-Rag1$^{-/-}$ mice was significantly slower, as seen by a significantly delayed increase in hematocrit (Figure 3.8A) and a lower reticulocyte count (Figure 3.8B). There was a correspondingly slower increase in EryC erythroblasts (Figure 3.8D), at both 24 and 72 hours. This sluggish response presumably prolonged the tissue hypoxia in these mice, as reflected by their higher serum Epo at 72 hours (Figure 3.8C). These results clearly show a delayed stress response in mice lacking Fas-mediated negative autoregulation of erythroblasts.

Unlike the response to injection of a fixed, high Epo dose (Figure 3.6), the slower erythropoietic response to hypoxia in the *gld*-Rag1$^{-/-}$ mice was not associated with a difference in the size of the ProE/ EryA pools at the early (24 hour) time point. Such a difference may have occurred earlier; alternatively, hypoxia may accelerate the maturation of EryA cells, so that reserve, Fas^{+} EryA cells in control mice do not contribute to an increase in the EryA pool but instead differentiate rapidly and contribute to the increase that we see in the EryC pool by 24 hours (Figure 3.8D). Indeed, it has been observed previously that hypoxic stress as a result of bleeding or phenylhydrazine stress accelerates erythroblast maturation [152-154]. The larger number of EryA in *gld*-Rag1$^{-/-}$ by 72 hours presumably reflects the higher Epo level at that time, in turn a result of the more prolonged stress these mice presumably experience, due to their sluggish

erythropoietic response to the initial hypoxic stimulus.

DISCUSSION

We investigated the role of Fas and FasL-mediated negative autoregulation in the early erythroblast pool. We generated *gld*-Rag1$^{-/-}$ and *lpr*-Rag1$^{-/-}$ mouse strains, deficient in FasL and Fas, respectively, bred onto two distinct genetic backgrounds. Both these strains showed similar erythropoietic deficits. They confirm the hypothesis that Fas and FasL are negative regulators of splenic EryA and ProE, resulting in negative regulation of erythropoiesis at the whole animal level. In addition, they show a striking, non-redundant role for Fas in stabilizing basal erythropoiesis. Surprisingly, in spite of the removal of a negative regulator and the consequent larger basal precursor pool, the response of the mutant mice to erythropoietic stress was significantly delayed. These findings reveal that an autoregulatory loop local to erythropoietic tissue can exert key dynamic properties on erythropoiesis as a whole. They also provide experimental evidence that regulation of erythroid precursors through apoptosis, though apparently wasteful, accelerates the response to erythropoietic stress.

The presence of a local negative autoregulatory loop in spleen erythropoietic tissue

Several lines of evidence suggest that EryA and ProE negatively regulate their own survival through their Fas and FasL-mediated interactions. First, the pattern of co-expression of both Fas and FasL by EryA and ProE [42,44]; second, the close apposition of cells within the erythroblastic island, making an interaction between Fas[+] and FasL^{+} cells

possible [44]; and last, our finding that a mathematical model in which EryA negatively regulate their own survival via the Fas/FasL interaction, accounts well for the experimental data correlating splenic EryA frequency with their Fas expression, across a wide range of Epo concentrations *in vivo* (Figure 3.2 and Text 3.1).

Fas-mediated negative autoregulation decreases erythropoiesis at the whole-animal level

Both acute and chronic inhibition of Fas suggest that it negatively regulates erythropoiesis at the level of the whole animal. An acute decrease in erythroblast FasL by transient administration of the decoy receptor Fas:Fc resulted in an acute increase in erythropoietic rate, reducing ProE and EryA apoptosis and doubling reticulocyte number by 48-72 hours (Figure 3.10).

Chronic loss of Fas function in the *gld*-Rag1$^{-/-}$ and *lpr*-Rag1$^{-/-}$ mice is likely to elicit compensation through the pO_2/Epo-mediated negative feedback loop, which automatically adjusts Epo levels and erythropoietic rate so as to maintain a near-normal basal hematocrit and tissue pO_2. Although *lpr*-Rag1$^{-/-}$ mice had normal reticulocytes and hematocrit, their plasma Epo was significantly lower, by 35%, than in matched Rag1$^{-/-}$ controls, evidence of compensatory adjustment. By contrast, *gld*-Rag1$^{-/-}$ mice were apparently unable to significantly lower their already low plasma Epo. Consequently, their reticulocyte numbers in peripheral blood, a direct measure of erythropoietic rate, more than doubled, and there was a corresponding significant 2.2% increase in hematocrit. This increase is equivalent to a third of the increase in hematocrit we

observed in mice housed in 12% oxygen, equivalent to hypoxia at 14,000 feet.

While many pathways have been implicated in the regulation of erythropoietic rate, a specific contribution to the stress response *in vivo* had been determined for very few. Of note, mice lacking ERK1, a recently described negative regulator of splenic erythropoiesis, showed a similar increase in hematocrit to that seen here for the *gld*-Rag1$^{-/-}$ mice, without a significant change in plasma Epo [155]. Taken together, both the *lpr*-Rag1$^{-/-}$ and *gld*-Rag1$^{-/-}$ strains show increased erythropoietic rate per unit plasma Epo when compared with matched controls, confirming that local negative regulation at the level of splenic erythropoietic tissue has a negative effect at the level of the whole animal.

There is no indication that Fas and FasL interact with alternative receptors or ligands. Therefore, the difference in the response of the *gld*-Rag1$^{-/-}$ and *lpr*-Rag1$^{-/-}$ mice at the level of the hematocrit and serum Epo is likely attributable to their different genetic backgrounds. The response of both these mouse strains at the level of the ProE and EryA precursors, the direct sites of action of Fas and FasL, was very similar.

Loss of Fas function results in a specific increase of spleen ProE and EryA pools

We found a significant 1.5- to 4-fold increase in the number of splenic, but not bone marrow, ProE and EryA in both the *gld*-Rag1$^{-/-}$ and *lpr*-Rag1$^{-/-}$ mice, consistent with the pattern of erythroid Fas and FasL expression [42]. We also identified an increase in CFU-e specific to spleen, suggesting that these cells are regulated by Fas, in agreement with their counterpart in fetal liver [44]. Bone marrow progenitor subsets were either normal or even decreased in number, possibly as a compensatory response to their

increase in spleen (Figure 3.4C,D).

The increase in spleen ProE, EryA and CFU-e is due to the absence of a spleen-specific negative regulator, rather than erythropoietic stress, since it is not associated with elevated serum Epo, and since there is no associated increase of bone marrow progenitors. It is unlikely that the increase in ProE/EryA is a consequence of expansion in an earlier, Fas-regulated progenitor compartment, since there was no significant change in bone marrow erythroid progenitors, platelets or white cells (Table 3.1). An earlier report of increased CFU-S in adult *lpr* and *gld* mice [156] is complicated by the autoimmune syndrome in these mice, which in the present work we addressed by breeding the *lpr* and *gld* mutant mice onto the immune-deficient Rag1^{-/-} background.

The expansion in ProE and EryA precursor pools in the *gld*-Rag1^{-/-} and *lpr*-Rag1^{-/-} mice represents a substantial non-redundant negative regulatory function of Fas. Nevertheless, it is likely to be an underestimate of the actual number of ProE/EryA that are regulated by Fas in wild-type mice, as suggested by the response to stress (see below). Compensatory mechanisms that could ameliorate the absence of Fas or FasL include upregulation of alternative negative regulators such as ERK1 [155], attenuation of alternative EpoR anti-apoptotic pathways such as Stat5-induced Bcl-x$_L$, phosphoinositol-3 kinase/AKT and suppression of Bim and Foxo3a [23,90,134], or a decrease in factors that stimulate erythropoiesis such as BMP4 [53].

A stabilizing function for the Fas and FasL-mediated negative autoregulatory loop

Random variation in the number of progenitors is an inevitable consequence of

inherent fluctuations in biological systems [157-159], found in mice that are genetically identical, of similar age and housed in similar stable conditions. The pO_2/Epo-mediated negative feedback loop (Figure 3.1A) adjusts overall mean erythropoietic rate in the face of such fluctuations over time, but the intrinsic delay in this loop may result in oscillations and limit the system's stability. Here we found that in the absence of Fas or FasL, there was a significant increase in variability, reflected by both increased variance and increased coefficient of variation, of splenic ProE, EryA and EryB in individual mice, compared with control mice (Figures 3.4B and 3.5A). Bone marrow erythroid subsets were not affected, but there was increased variability of overall erythropoietic rate, as reflected by the reticulocyte counts. Therefore, Fas-mediated autoregulation in spleen has a stabilizing effect on erythropoiesis at the whole animal level, offsetting the limitations of the pO_2/Epo-mediated negative feedback loop.

The stabilizing influence of the Fas/FasL interaction is a result of its sensitivity to the size of the erythroblast pool. For comparison, a recently identified cell-autonomous negative regulator of splenic erythropoiesis *in vivo*, ERK1, does not appear to contribute to the stability of erythropoiesis [155]. Fas-mediated apoptosis of ProE or EryA depends on the probability that two cells expressing Fas and FasL respectively, encounter each other within the erythropoietic niche. This probability is dependent on their frequency in tissue (Figure 3.2 and Text 3.1*)*. Should their frequency be in excess, Fas-mediated loss of EryA would accelerate, providing an automatic correction. Conversely, a shortage of EryA would lower the probability of their interaction and death, allowing their number to increase. Both negative and positive corrections take place locally in erythropoietic

tissue, with little delay and without the need to engage the pO$_2$/Epo-mediated negative feedback loop, avoiding potentially deleterious corrective swings in systemic tissue pO$_2$.

Fas-mediated negative autoregulation accelerates the stress response

Unexpectedly for mice lacking a negative erythropoietic regulator, the response of *gld*-Rag1$^{-/-}$ and *lpr*-Rag1$^{-/-}$ mice to acute Epo administration was delayed. The splenic EryA pool expanded 30-fold its basal size in control mice by day 2; this massive increase was reduced by 30% in the *gld*-Rag1$^{-/-}$ and *lpr*-Rag1$^{-/-}$ mice, reflecting a significant shortfall, equivalent to 10 times the size of the basal EryA pool. This shortfall occurred in spite of a larger than normal basal EryA pool in the mutant mice. We found a similar delay in the expansion of ProE cells in the *gld*-Rag1$^{-/-}$ and *lpr*-Rag1$^{-/-}$ mice.

To explain this phenomenon, we propose the model illustrated in Figure 3.9. EryA are continuously formed from earlier progenitors (=EryA input) but the majority dies, with only a small fraction remaining as the basal EryA pool. However, the apoptosis-prone EryA form a reserve population that may be rapidly recruited by high Epo during stress. We propose that the rapid, 30-fold expansion in EryA within 2 days of Epo administration corresponds to the size of the reserve EryA population. The smaller initial expansion in the *gld*-Rag1$^{-/-}$ and *lpr*-Rag1$^{-/-}$ mice suggests that part of the EryA reserve is regulated through Fas, and is missing in these mutant mice.

These observations suggest that the high apoptotic rates of ProE and EryA in the basal state, in part due to Fas, provide a mechanism that accelerates the stress response. The rescue of ProE/EryA from apoptosis allows a faster increase in their number

compared with their generation by cell division from earlier progenitors. This faster increase accelerates erythropoietic rate and prevents a prolonged tissue hypoxia. We found that the response of the erythropoietic system to reduced atmospheric oxygen was similarly delayed in *gld*-Rag1^{-/-} mice, as reflected by lower reticulocyte counts and a slower increase in hematocrit. In this more complex, hypoxic stimulus to the system, we noted that the principal difference in the erythroblast pools between *gld*-Rag1^{-/-} and control mice appeared at the EryC stage, rather than in the earlier, ProE and EryA stages. We suggest that this may be due to accelerated maturation of erythroblasts, noted in the older literature in response to hypoxic stress [152-154].

Of note, in ERK1^{-/-} mice, the stress response is timely and somewhat amplified [155]. Unlike Fas-mediated autoregulation, which is exerted at the level of erythroblasts, ERK1 appears to suppress a much earlier, BMP-dependent BFU-e progenitor, which is therefore unlikely to contribute to the initial, acute phase of stress.

The negative autoregulatory motif

Negative autoregulation is a frequent motif in biological networks. Computational and experimental approaches in simple transcriptional networks in E.Coli suggested that it has two principal effects: conferring resistance to random fluctuations, and accelerating the response to a stimulus [141-144,160,161]. To our knowledge, the functional role of negative autoregulation within higher-level intercellular networks had not been tested experimentally. Our work suggests that the negative regulatory motif may exert similar 'logic' in higher-level networks, helping to maintain both stability and a fast stress

response of tissue progenitors.

Acknowledgements
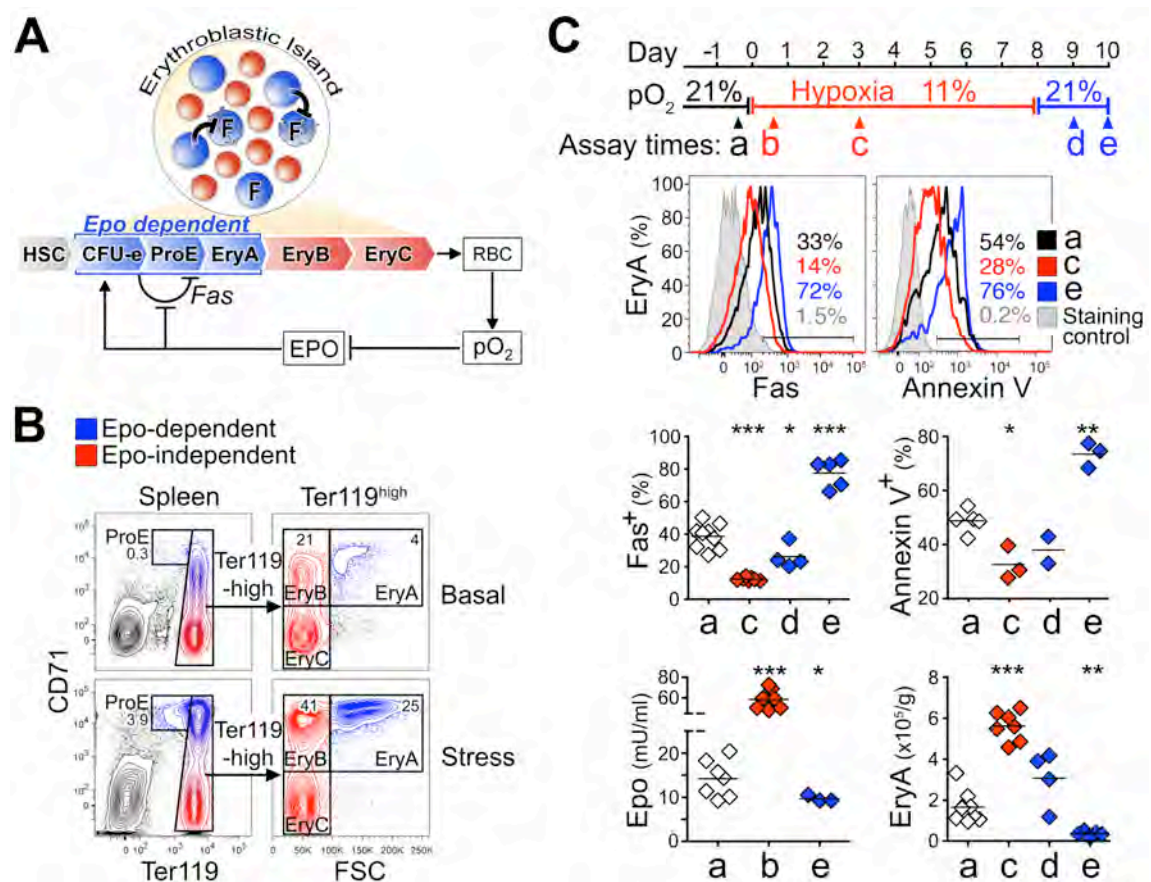
Figure 3.1

Figure 3.1   Epo regulation of erythropoiesis through Fas-mediated apoptosis.

(A)   Epo-dependent erythroblastic island precursors CFU-e, ProE and EryA (in blue) co-express Fas and FasL, and mature into Epo-independent EryB, EryC and red blood cells (RBC, in red). 'F' =Fas expressing cells, shown undergoing cell death as a result of interaction with FasL-expressing cells within the Epo-dependent (blue) compartment (black flat-headed arrow). A negative feedback loop driven by tissue pO_2 regulates Epo levels in blood, which in turn enhance erythroblast survival, by either suppressing Fas and FasL expression, or by non-Fas dependent pathways. HSC =hematopoietic stem cells.

(B)   Flow-cytometric identification of Epo-dependent ProE and EryA subsets (in blue) and Epo-independent EryB and EryC (in red), in adult Balb/C mouse spleen, in basal conditions (top panels) or 48 hours following Epo injection (300 U /mouse, lower panels). ProE are defined as $Ter119^{med}CD71^{high}$ cells; $Ter119^{high}$ cells are further subdivided based on forward scatter (FSC) and CD71 expression into EryA ($CD71^{high}Ter119^{high}FSC^{high}$), EryB ($CD71^{high}Ter119^{high}FSC^{low}$) and EryC ($CD71^{low}Ter119^{high}FSC^{low}$).

(C)   The erythropoietic response of mice to a hypoxic environment. Mice (Balb/C) were examined either in the basal state ('a', 21% atmospheric oxygen), when housed in 11% oxygen for 8 days (assay times 'b' and 'c' at 13 hours and 3 days, respectively), and when placed back in normoxia (21%; assay times 'd' and 'e', at 1 and 2 days post-hypoxia). Top panels show representative flow-cytometric histograms of Fas expression and Annexin V binding at the indicated assay times. Gates refer to the Fas^+ and Annexin

V$^+$ populations, determined with reference to staining controls in which either the anti-Fas antibody (left panel) or Annexin V (right panel) were omitted. The fraction of cells positive for Fas or Annexin V at each time point is noted. Middle panel shows a summary of similar data, 2 to 9 mice per time point. Lower panels show corresponding serum Epo levels and EryA cell number in spleen (expressed as total EryA cells /gram body weight). *p<0.05, **p<0.002, ***p<0.0001 (two-tailed t-test, unequal variance).

Figure 3.2
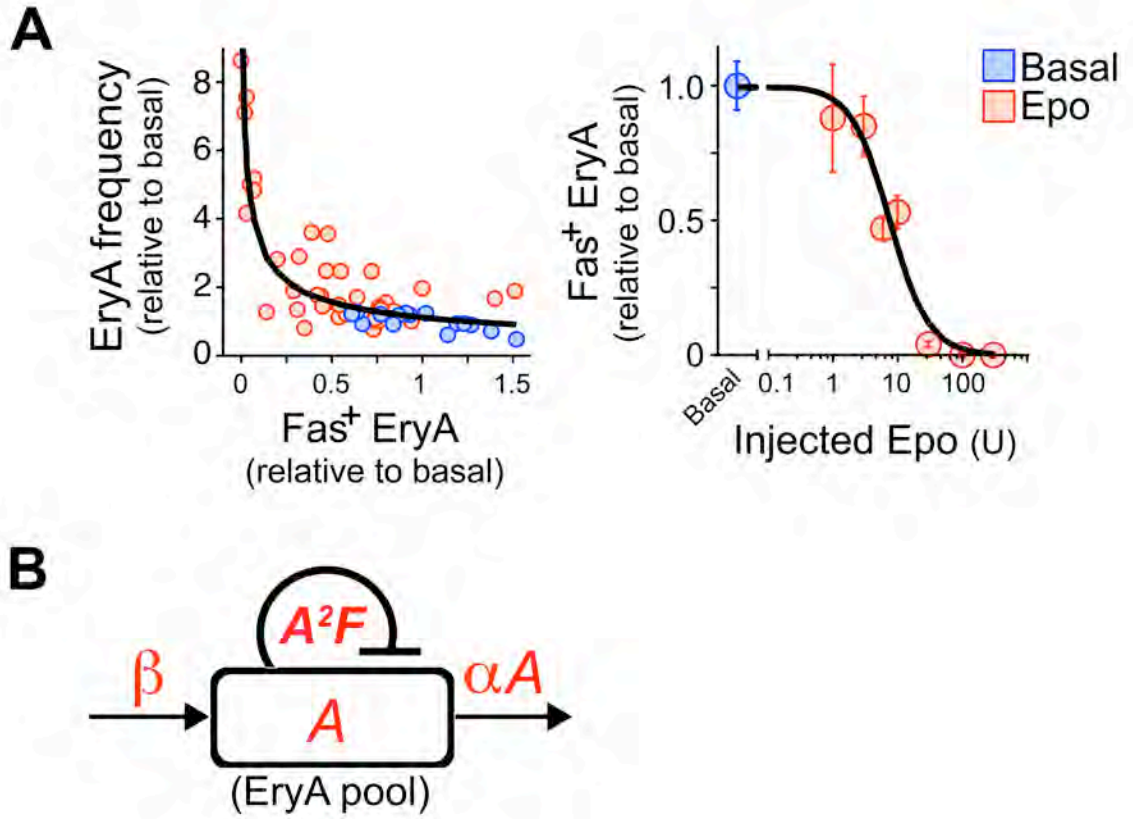
Figure 3.2   Fas and FasL-mediated negative autoregulation of the EryA pool.

(A)   Wild-type Balb/C mice were injected with a single Epo injection subcutaneously, of 1, 3, 6, 10, 30, 100 or 300 U /25 g body weight. Spleen EryA were examined on day 3 post injection. *Left panel* shows EryA cell frequency (of total erythroid cells) relative to basal frequency, plotted against the number of EryA cells that express Fas (Fas$^+$ EryA, expressed as a ratio to basal levels). Data points represent individual mice. Blue =mice in the basal state (n=15), red =mice injected with Epo (n=38). For clarity only mice injected with 30 U (which maximally suppress Fas) or less are included in the left panel (for 30 U, 6 highest data points lie at the maximal Fas suppression and maximal EryA frequency). Data are fitted with a curve derived from the mathematical model described in panel (B) and in the Text 3.1. *Right panel* shows the dependence of Fas$^+$ EryA on the dose of injected Epo, in the same dataset as in the left panel; all mice injected with a given Epo dose were pooled into one data point, mean ±SEM.

(B)   Schematic of the factors that regulate the size of the EryA pool, '*A*', measured as the fraction of all Ter119$^+$ cells that are EryA. *F* =fraction of EryA cells that express Fas. ß =input into the EryA pool from earlier progenitor stages. α*A* =output from the EryA pool into later erythroid subsets (EryB). A^2F =Fas-mediated cell loss. See mathematical model described in Text 3.1. In panel (A) of this figure, *A* is plotted against *F*, expressed as a ratio to the *A* and *F* values in the basal state, respectively.

Figure 3.3
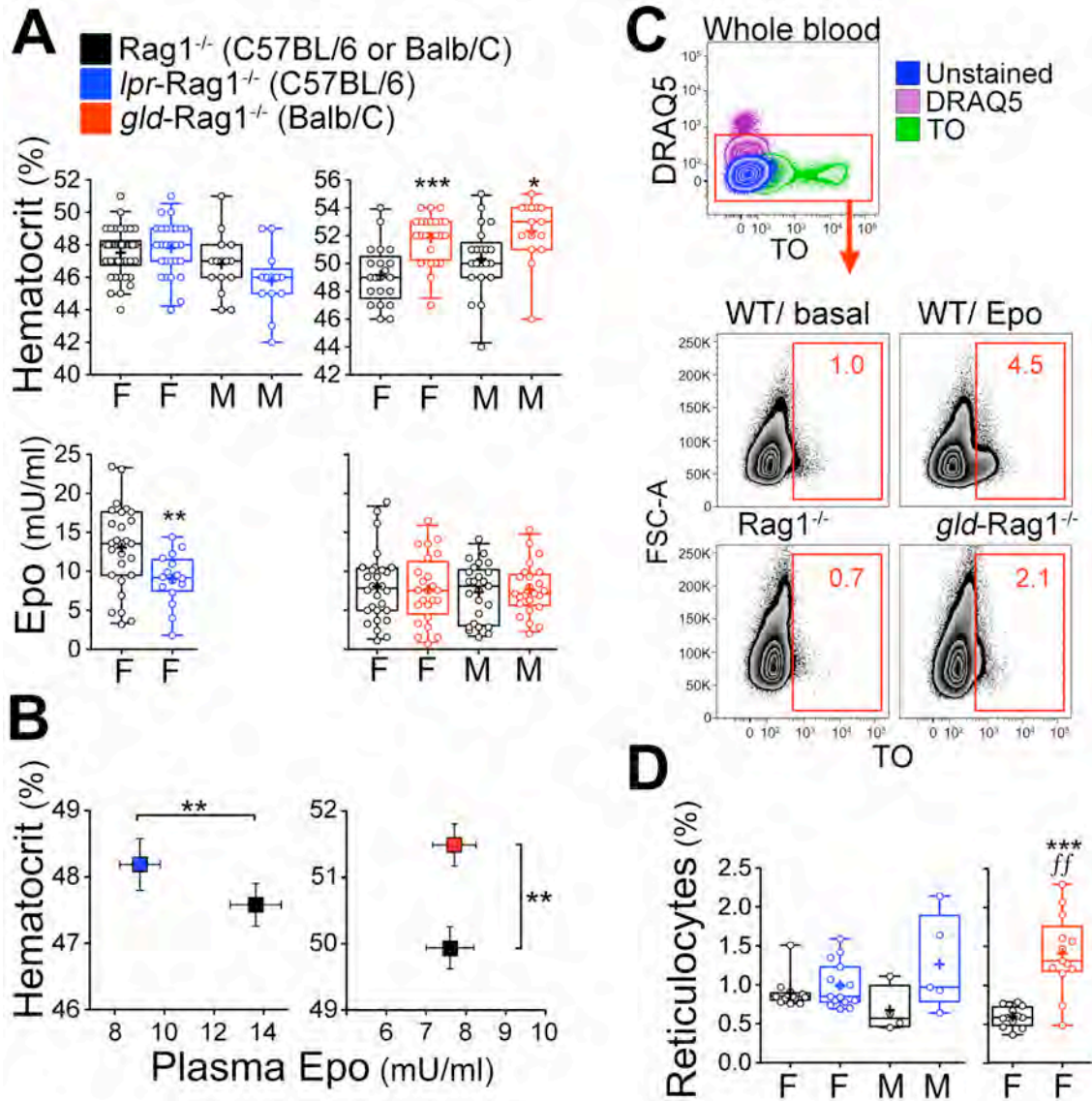
Figure 3.3   Increased erythropoiesis in mice deficient in the Fas pathway.

Legend in (A) also applies to panels (B) and (D). *lpr*-Rag1$^{-/-}$ mice are on the C57BL/6 background (in blue), and are compared with control Rag1$^{-/-}$ mice on the C57BL/6 background. *gld*-Rag1$^{-/-}$ mice are on the Balb/C background (in red), and are compared with control Rag1$^{-/-}$ mice on the Balb/C background.

(A)   Hematocrit (=fraction of the blood volume that is due to red cells) and Plasma Epo of *lpr*-Rag1$^{-/-}$, *gld*-Rag1$^{-/-}$ and Rag1$^{-/-}$ age- and strain-matched control mice. M= males. F= females. Box and whiskers delineate the central 50% and 90% of readings, respectively. Median is indicated with a horizontal line; arithmetic mean with a '+'. Data points correspond to individual mice. Between 11 and 40 mice examined per genotype. *p<0.05, **p<0.005, ***p<0005 (ANOVA).

(B)   Hematocrit *vs.* plasma Epo in the subset of mice where both values were measured, in the basal state, for *lpr*-Rag1$^{-/-}$ and matched Rag1$^{-/-}$ control mice (left panel), and for *gld*-Rag1$^{-/-}$ and matched Rag1$^{-/-}$ controls (right panel). Data are mean ±SEM of ≥16 mice. *p≤0.001 (two-tailed t-test, unequal variance).

(C)   Flow-cytometric measurement of reticulocyte number. Top: whole blood stained with either DRAQ5 (detects DNA) or Thiazole Orange (TO, detects both DNA and RNA). Reticulocytes lack a nucleus but retain RNA. They therefore form a DRAQ5-negative, TO-positive population. Bottom panel shows analysis in wild-type (WT) mice either in the basal state or following Epo injection; and in *gld*-Rag1$^{-/-}$ and control Rag1$^{-/-}$ mice.

(D)   Reticulocytes in *lpr*-Rag1$^{-/-}$, *gld*-Rag1$^{-/-}$ and matched Rag1$^{-/-}$ controls, measured

by flow cytometry. ***p<0.0001, two-tailed t-test, unequal variance; *ff*= p<0.001, F test.

Figure 3.4
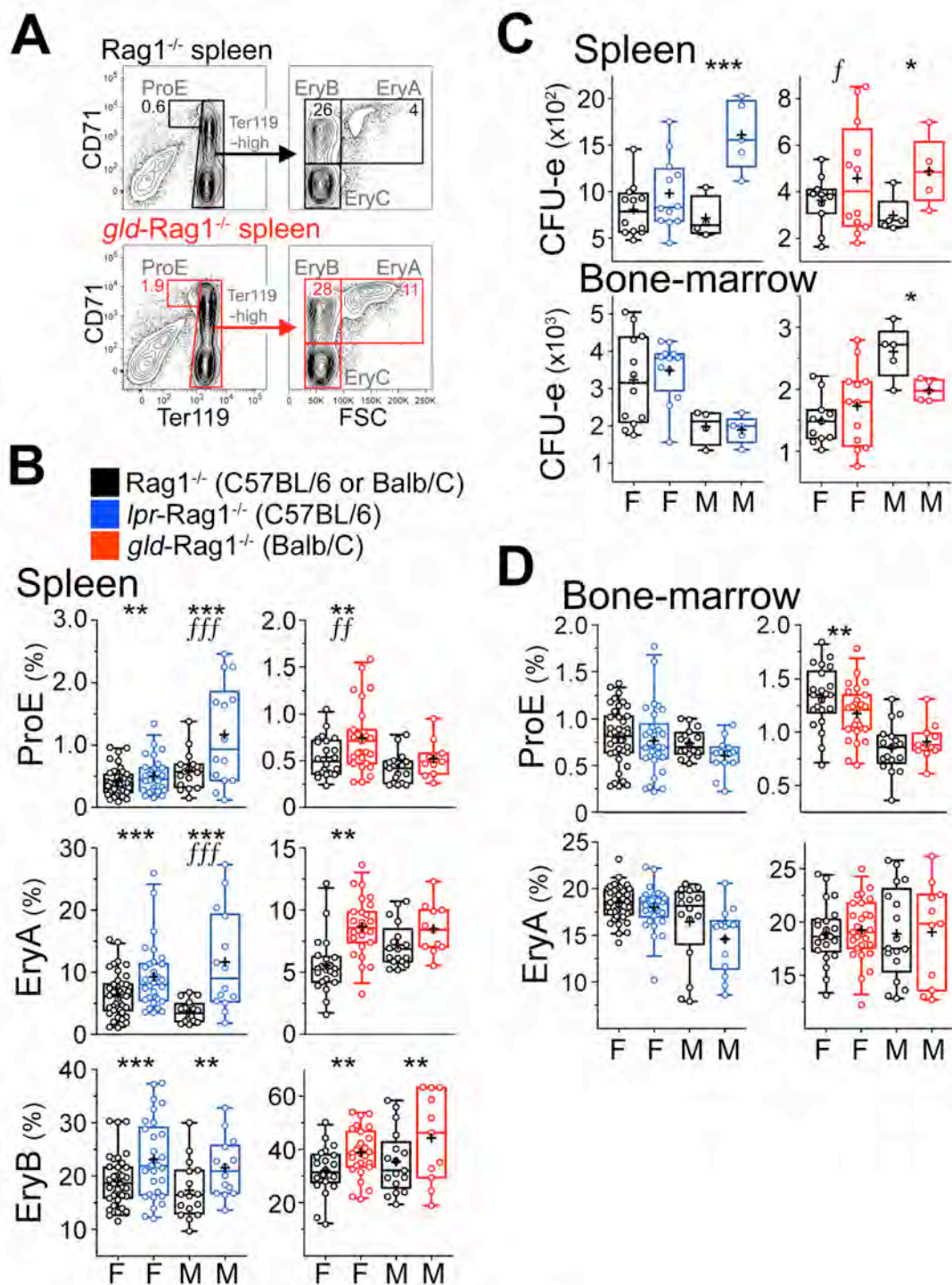
Figure 3.4   Increased frequency of spleen, but not bone-marrow, erythroid progenitors and precursors in mice deficient in the Fas pathway.

The Legend in panel (B) also applies to (C) and (D).

(A)   Representative flow-cytometric analysis of spleen erythroid subsets in *gld*-Rag1$^{-/-}$ and matched Rag1$^{-/-}$ controls, showing increased frequency of ProE and EryA within Ter119^{+} cells.

(B)   Frequency of erythroblast subsets in spleen erythropoietic tissue, measured as in (A), expressed as fraction of all spleen Ter119^{+} cells. F=female M=male. Box and whiskers delineate the central 50% and 95% of readings, respectively, with the median indicated with a horizontal line and arithmetic mean with a '+'. Data points are individual mice (11-40 mice per sex/genotype combination). Data were pooled from several independent experiments.

(C)   CFU-e progenitors in spleen and bone marrow (per 1x10^{6} plated cells). Data pooled from two independent experiments for females, and one experiment for males, for each genotype.

(D)   Frequency of erythroblast subsets in bone marrow expressed as fraction of all spleen Ter119^{+} cells.

For all panels, *p<0.05 **p<0.02, ***p<0.002 (ANOVA, for difference in means). *f*= p <0.05 ,*ff*= p<0.02, *fff*= p<0.002 (F test, for difference in variance).

Figure 3.5
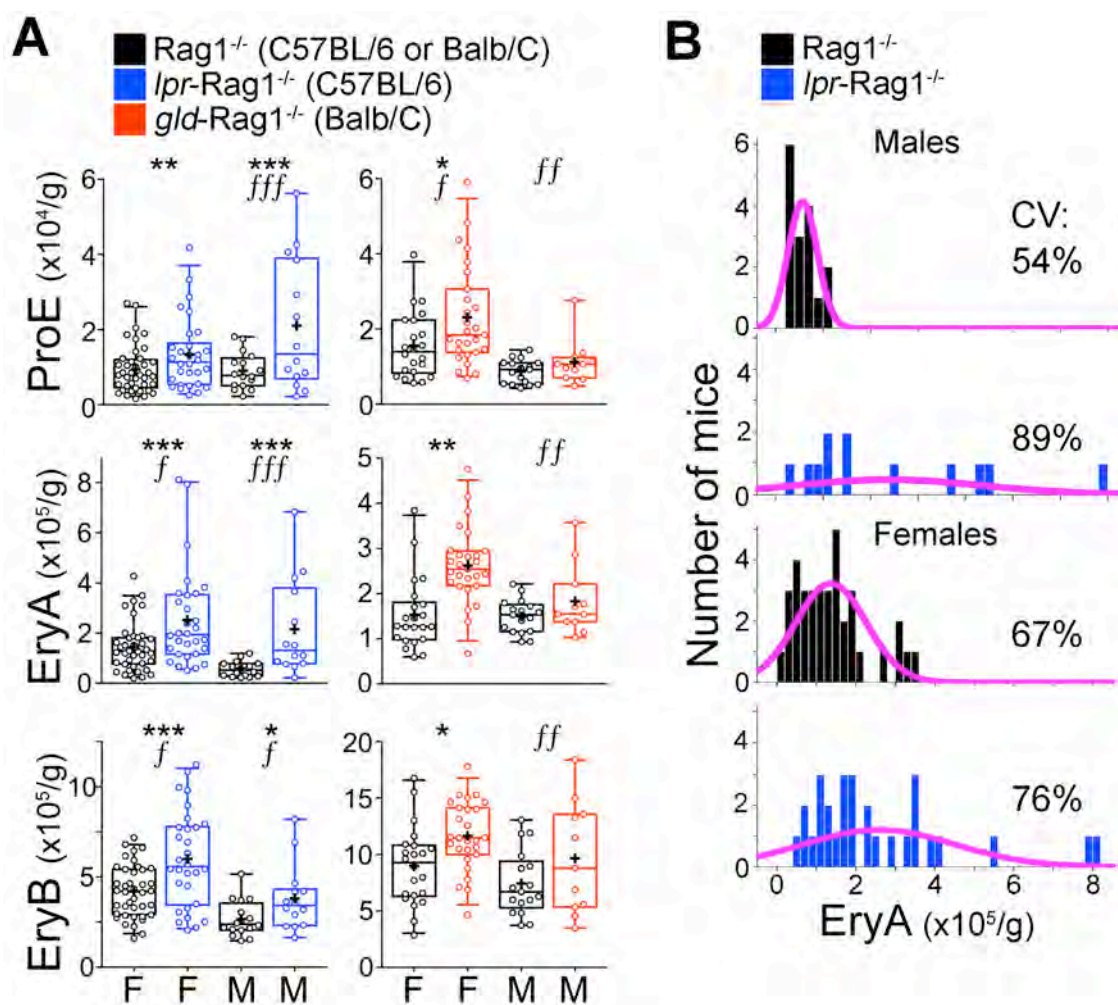
Figure 3.5   Loss of Fas function results in a larger and more variable basal spleen erythroid progenitor pool.

(A)   Spleen erythroid subsets ProE, EryA or EryB, expressed as absolute number of cells per gram body weight, in *gld*-Rag1$^{-/-}$, *lpr*-Rag1$^{-/-}$ and matched Rag1$^{-/-}$ controls, shown separately for male (M) and female (F) mice. Data correspond to the same mouse dataset as in Figure 3.4. Box and whiskers delineate the central 50% and 90% of readings, respectively, with the median indicated with a horizontal line and arithmetic mean with a '+'. Data points correspond to individual mice. Between 11 and 40 mice were examined per genotype; data pooled from several independent experiments. *p<0.05, **p<0.005, ***p<0.0005 (ANOVA, for difference in means); *f* =p<0.05, *ff* =p<0.005, *fff* =p<0.0005 (F test, for difference in variance).

(B)   Frequency distribution histograms for EryA, in male and female *lpr*-Rag1$^{-/-}$ and matched Rag1$^{-/-}$ controls. The coefficient of variation for each group is shown. Purple line is the fitted normal distribution curve. Same dataset as in panel (A).

Figure 3.6
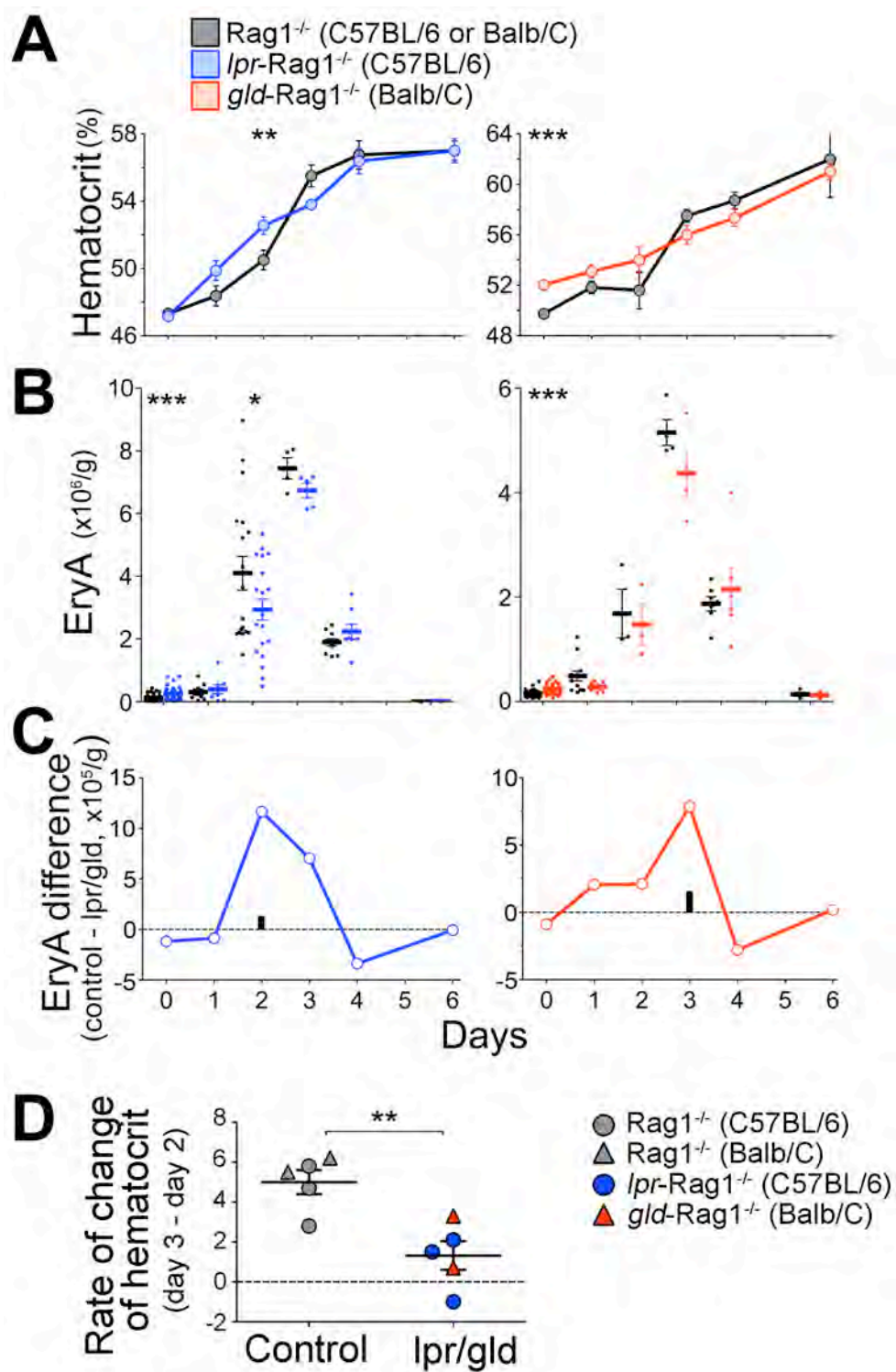
Figure 3.6 **Delayed response to Epo-induced stress in mice deficient in the Fas pathway.**

(A-D) *gld*-Rag1$^{-/-}$, *lpr*-Rag1$^{-/-}$ and matched Rag1$^{-/-}$ control mice were injected with Epo (300 U /25 g body weight) subcutaneously at t=0. The erythropoietic response was followed for 6 days. Data are mean ±SEM for 3 to 18 mice per time point per genotype, pooled from up to 3 experiments per time point. Data at t=0 are the basal state data shown in Figures 3.3A and 3.5A, pooled for males and females.

(A)   Hematocrit measurements.

(B)   Spleen EryA (cells per gram body weight) in the same mouse set as in the top panel. Data points are individual mice, with the mean ±SEM for each day marked as a horizontal line.

(C)   The difference in mean EryA number (shown in panel B) between the mutant *gld*-Rag1$^{-/-}$ or *lpr*-Rag1$^{-/-}$ and their matched Rag1$^{-/-}$ controls, for each day. The size of the corresponding control (Rag1$^{-/-}$) EryA pool is marked with a black bar.

(D)   The rate of change in hematocrit between days 2 and 3 following Epo injection. The same dataset as in panel (A), showing the differences in hematocrit measured in multiple independent experiments on days 2 and 3. Altogether 5 independent comparisons are shown.

For all panels, *p<0.05, **p<0.005, ***p<0.0005 (t-test, unequal variance).

Figure 3.7
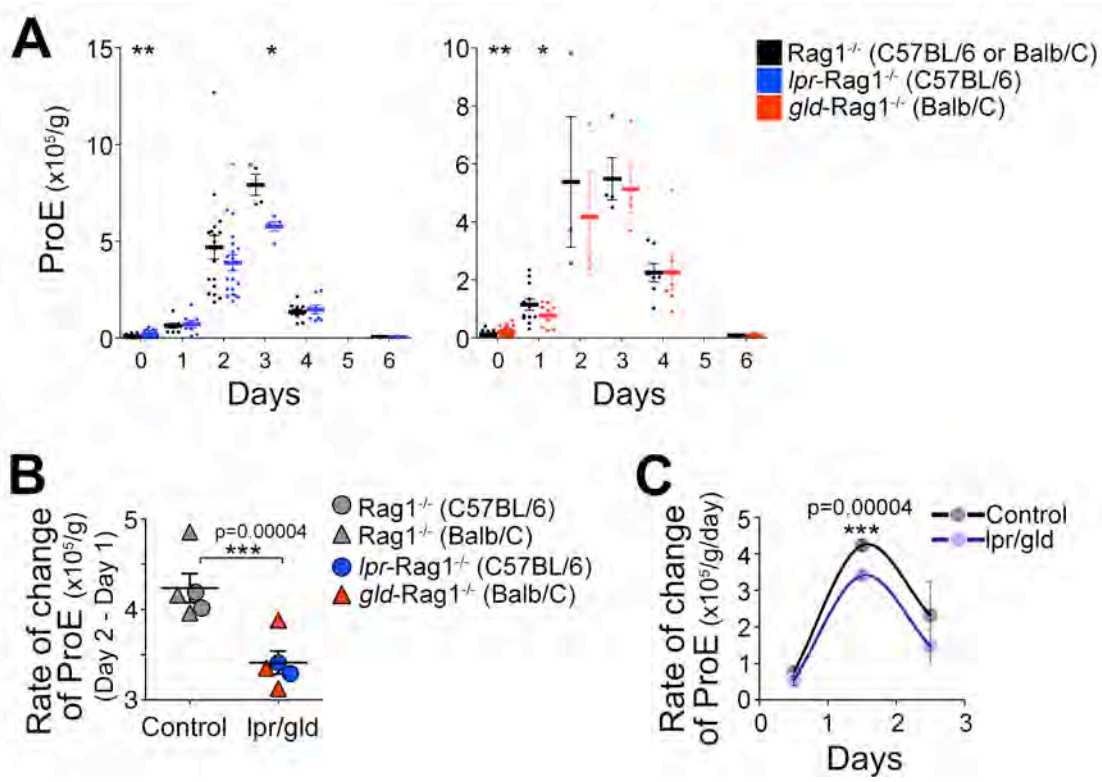
Figure 3.7   Delayed response to Epo-induced stress in mice deficient in the Fas pathway.

(A-C) Analysis of the ProE response to Epo injection. The same experiment and dataset as in Figure 3.6.

(A)   Spleen ProE (cells per gram body weight). Data points are individual mice, with the mean ±SEM for each day marked as a horizontal line. Data pooled from 1 to 3 experiments with 3 to 18 mice per genotype.

(B)   The rate of change in spleen ProE between days 1 and 2 post-Epo injection in the mutant *gld*-Rag1$^{-/-}$ (indicated in red) or *lpr*-Rag1$^{-/-}$ (blue) and their matched Rag1$^{-/-}$ controls. Dataset as in panel (A). Each point represents the mean difference in ProE between independent experiments done on days 2 and 3, in 5 independent comparisons.

(C)   The rate of change in spleen ProE throughout the first 3 days of response to Epo, computed as in panel B. The rate of change between days 0 and 1, days 1 and 2, and days 2 and 3, were plotted on days 0.5, 1.5 and 2.5, respectively. Data points represent pooled mutant (*lpr/gld*) or control differences (mean ±SEM).

For all panels, $*p<0.05$, $**p<0.005$, $***p<0.0005$ (t-test, unequal variance).

Figure 3.8
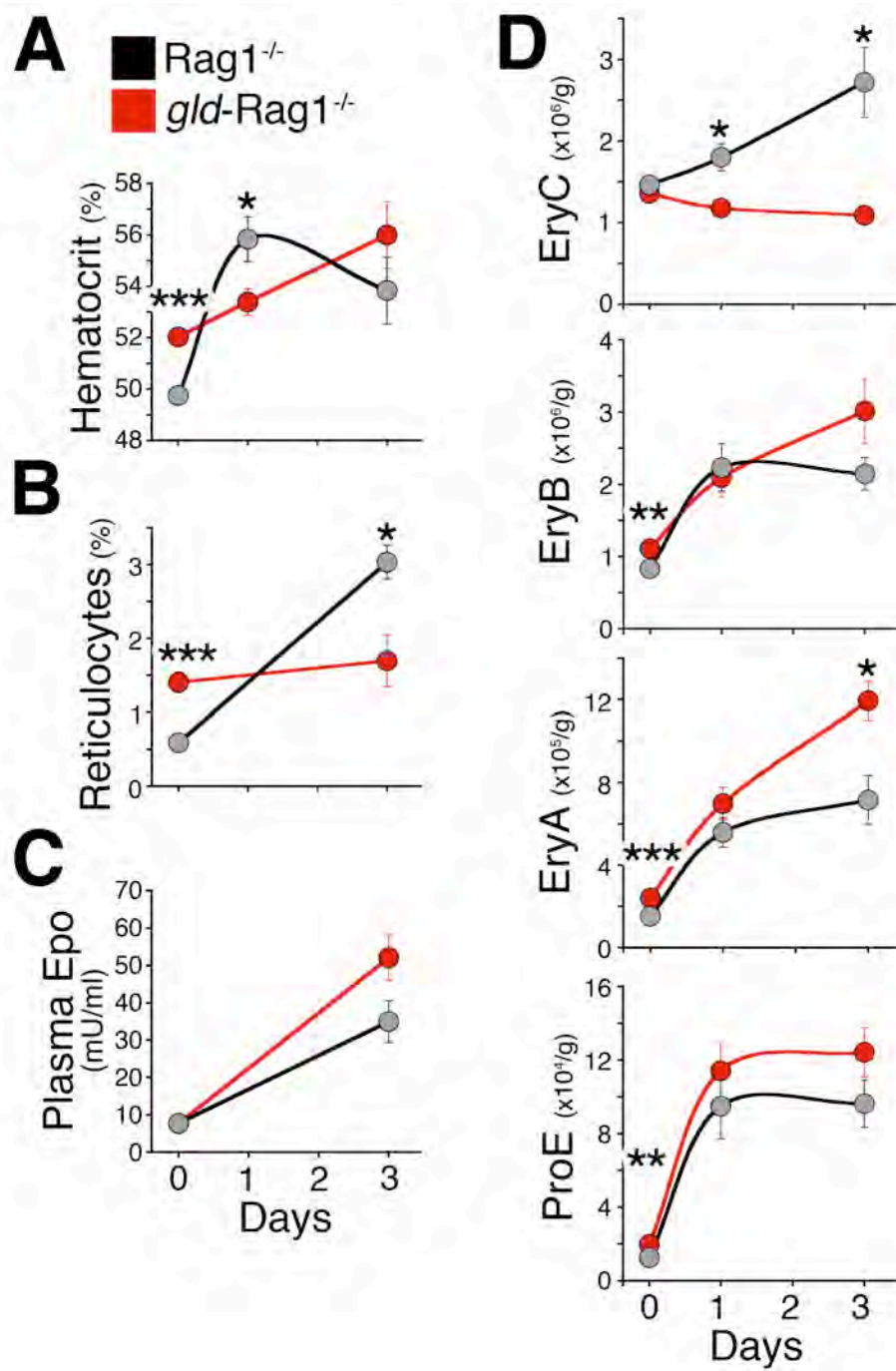
Figure 3.8   Delayed response to hypoxia-induced stress in mice deficient in the Fas pathway.

(A-D) *gld*-Rag1$^{-/-}$ or control mice were transferred to a hypoxia chamber with ambient 11% oxygen for 1 or 3 days. Data are mean ±SEM for 4 to 9 age- and gender-matched mice per time point per genotype. Data at t=0 are the basal state data shown in Figures 3.3A and 3.5A, pooled for males and females.

(A)   Hematocrit measurements, performed via CritSpin microcentrifugation.

(B)   Reticulocyte measurements, performed flow-cytometrically, as in Figure 3.3C.

(C)   Plasma Epo, measured by ELISA.

(D)   Spleen erythroid subsets ProE, EryA, EryB and EryC, expressed as absolute number of cells per gram body weight in *gld*-Rag1$^{-/-}$ and matched Rag1$^{-/-}$ controls.

For all panels, *p<0.05, **p<0.005, ***p<0.0005 (t-test, unequal variance).

Figure 3.9
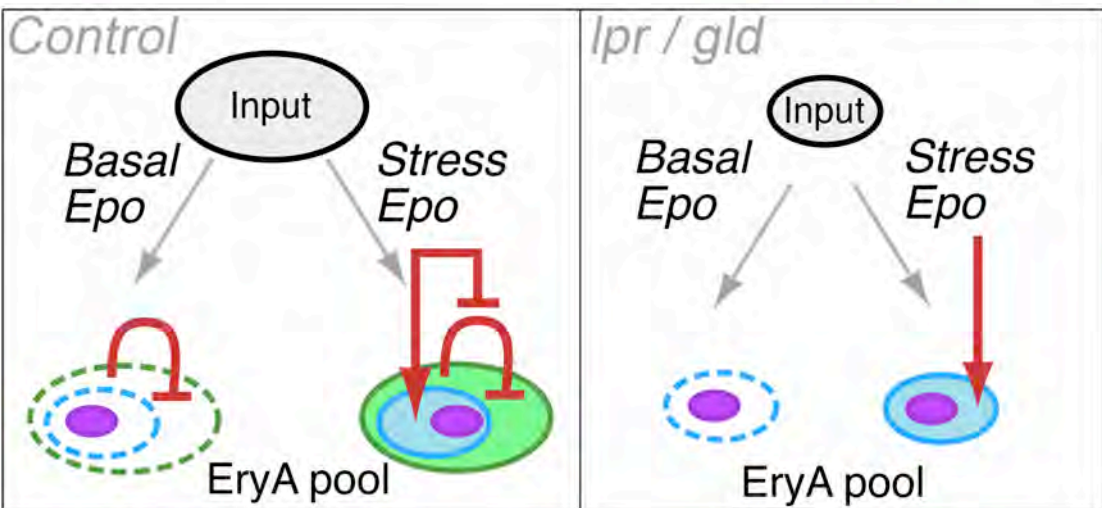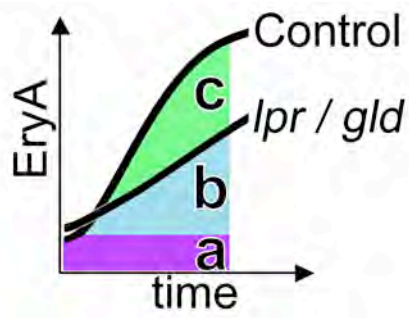
Figure 3.9   **Absence of a Fas-regulated EryA reserve delays the response to stress.**

EryA cells are continuously formed from earlier precursors ('input'). In the basal state, when Epo concentrations are low, only a small fraction of these cells survive, forming the 'basal EryA pool' (in purple). The remaining EryA undergo apoptosis, either through Fas ('Fas-regulated reserve', green) or alternative mechanisms ('Alternative reserve', blue). Together, the EryA reserve pools are 30- to 60-fold the size of the basal pool (see Figure 3.6). During the initial response to stress, high Epo levels rescue the EryA reserve pools from apoptosis, resulting in an immediate increase in the size of the surviving EryA pool and an increase in erythropoietic rate (solid colors indicate surviving cells, dashed lines indicate cells that underwent apoptosis).

We suggest that *lpr* and *gld* mice partially compensate for the absence of the Fas-regulated reserve by generating fewer EryA cells (a smaller input). In this way, the absence of Fas-mediated apoptosis does not excessively increase the basal EryA pool (which does increase 1.5- to 4-fold, see Figure 3.5; this increase is much smaller than the stress-induced increase and is not shown). During stress, the absence of the Fas-regulated reserve in *lpr* and *gld* mice reduces the number of EryA that may be immediately recruited into the surviving EryA pool and consequently delays the stress response.

Figure 3.10
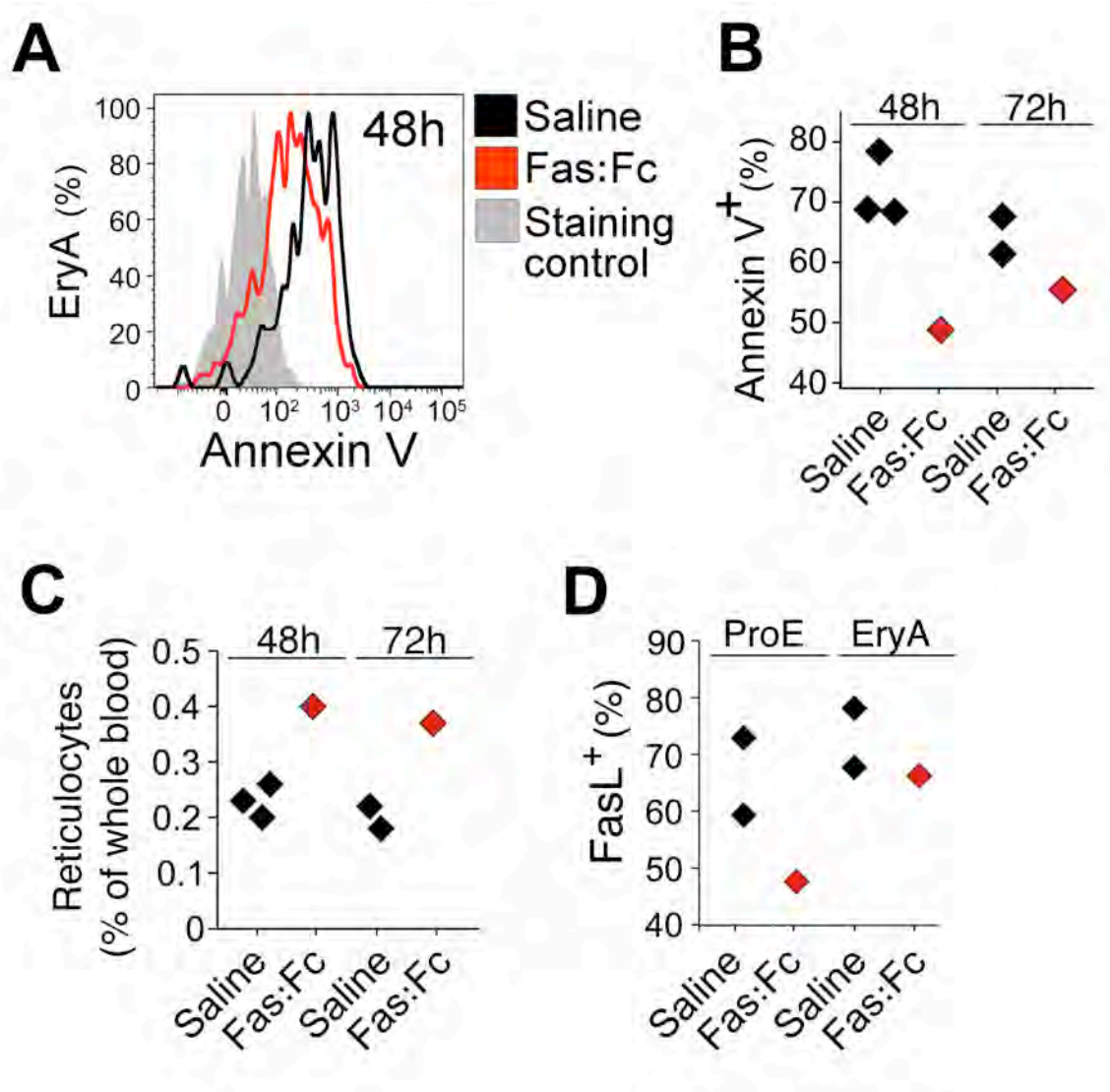
Figure 3.10, associated with Figure 3.1. Inhibition of Fas with Fas:Fc decreases EryA death and increases erythropoietic rate.

MyD88$^{-/-}$ mice (C57BL/6 background) were each injected intraperitoneally with 100 µg of human purified Fas:Fc chimeric protein (BD Biosciences), or with an equal volume of saline (200 µl).

(A)   Flow-cytometric histogram of Annexin V binding of spleen EryA cells, showing decreased apoptosis 48 hours following injection of Fas:Fc.

(B)   Summary of Annexin V binding in two independent experiments, at 48 hours and at 72 hours post-injection. Data points correspond to individual mice.

(C)   Summary of reticulocyte count (red blood cells younger than 24 hr, identifiable by their cytoplasmic RNA, which is absent in older red cells) in the same mice/experiments as in panel (B). Fas:Fc caused an increase in reticulocytes, reflecting increased erythropoietic rate.

(D)   Summary of FasL-positive frequency in spleen ProE and EryA 24 hours post-Fas:Fc. Fas:Fc treatment blocked immunodetection of FasL on the cell surface.

Figure 3.11
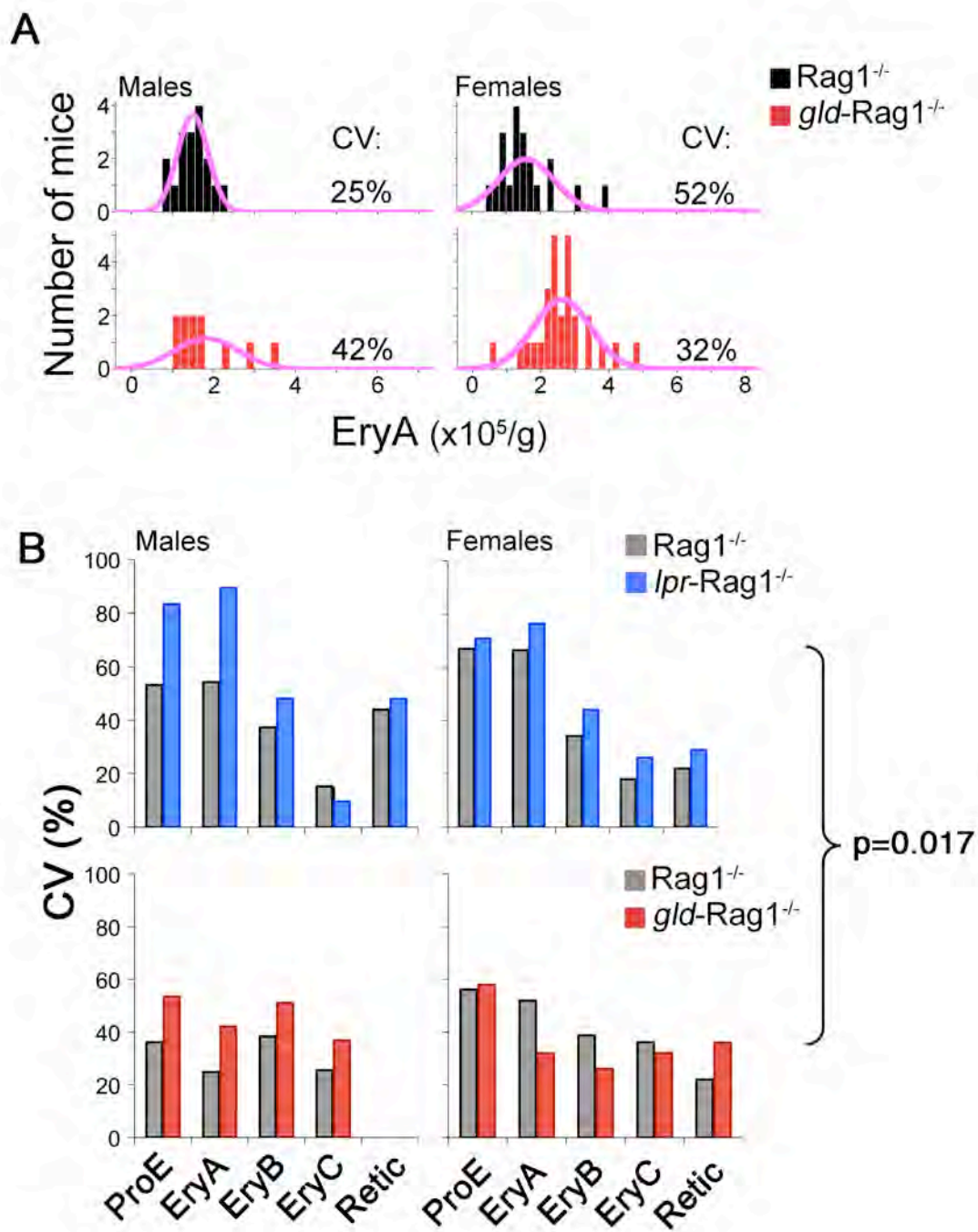
Figure 3.11, associated with Figure 3.5. Increased variance in *lpr/gld* erythroid progenitor subsets.

(A)   Frequency distribution histograms for EryA, in male and female *gld*-Rag1$^{-/-}$ and matched Rag1$^{-/-}$ controls. The coefficient of variation for each group is shown. Purple line is the corresponding normal distribution curve. Same dataset as in Figure 3.5. A similar analysis for the *lpr*-Rag1$^{-/-}$ mice is shown in Figure 3.5B.

(B)   Coefficient of variation (CV) for subsets ProE, EryA-C and reticulocytes in male or female *lpr*-Rag1$^{-/-}$ or and *gld*-Rag1$^{-/-}$ mice and corresponding Rag1$^{-/-}$ controls. The difference in CV between control and *lpr/gld* is significant at p=0.017 (paired t-test, treating the CV as a standard statistical variable).

Figure 3.12
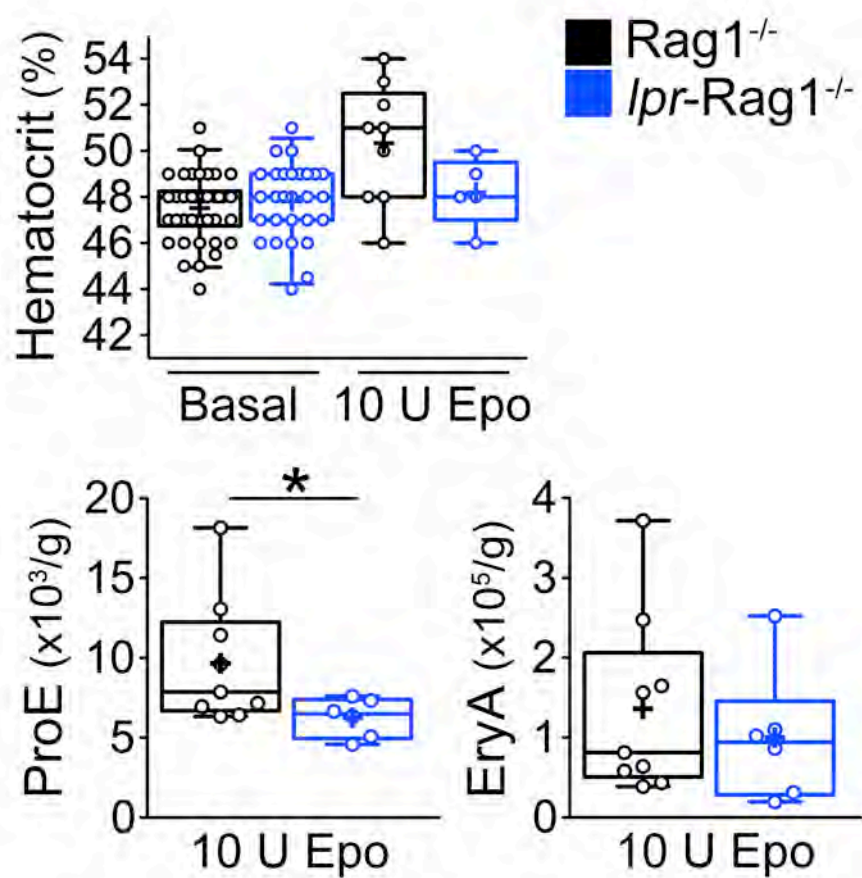
Figure 3.12, associated with Figure 3.6   Delayed response to Epo injection in *lpr*-Rag1$^{-/-}$ mice.

Female mice were injected with 10 U of Epo subcutaneously. Hematocrit, ProE and EryA progenitors were measured on day 3 post injection. *p<0.05 (two-tailed t-test, unequal variance). Basal hematocrit values are for *lpr*-Rag1$^{-/-}$ females.

Table 3.1

Genotype		n	HCT (%)	HGB (g/dL)	RBC (10⁶/ul)	MCV (fL)	WBC (10³/ul)	PLT (10³/ul)
Balb/C Rag1⁻		6	47.8 ± 1.3	13.9 ± 0.4	9.1 ± 0.2	52.5 ± 0.6	3.9 ± 0.6	785 ± 126
	Experiment 1							
Balb/C *gld*-Rag1⁻		7	50.4 ± 0.7	14.9 ± 0.2	9.5 ± 0.1	53.1 ± 0.2	2.5 ± 0.1	831 ± 29
	t test		0.1	0.04*	0.2	0.4	0.06	0.73
Balb/C Rag1⁻		5	48.4 ± 0.3	15.7 ± 0.1	9.9 ± 0.1	48.9 ± 0.7	4.5 ± 0.5	1100 ± 18
	Experiment 2							
Balb/C *gld*-Rag1⁻		5	51.9 ± 0.9	16.5 ± 0.3	10.4 ± 0.1	49.8 ± 0.4	4.5 ± 0.3	1222 ± 63
	t test		0.02*	0.05*	0.04*	0.29	1	0.12
	Experiments 1+2, t test		0.003*	0.07	0.12	0.36	0.11	0.54
C57BL/6 Rag1⁻		5	40.4 ± 0.8	13.4 ± 0.3	9.2 ± 0.2	43.9 ± 0.3	4.0 ± 1.0	971 ± 30
C57BL/6 *lpr*-Rag1⁻		6	40.3 ± 0.8	13.4 ± 0.2	9.1 ± 0.2	44.1 ± 0.1	3.7 ± 0.2	975 ± 31
	t test		0.9	0.9	0.7	0.4	0.8	0.9

Table 3.1, associated with Figure 3.3.

Complete blood counts (CBC) for the indicated mouse strains. n =number of mice used for each strain in each experiment. HCT =hematocrit. HGB =hemoglobin. RBC =red blood cells. MCV =mean corpuscular volume. WBC =white blood cells. PLT =platelets. All data are mean ±SEM. t-test (unequal variance) p-values are indicated.

Text 3.1   Regulation of the EryA progenitor pool by Fas.

The data in Figure 3.2A (left panel) can be fitted by a model in which Fas acts as a negative autoregulator of the EryA pool (Figure 3.2B).

Let the number of EryA cells within the erythroblastic island be *'A'*. *'A'* is expressed relative to the basal frequency of EryA within the erythroblastic island, (measured experimentally as the fraction of Ter119$^+$ cells that are 'EryA' in the basal state).

'A' is the result of three principal factors (Figure 3.2B):

- a continuous input from earlier progenitors, *β*;

- a continuous output, *αA*, into more differentiated progenitor subsets;

- Fas-dependent loss through cell death.

The probability of Fas-mediated cell death is proportional to the probability of a Fas-positive EryA cell encountering an EryA cell that expresses FasL, at sufficiently close quarters to result in activation of the Fas receptor. If the fraction of EryA cells that expresses Fas is denoted by *'F'*, then the frequency of Fas-positive EryA cells in the erythroblastic island is *'AF'*; similarly, if the frequency of FasL expression amongst EryA is *'L'*, the frequency of FasL-positive EryA cells in the island is *'AL'*. The probability of this encounter is therefore proportional to $AF * AL = A^2 FL$. However, since nearly all EryA cells express FasL, and since the change in FasL expression in response to Epo is relatively small, we can substitute $L \approx 1$. The probability of Fas-mediated cell death is therefore proportional to *'A^{2}F'*, a term that varies with the square of the frequency of EryA in the erythroblastic island, for any given level of Fas.

This model allows us to predict how the frequency of EryA changes with Fas expression in response to Epo. Thus, change in EryA pool over time, $\frac{dA}{dt}$, is given by:

$$\frac{dA}{dt} = \beta - kA^2F - \alpha A \tag{1}$$

where 'k' is a proportionality constant. When a new steady state is attained between days 2 and 3 following an Epo injection (Liu et al), there is no net change in 'A', making $\frac{dA}{dt} = 0$. Therefore, equation (1) becomes:

$$\beta - kA^2F - \alpha A = 0 \tag{2}$$

For a given constant value of β, α and F, the corresponding value of 'A' may be found by solving equation (2) as a simple quadratic equation:

$$A = \frac{\alpha \pm \sqrt{\alpha^2 + 4kF\beta}}{-2kF} \tag{3}$$

Epo levels change with erythropoietic stress, suppressing F. We assume that the input β and the output coefficient, α, remain relatively constant in spite of changes in the level of Epo. The inverse relationship between EryA ('A', *expressed relative to the basal frequency of EryA within Ter119$^+$ cells*) and the number of Fas$^+$ EryA ('F', *expressed relative to the frequency of Fas$^+$ cells within EryA cells*) in Figure 3.2A is fitted well by a hyperbolic curve that represents the (positive) solutions for 'A' in equation (3), for different steady-state levels of Fas ('F') (R^2=0.89).

The initial fitted constants were β=1.3, α=0, k=0.5. R^2=0.88.

The zero value fitted by the 'solver' software for α reflects its low actual value relative to β, with the result that the curve fitting for equation (3) is relatively insensitive to small changes in α around zero. To find the actual value for α:

As F$\rightarrow$0, then, from equation (2),

$$A = \frac{\beta}{\alpha} \qquad (4)$$

Experimentally, we know that under these circumstances, 'A' is in the order of 30- to 60-fold the basal EryA pool (This increase is the measured expansion of EryA. Figure 3.4A and main text). From equation (4), and from the value for β obtained by the curve fitting, this gives a value for α between 0.02 and 0.04. Substituting these values in the equation describing the curve in Figure 3.2A does not substantially alter the curve and its fitness to the data (R^2 remains 0.89).

Chapter IV Attributions and Copyright information

The material in this chapter has been submitted for publication in Blood Journal in a modified format. This chapter represents original work by the authors.

Contrasting Dynamic Responses *in vivo* of the Bcl-x$_L$ and Bim Erythropoietic Survival Pathways

Miroslav Koulnis[1#], Ermelinda Porpiglia[1#], Alberto Porpiglia[1], Ying Liu[1], Kelly Hallstrom[1] and Merav Socolovsky[1]

[1]Department of Pediatrics and Department of Cancer Biology, University of Massachusetts Medical School, Worcester MA USA.

[#] authors contributed equally

Specific Authorship Contributions:

MK performed experiments presented in Figure 4.1A-E, Figure 4.2D, Figure 4.3B and part of 4.3C, Figure 4.4A-I, part of Figure 4.5A, Figure 4.5B and C, Figure 4.6C-E, Figure 4.8A and C-E, Figure 4.9, Figure 4.11, and Figure 4.12. He also designed and drew models shown in Figure 4.7. MK, with guidance from MS, also analyzed the majority of data [with the exception of Figure 4.2A-C and E, Figure 4.3A, Figure 4.5A (left panels), Figure 4.6A-B and F, Figure 4.8B, and Figure 4.10]. MK created and adjusted all figures for publication, and wrote part of the manuscript.

EP performed experiments, analyzed the results, and presented data for Figure 4.6A, B and F.

AP, together with MK, performed experiments and analyzed part of the results in Figures 4.1A-E, Figure 4.3B-C, Figure 4.4G-I, Figure 4.5A and C, Figure 4.8A, D and E.

YL performed experiments presented in Figure 4.2A-C and E, Figure 4.3A and part of 4.3C, Figure 4.5A, and Figure 4.10.

KH performed experiments presented in Figure 4.8B, and helped MK perform experiments in Figure 4.8C.

MS designed research, analyzed and interpreted data and wrote the manuscript.

Disclosure of Conflicts of Interest:

None of the authors have any conflicts of interest to declare.

CHAPTER IV

CONTRASTING DYNAMIC RESPONSES IN VIVO OF THE BCL-X$_L$ AND BIM ERYTHROPOIETIC SURVIVAL PATHWAYS

ABSTRACT

Survival signaling by the erythropoietin (Epo) receptor (EpoR) is essential for erythropoiesis and for its acceleration in hypoxic stress. A number of apparently redundant EpoR survival pathways were identified *in vitro*, raising the possibility of their functional specialization *in vivo*. Here we used mouse models of acute and chronic stress, including a hypoxic environment and β-thalassemia, to identify two markedly different response dynamics for two early erythroblast survival pathways *in vivo*. Induction of the anti-apoptotic protein Bcl-x$_L$ is rapid but transient, whilst suppression of the pro-apoptotic protein Bim is slower but persistent. Similar to sensory adaptation, however, the Bcl-x$_L$ pathway 'resets', allowing it to respond afresh to acute stress superimposed on a chronic stress stimulus. Using 'knock-in' mouse models expressing mutant EpoRs, we found that adaptation in the Bcl-x$_L$ response is due to adaptation of its upstream regulator Stat5, both requiring the EpoR distal cytoplasmic domain. We conclude that survival pathways show previously unsuspected functional specialization for the acute and chronic phases of the stress response. Bcl-x$_L$ induction provides a 'stop-gap' in acute stress, until slower but permanent pathways are activated. Further, pathological elevation of Bcl-x$_L$ may be the result of impaired adaptation, with implications for myeloproliferative disease mechanisms.

INTRODUCTION

Hypoxic stress accelerates the production of red cells by up to ten-fold [162]. Erythropoietin (Epo) is essential for both basal and stress erythropoiesis. Epo exerts its effect by activating its receptor, EpoR, on the surface of erythroid progenitors [163]. Colony-forming unit-erythroid (CFU-e) progenitors and their immediate proerythroblast and basophilic erythroblast progeny are Epo-dependent [2]. Until recently, the rarity of these cells within hematopoietic tissue confined their biochemical study to *in-vitro* culture systems, where they were found to undergo apoptosis when deprived of Epo [73]. It was therefore suggested that Epo regulates erythropoietic rate through the number of erythroid progenitors it rescues from apoptosis [73].

Recently, we [42] and others [47,164] made use of cell-surface markers to identify maturation-specific erythroblast subsets directly within freshly isolated mouse hematopoietic tissue [42], including the Epo-responsive ProE (proerythroblasts, CD71^{high}Ter119^{medium}) and EryA (early basophilic erythroblasts, CD71^{high}Ter119 ^{high} FSC^{high}). This approach confirmed the central role of apoptosis in the erythropoietic stress response, showing that a substantial fraction of the early erythroblast compartment, particularly splenic ProE and EryA, undergo apoptosis *in vivo* in the normal basal state. Stress-induced high Epo levels suppress apoptosis and consequently promote early erythroblast expansion and an increase in erythropoietic rate [42].

Although a number of EpoR-activated survival pathways have been identified [67,76,81,90,136], relevance to erythropoiesis *in vivo* was documented for only a few, largely through gene 'knockout' studies revealing abnormal basal or stress erythropoiesis

[43,76,84,155,165]. Importantly, it is unknown how multiple survival pathways integrate *in vivo* to provide a coherent erythropoietic stress response, and whether the large number of survival pathways represents redundancy or functional specialization. The study of these pathways *in vivo*, now made possible with the advent of flow-cytometric techniques (Chapter V) [42,47,164], may assist in answering this question.

We recently investigated the role of the death receptor Fas, and its ligand, FasL, which are co-expressed by early erythroblasts and suppressed by EpoR signaling *in vivo* [42,44] (Chapter III). We found that, in addition to regulating cell survival, this pathway stabilizes basal erythropoiesis and accelerates its response to stress (Chapter III). Therefore, anti-apoptotic pathways may have system-level functions that are not immediately apparent from their anti-apoptotic effects in culture. Here we set out to investigate two apoptotic regulators of the Bcl-2 protein family that are targeted by EpoR signaling, the anti-apoptotic protein Bcl-x_L, and the pro-apoptotic Bim protein. Bcl-x_L induction is a major survival pathway in erythroblasts [96,97], where it is regulated by EpoR-activated Stat5 [76,78] synergistically with GATA1 [101]. Bcl-$x_L^{-/-}$ mice die *in utero* of anemia, and Bcl-$x_L^{-/-}$ ES cells do not contribute to erythropoiesis in chimeric mice [166]. In a Stat5-deficient mouse [167], reduced Bcl-x_L in early erythroblasts results in ineffective erythropoiesis and anemia [43]. Severe ineffective erythropoiesis in adult erythroblasts conditionally-deleted for Bcl-x_L [165] is corrected if mice are also deleted for the pro-apoptotic proteins Bax and Bak [88], suggesting that the requirement for Bcl-x_L in erythropoiesis is due to its anti-apoptotic effect.

In spite of the clear role for Bcl-x_L in basal erythropoiesis, it is not known

whether erythroblast Bcl-x_L levels increase further during stress, contributing to enhanced erythroblast survival. Elevated levels of erythroblast Bcl-x_L have been implicated in Polycythemia Vera [168,169], suggesting that Bcl-x_L-mediated enhanced erythroblast survival has the potential to increase erythropoiesis above the basal rate [169]. It is not, however, known if this happens physiologically.

We contrasted Bcl-x_L with Bim, a BH3-only pro-apoptotic Bcl-2 family protein [170]. Bim downregulation is a key component of survival signaling by cytokines and oncoproteins such as Bcr-Abl or Jak2V617F in hematopoietic progenitors [171,172]. EpoR survival signaling *in vitro* was recently shown to be in part due to decreased Bim mRNA [89,90] and to ERK-mediated phosphorylation and degradation of the Bim protein [89]. Further, Bim$^{-/-}$ mice have normal red cell numbers but these arise from a smaller pool of progenitors with enhanced survival [89]. Like Bcl-x_L, in addition to EpoR signaling, Bim suppression is also mediated by GATA-1, via its transcriptional target LRF [106]. LRF$^{-/-}$ mice, which die *in utero* secondary to severe erythroblast apoptosis and anemia, were partly rescued by Bim deletion [106]. In spite of the clear role of Bim suppression in erythroblast survival, it is not known whether this pathway participates in the stress response.

Here we used intracellular multiparameter flow cytometry to measure Bcl-x_L and Bim in stage-specific erythroblasts directly in erythropoietic tissue of fetal and adult mice as they are undergoing differentiation and responding to stress *in vivo*. We found a similar, highly dynamic activation of the Bim and Bcl-x_L survival pathways in the fetus that was dependent on both developmental day and erythroblast differentiation stage.

These pathways diverge, however, in the adult, where their contrasting dynamic responses suggest a clear segregation of function during the acute and chronic phases of the stress response.

RESULTS

Erythroid developmental delay in Stat5^{-/-} embryos

The definitive erythropoietic lineage generates enucleated red cells and first begins in the murine fetal liver on embryonic day 11.5 (E11.5). Using cell surface markers CD71 and Ter119, we divided fresh fetal liver into a developmental sequence of increasingly mature subsets S0 to S5 [46] (Figure 4.1A). Most S0 cells (≥70%) are erythroid progenitors at the colony-forming unit stage (CFU-e), just preceding the onset of Epo/EpoR dependence that takes place at the transition from S0 to S1 [46]. Subsets S1 to S5 contain increasingly mature Epo-dependent CFU-e, proerythroblasts and erythroblasts [46]. Between E11.5 and E14.5, fetal liver cell number increases 1000-fold, and the majority shift in maturational stage from earlier erythroid progenitors and precursors (S0/S1/S2) at E11-E12, to late erythroblasts at E13-E14 [44] (Figure 4.1A). We previously showed that these dynamic changes are associated with an apoptosis rate that is dependent on both differentiation stage and developmental day [44]. Apoptosis is seen principally in CFU-e and early erythroblasts (S1-S2), where it is highest on E11.5, decreasing to a low value on E12-E12.5 and rising again on E13-E14 [44].

Given this dynamic picture, we set out to characterize the developmental and maturation-stage-specific expression of Bcl-x_L and Bim in wild-type and in Stat5^{-/-} mice

(Figure 4.1). The Stat5$^{-/-}$ mice [77] are anemic *in utero* leading to perinatal death, a similar but more severe phenotype to that of the hypomorphic Stat5 mouse in which only the first Stat5 exon is deleted [76,167]. We first analyzed the CD71/Ter119 profiles on sequential developmental days and found that erythroblast maturation in the Stat5$^{-/-}$ embryos was delayed, as seen by their delayed progression from the S1 to S3 (Figure 4.1A,B). Specifically, on E12.5, the S1 subset contained only 10% of wild-type fetal liver cells, but 35% of the Stat5$^{-/-}$ fetal liver cells (p<0.005); by contrast, the more mature S3 subset contained ≥60% of wild-type, but only 20% Stat5$^{-/-}$ fetal liver (p=0.005). This pattern was not simply due to delayed expression of the cell surface markers Ter119 or CD71, as evident from cell size analysis of the S1 and S3 subsets using the flow-cytometric forward scatter parameter, which was unaltered for cells in each respective subset.

Bcl-x$_L$ and Bim expression in fetal liver is differentiation-stage and embryonic-day dependent

We assessed Bcl-x$_L$ and Bim protein expression using intracellular flow cytometry (Figure 4.1C,D), employing an anti-Bcl-x$_L$ antibody that we previously verified for its specificity [43], and an anti-Bim antibody whose specificity we verified using Bim$^{-/-}$ splenocytes (Figure 4.8A). We found that, consistent with previous findings *in vitro* [78,97], Bcl-x$_L$ is expressed at very low levels in the early S0-S2 compartment and increases with erythroblast differentiation (Figure 4.1C,D, upper panels). However, in addition, Bcl-x$_L$ expression was highly dependent on developmental day, with high levels in the early S0-S2 subsets of E11.5 embryos, decreasing rapidly in the same subsets with

embryonic age (Figure 4.1D, upper panel).

Expression of the anti-apoptotic Bim protein is also dependent on both differentiation stage and embryonic day. We found a highly significant increase in both the long (Bim_L) and extra-long (Bim_{EL}) transcripts (Figure 4.8B, p<0.0001) and in the Bim protein (Figure 4.1D, lower panel, p<0.0001) with the transition from S0 to S1, a transition that marks the onset of erythroid progenitor dependence on EpoR [46]. This raised the possibility that induction of the pro-apoptotic Bim protein at the S0/S1 transition may be the cause of EpoR dependence. However, we found no significant differences in Epo dependence or in the sensitivity of $Bim^{-/-}$ fetal liver erythroid progenitors to Epo using a CFU-e assay *in vitro* (Figure 4.8C).

Bim protein expression peaks in S1 and is gradually suppressed with erythroid differentiation, reaching its lowest values in mature erythroblasts (Figure 4.1D, lower panel). Similar to $Bcl-x_L$, Bim expression was also a function of developmental day. For a given maturation subset, Bim expression is lowest on E11.5, peaking on E12.5, and decreasing in older embryos (Figure 4.1D). The changing fetal liver $Bcl-x_L$ and Bim during embryonic days E11.5-E12.5 match our previous findings of large changes in apoptosis, cell number and Fas expression at this time [44].

Bim and Bcl-x_L expression in fetal liver are regulated by Stat5

The rapidly changing expression of Bim and $Bcl-x_L$ during E11.5-E12.5 (Figure 4.1D), and the developmental delay in the $Stat5^{-/-}$ fetal liver (Figure 4.1A,B), together impede our ability to assess the role of Stat5 in regulating Bim and $Bcl-x_L$ expression at

this time. However, the CD71/Ter119 profiles and Bim and Bcl-x_L expression begin to stabilize at E13.5, and the Stat5$^{-/-}$ fetal liver profile approaches that of wild-type embryos (Figure 4.1D, Figure 4.1A,B). We therefore compared Bim and Bcl-x_L expression in Stat5$^{-/-}$ fetal liver and wild-type littermates on E13.5-E14.5 (Figure 4.1E, Figure 4.8D,E).

Bcl-x_L expression in the Stat5$^{-/-}$ fetal liver was 1.5- to 2-fold lower in the early erythroblast subsets S1 (p=0.01), S2 (p=0.03) and S3 (p=0.002). Bim levels in Stat5$^{-/-}$ fetal liver were 30% and 40% higher, respectively, in the S3 and S4/5 subsets (p<0.01), suggesting Stat5 regulates its expression. For comparison, we also assessed expression of the erythroblast apoptotic regulators Fas and FasL in the Stat5$^{-/-}$ fetal liver. We found no significant difference in Fas expression between Stat5$^{-/-}$ embryos and wild-type littermates (Figure 4.9).

Bcl-x_L is rapidly induced in adult early erythroblasts in response to a single Epo injection

We examined Bcl-x_L expression in response to a single dose of Epo, the principal mediator of the stress response. A single subcutaneous injection (300 U /25 g) results in a rapid increase in serum Epo, peaking by 6 hours, persisting for 24 hours and declining to baseline by 36 hours (Figure 4.2A). We measured Bcl-x_L expression by intracellular flow cytometry, in each of the adult flow-cytometric erythroblast subsets ProE, EryA, EryB and EryC [42] (Chapter V and Figure 4.2B), in freshly explanted bone-marrow and spleen at the indicated time points (Figure 4.2C-E). In control, saline-injected mice, Bcl-x_L expression increases 6-fold with differentiation from ProE to EryC in both bone-marrow

and spleen, a pattern similar to that of fresh fetal liver (representative histograms in Figure 4.2C; summary of several experiments in Figure 4.2E). Injected Epo caused a further induction of Bcl-x_L expression in all erythroblast subsets (Figure 4.2C,E). Proportionally, this increase was largest and most rapid in the earliest subsets, where basal Bcl-x_L levels are lowest, and where it peaked 5-fold its basal level within 16 hours of Epo injection in splenic ProE (p=0.0006) and 3-fold by 18 hours in splenic EryA (p=0.0009) (Figure 4.2C,E).

To assess the sensitivity of the Bcl-x_L pathway to injected Epo, we carried out a dose/response curve *in vivo*, injecting mice with the indicated Epo dose and examining peak Bcl-x_L expression at 18 hours in splenic EryA (Figure 4.2D). This analysis shows that half the maximal response is obtained with the injection of 3 U /25 g, estimated to result in a serum concentration of 0.3 U/mL, approximately a ~10-fold increase above basal serum Epo. This response is more sensitive than that of the Fas-suppression pathway, where we found a half-maximal response with an injection of 10 U /25 g (Chapter III).

Induction of the Bcl-x_L protein is associated with an increase in the Bcl-x_L mRNA that follows a similar time course (Figure 4.3A).

Expression pattern of Bim in basal and stress adult erythropoiesis

We used intracellular flow cytometry in adult spleen and bone-marrow, freshly explanted at the indicated time points following either saline or Epo injection (300 U /25 g), to examine Bim expression. Bim is expressed at its highest levels in the early, ProE

subset, declining gradually in subsequent differentiation subsets and reaching a quarter of its ProE level in EryC (Figure 4.3B). In response to an Epo injection Bim levels decreased further in all subsets (Figure 4.3B,C), with the largest decline in the early bone-marrow and spleen ProE progenitors, where they fell ~2-fold (p<0.0001).

Importantly, the time course of Bim suppression in response to Epo injection was much slower, and more prolonged, than the Bcl-x_L response. Maximal Bim suppression was reached at 72 hours post injection in most subsets, a time when the Bcl-x_L induction had already peaked and returned to baseline (Figure 4.3C).

The erythroblast response to reduced atmospheric oxygen

The modulation of erythroblast Bim and Bcl-x_L levels by an Epo injection *in vivo* suggested that these pathways are likely to play a role in the physiological stress response. To test this, we placed mice in a reduced oxygen environment in which atmospheric partial oxygen pressure was reduced to 11% for up to 5 days (Figure 4.4). Epo levels in blood plasma rose rapidly in the first 24 hours, from a basal level of 12 mU/mL, to a peak of 29 mU/mL (p=0.001). This high Epo level was sustained until day 3. On days 4 and 5 Epo began to decline to a new, lower plateau of 18 mU/mL (Figure 4.4A).

The hematocrit response was rapid, rising from 51.5% to 56% in the first 24 hours, and reaching a sustained plateau of 57% (Figure 4.4B). The rapid initial increase in hematocrit is likely in part to be the result of plasma volume adjustment in response to hypoxia [19,173].

We examined the response of individual flow-cytometric erythroblast subsets in freshly explanted tissue at the indicated time points (Figure 4.4C-I). The results shown are from 23 pooled experiments, with at least 6 mice per time point. To evaluate the various responses in relation to the plasma Epo levels, the Epo response in Figure 4.4A is replicated as a gray line in subsequent panels (Figure 4.4E-I).

The absolute numbers of spleen ProE and EryA erythroblasts increased over the initial 3 days, reaching new plateaus that were 4- and 3-fold higher than basal values, respectively (Figure 4.4C,D). This increase in cell number was associated with a marked and significant reduction in apoptosis, with the number of Annexin V^+ cells declining from 55% to 32% (p=0.002) and 42% to 30% (p=0.001) in the ProE and EryA subsets, respectively (Figure 4.4E).

The response of erythroblast Bim, Fas and Bcl-x$_L$ to reduced atmospheric oxygen

Given the clear changes in ProE and EryA apoptosis, we investigated their expression of the apoptotic regulators Fas, Bim and Bcl-x$_L$. We previously showed that cell surface Fas on spleen ProE and EryA decreases in response to a number of acute and chronic erythropoietic stress conditions. Maximal Fas suppression is reached within 24 to 48 hours and is maintained for the duration of the stress stimulus (Figure 4.4F) (Chapter III) [42].

The Bcl-x$_L$ response was rapid and transient, its expression peaking by 18 hours in both ProE and EryA, and then rapidly dipping below baseline by 24 hours, in spite of the persisting high Epo levels (Figure 4.4G). The response of Bim, by contrast, was

slower, reaching maximal suppression at 48 hours, with low levels maintained for the duration of high Epo levels (Figure 4.4H,I).

We examined the possibility that the transient increase in Bcl-x_L may be due to the relatively modest increase in plasma Epo generated by the hypoxic environment. We injected mice with Epo (300 U /25 g) daily for 3 consecutive days, which generates increasingly high plasma Epo equivalent to that of maximal stress conditions [162] (Figure 4.2A). We measured the Bcl-x_L response 18 hours following each injection (Figure 4.10). The amplitude of the Bcl-x_L response was larger in response to this higher Epo dose than in the response to the hypoxic environment, as expected from the Epo dose/Bcl-x_L response curve (Figure 4.2D). However, the response to the second and third Epo injections was smaller or absent (Figure 4.10), suggesting that the transience of the Bcl-x_L response is unrelated to Epo dose.

Response of the Bim and Bcl-x_L pathways to chronic erythropoietic stress

We went on to assess the Bim and Bcl-x_L response to chronic erythropoietic stress. The Bcl-x_L expression profiles in the ProE/EryA-C subsets in either spleen or bone-marrow was unaltered by 3 distinct erythropoietic stress conditions: pregnancy at mid-gestation, chronic anemia due to β-thalassemia [174], and chronic erythrocytosis due to tissue-specific deletion of the von Hippel-Lindau gene that results in elevated Epo (ts-VHL$^{-/-}$) [9] (Figure 4.5A). Plasma Epo is elevated to 30 mU/mL and 220 mU/mL in the ts-VHL$^{-/-}$ and β-thalassemia mice, respectively (Figure 4.11), a concentration range in which Bcl-x_L induction was seen in acute stress (Figure 4.4). Further, we have previously

shown that cell surface Fas and FasL are downregulated in the same chronic stress models [42].

Unlike Bcl-x_L, Bim expression in the β-thalassemia mice was suppressed in all erythroblast subsets (Figure 4.5B), to levels similar to those seen in response to an acute Epo injection (Figure 4.3B).

The Bcl-x_L response to an 'acute on chronic' stress stimulus

The transience of the Bcl-x_L response to stress is reminiscent of sensory systems that undergo adaptation, such as neutrophil chemotaxis or sensory neural adapting systems. These systems respond to a change in the stimulus, rather than to absolute stimulus levels [175]. We therefore asked whether the desensitization of the Bcl-x_L pathway to chronic stress was permanent, or whether an acute change in the level of stress, superimposed on a chronic stress stimulus, would re-stimulate Bcl-x_L induction.

We injected β-thalassemia mice with a single Epo dose of 300 U /25 g, and examined their Bcl-x_L response at 18 hours post injection. We found a clear induction in Bcl-x_L in all erythroblast subsets in the β-thalassemia mice, closely resembling that of control mice in the bone-marrow, and only a little short of the wild-type response in the spleen (Figure 4.5C). This experiment suggests that while the Bcl-x_L response desensitizes to chronic stress, it rapidly responds to new changes in stress superimposed on the chronic stress levels.

Stat5 activation *in vivo* undergoes adaptation

We asked whether adaptation in the Bcl-x$_L$ stress response is due to adaptation in Stat5, its upstream regulator. We first examined the time course of Stat5 activation *in vivo* following Epo injection (300 U /25 g), using intracellular flow cytometry in freshly explanted spleen and bone-marrow at the indicated time points post-injection (Figure 4.6A). The number of ProE and EryA containing active, phosphorylated Stat5 (p-Stat5) increased rapidly following injection, peaking by 30 minutes, but declining rapidly to a lower level by 6 hours (Figure 4.6A). Of note, plasma Epo peaked at 6 hours (Figure 4.2A), suggesting the decline in p-Stat5 is intrinsic to the p-Stat5 response and is not due to declining Epo.

Signal adaptation may be due to negative feedback [176,177]. p-Stat5-mediated transcriptional activation of SOCS family proteins results in their feedback inhibition of the Jak2 and Stat5 response [178]. This negative regulation in part depends on SOCS protein binding to phosphotyrosines on the activated EpoR cytoplasmic domain [163]. To investigate the possibility that Stat5-mediated negative feedback is responsible for adaptation in the p-Stat5 response, we investigated two 'knock-in' mouse models, expressing the EpoR mutants EpoR-H and EpoR-HM [75], both lacking the negative regulatory distal portion of the EpoR cytoplasmic domain containing 7 of its 8 phosphotyrosines, including SOCS family docking sites [163]. In EpoR-HM, the remaining Y343, a Stat5 docking site, is mutated to phenylalanine [75]. The EpoR-H mouse has a mildly elevated basal hematocrit. By contrast, the EpoR-HM mouse has only a mild anemia in the basal state but a deficient stress response [75].

We tested the response of freshly harvested fetal liver early erythroblasts derived

from EpoR-H, EpoR-HM and wild-type embryos to continuous stimulation with Epo for up to 6 hours *in vitro*. The time course of response of wild-type erythroblasts was similar to that of adult erythroblasts *in vivo* (Figure 4.6A,B). The peak p-Stat5 response to Epo stimulation in EpoR-HM erythroblasts was 15% of the response in wild-type or EpoR-H mice, in agreement with previous results [179]. In EpoR-H erythroblasts, peak p-Stat5 was similar to that of the wild-type response, though baseline p-Stat5 was higher. In both EpoR-HM and EpoR-H, duration of the initial p-Stat5 peak was prolonged substantially (Figure 4.6B). These findings suggested that the distal EpoR cytoplasmic domain, likely through binding to Stat5-induced SOCS family proteins, is responsible for curtailing the p-Stat5 response.

The Bcl-x$_L$ and Bim stress responses in EpoR-H and EpoR-HM mice

The finding that the p-Stat5 signal undergoes adaptation (Figure 4.6A,B) suggests it may be responsible for the adaptation in the Bcl-x$_L$ response. To test this, we asked whether failure of p-Stat5 adaptation in the EpoR-H mice (Figure 4.6B) would prevent adaptation of the Bcl-x$_L$ response.

We therefore injected EpoR-H mice with Epo (300 U /25 g) and examined the resulting induction in Bcl-x$_L$. The peak Bcl-x$_L$ response was closely similar to that of matched wild-type control mice (Figures 4.6C and 4.12A). There was little increase in Bcl-x$_L$ in EpoR-HM mice, consistent with p-Stat5 as the principal regulator of the Bcl-x$_L$ stress response (Figures 4.6C and 4.12A). Importantly, there was a failure of adaptation of the Bcl-x$_L$ response in EpoR-H mice. Bcl-x$_L$ levels remained elevated well above their

initial baseline at 36 and 48 hours post-injection in spleen ProE, and at 36 hours in EryA

and EryB (p<0.005, Figure 4.6D), even though Bcl-x_L levels in wild-type mice (Figure

4.6D) and serum Epo (Figure 4.2A) had returned to baseline. This strongly suggests that

adaptation in the Bcl-x_L response requires the EpoR distal cytoplasmic domain and is

most likely a result of adaptation in the p-Stat5 response, also dependent on this domain

(Figure 4.6B).

Bim expression was suppressed in EpoR-HM mice in response to a single Epo

injection (300 U /25 g). However, suppression was less efficient than in wild-type mice,

by a small but statistically significant amount (Figures 4.6E, 4.12B, p=0.03 and p=0.001

in ProE and EryA, respectively). These results suggest that, in addition to Stat5, other

pathways, likely ERK, regulate the EpoR-mediated Bim suppression [89].

The p-Stat5 response to an 'acute on chronic' stress stimulus

Although Bcl-x_L expression is not elevated in chronic stress, it is induced in

response to an acute stimulus superimposed on the chronic stress stimulus (Figure 4.5C).

Given the proposed role of Stat5 activation in Bcl-x_L induction, we similarly examined

the p-Stat5 response to chronic and 'acute on chronic' stress stimuli. We found no

increase in the level of p-Stat5 activation in ProE freshly isolated from β-thalassemic

mice (Figure 4.6F, upper panel), in spite of the chronically elevated plasma Epo in these

mice (Figure 4.11). A single injection of Epo (300 U /25 g) however, resulted in a rapid

increase in p-Stat5 activation in both β-thalassemic mice and in matched control mice

(Figure 4.6F, lower panels). Therefore, both the p-Stat5 and Bcl-x_L responses 'reset'

during chronic stress, allowing them to respond afresh to an acute change in stress.

DISCUSSION

We examined Bim suppression and Bcl-x_L induction, two EpoR-activated erythroblast survival pathways in fetal and adult basal and stress erythropoiesis. Their analysis *in vivo* revealed previously unsuspected functional specialization of EpoR-pathways to either the chronic or acute phases of the stress response. Bcl-x_L induction behaves like a classical sensory adapting pathway, being insensitive to the prevailing level of stress, and instead responding only to changes in stress level. Adaptation allows Bcl-x_L to provide a stop-gap at the onset of stress that rapidly rescues early erythroblasts from apoptosis, until slower but persistent stress pathways, such as Bim or Fas suppression, are activated. Mechanistically, we suggest that adaptation in the Bcl-x_L response is the result of adaptation in the response of p-Stat5, its upstream regulator.

Regulation of Bim and Bcl-x_L expression in early *vs.* late erythroblasts

We delineated the expression pattern of both Bim and Bcl-x_L proteins throughout erythroid maturation in adult and fetal hematopoietic tissue *in vivo*. The basal pattern observed in the absence of stress is one of low Bcl-x_L and high Bim in early erythroblasts, gradually inverting with differentiation so that in mature erythroblasts Bim levels are low, and Bcl-x_L levels are high (Figure 4.7A). These results are consistent with the previously reported increase in Bcl-x_L transcript and protein with erythroid differentiation *in vitro* [78,97], and with the increase in Bcl-x_L and decrease in the pro-apoptotic Bid and

Bax transcript with the transition from early to late erythroblasts in murine bone-marrow [164]. Together with our previous findings of high Fas and FasL co-expression in early, but not late, erythroblasts [23,42,44], a strong pattern emerges of apoptosis-prone early erythroblasts, containing high levels of pro-apoptotic regulators and only low levels of anti-apoptotic proteins, gradually transitioning into apoptosis-resistant late erythroblasts in which anti-apoptotic proteins predominate. This underlying pattern explains why high levels of apoptosis are seen in early erythroblasts but not in late erythroblasts during normal fetal and basal adult erythropoiesis *in vivo* [23,42,44] (Chapter III; Figures 4.1D, 4.2E and 4.3B), and was recently suggested as being responsible for the sensitivity of early erythroblasts to irradiation [164].

Bcl-x_L expression is regulated by both GATA-1 and by EpoR-activated Stat5 [101]. Similarly, Bim suppression is regulated by both EpoR-activated ERK [89] and by GATA-1-induced LRF [106]. Here we find that in addition, Bim is regulated by EpoR-activated Stat5, as suggested by higher Bim levels in the Stat5$^{-/-}$ fetal liver and to a lesser extent in the adult EpoR-HM mouse (Figures 4.1E, 4.6E and 4.12B). Lower Bcl-x_L in the S1-S3 subsets of the Stat5$^{-/-}$ fetal liver, and in EpoR-HM mice in the basal state, support older reports of the role of Stat5 in the induction of erythroid Bcl-x_L [43,76,78]. The role of Stat5 is especially notable, however, in the Bcl-x_L stress response, which is absent in the EpoR-HM mice (Figure 4.6C).

Based on their expression patterns, we propose that EpoR and GATA-1 -mediated regulation of Bim and Bcl-x_L are largely segregated into the early and late erythroblast compartments, respectively (Figure 4.7A). Specifically, the underlying, largely stress-

insensitive gradual increase in Bcl-x_L and gradual suppression of Bim with differentiation, is likely to be mediated by GATA-1. Superimposed on this pattern are Epo-mediated, stress-dependent adjustments that accelerate Bcl-x_L induction and Bim suppression in early erythroblasts (Figures 4.2, 4.3 and 4.7A). Thus, only the apoptosis-prone CFU-e, proerythroblasts and early basophilic erythroblasts (='early erythroblast compartment') are dependent on EpoR signaling for survival in the basal state. Further, during hypoxic stress, it is principally the early erythroblast compartment that is Epo-responsive, undergoing expansion as a result of a rapid drop in apoptosis [23,42,44] (Chapter III and Figure 4.4E). The susceptibility of the early erythroblast compartment to apoptosis is precisely the characteristic that gives plasticity to the erythropoietic system, allowing the level of EpoR signaling to determine erythropoietic rate.

We previously showed that Epo-mediated suppression of early erythroblast apoptosis during stress is strongly correlated with suppression of early erythroblast Fas. Using Fas and FasL-mutant mice, we recently found that the Fas suppression pathway accounts for ~30% of the early erythroblast expansion in stress (Chapter III). Bim suppression and Bcl-x_L induction are therefore likely to cooperate with Fas suppression, and potentially with as yet uncharacterized other anti-apoptotic pathways, in achieving the full expansion of the early erythroblast compartment during stress.

In late erythroblasts, Bim, Bcl-x_L and Fas expression are relatively unaffected by EpoR-stress signaling. Consistent with this, in Stat5$^{-/-}$ embryos and in EpoR-HM mice, where EpoR-Stat5 signaling is deficient, Bcl-x_L levels are only modestly lower in late erythroblasts; the underlying pattern, likely GATA-1-mediated, of a gradual increase in

Bcl-x$_L$ and decline in Bim, is preserved.

Importantly, our results show that Stat5-regulated Bcl-x$_L$ expression *in vivo* varies with differentiation stage, with embryonic day, and with the phase of the stress response. These factors should therefore be considered in the interpretation of Bcl-x$_L$ measurements *in vivo* and in models of this system *in vitro*.

Adaptation allows functional specialization of the Bcl-x$_L$ response to the acute phase of stress

The acute and chronic phases of the stress response differ in their requirements. At the onset of stress the speed of the response is paramount, a property that is unimportant during the chronic, maintenance phase. Here we find that the Bcl-x$_L$ response is significantly faster than Bim or Fas suppression. In addition, the Bcl-x$_L$ response undergoes rapid adaptation, which makes it insensitive to the prevailing absolute level of stress. Like other classical sensory adapting mechanisms, though, it is re-activated as soon as a new change in stress takes place. In this way, the dynamic range of the Bcl-x$_L$ response is extended, allowing a rapid response to changes in stress irrespective of the baseline stress levels. Our new data on the Bcl-x$_L$ pathway show that distinct molecular mechanisms regulate the acute and chronic phases of stress. The EpoR is therefore capable of generating at least two broad types of signal: persistent, giving rise to persistent suppression of Bim and Fas, and a rapidly adapting signal, responsible for the adaptation of the Bcl-x$_L$ response (Figure 4.7B).

Mechanism of adaptation in the Bcl-x$_L$ response

We identified adaptation in the p-Stat5 response in erythroblasts *in vivo* and suggest this to be the mechanism of adaptation in the Bcl-x$_L$ response. Both p-Stat5 and Bcl-x$_L$ respond similarly to an 'acute on chronic' stress stimulus, a response typical of other biological adapting systems like sensory adaptation or neutrophil chemotaxis. Adaptation of both p-Stat5 and Bcl-x$_L$ depends on the distal domain of the EpoR, a previously documented negative regulatory domain that contains docking sites for the Stat5-induced SOCS family of negative regulators [163] (Figure 4.7C). Negative feedback is a well-documented mechanism of adaptation in sensory systems [176,177]. Stat5 transcriptionally activates SOCS inhibitors that feed back to limit Jak2 and Stat5 activation [178]. Though well-documented, the precise effect of this pathway on the p-Stat5 signal was not previously investigated. Here we found that in EpoR-H mice that lack this feedback inhibition, peak p-Stat5 signal intensity is not higher than in wild-type. However, the duration of the peak is prolonged (Figure 4.6D). Therefore, p-Stat5-mediated negative feedback is likely responsible for the adaptation of both the p-Stat5 and Bcl-x$_L$ responses.

Implications for myeloproliferative disease mechanisms

The rapid adaptation of the Bcl-x$_L$ response to stress raises the possibility that prolonged periods in which Bcl-x$_L$ is elevated may be harmful. Indeed, persistently elevated levels of Bcl-x$_L$ are characteristic of Polycythemia Vera and other myeloproliferative syndromes [168,169,180]. High Bcl-x$_L$ was suggested as a cause of Epo-

independent erythroid differentiation in Polycythemia Vera and of the apoptosis resistance of other myeloproliferative syndromes and neoplasms [168,180,181]. Our results, supported by recent reports of SOCS protein inactivation in myeloproliferative disease [182,183], suggest that impairment of p-Stat5 and Bcl-x$_L$ adaptation may contribute to their prolonged activation. Together these results point to the importance of adaptation in the Bcl-x$_L$ response as a homeostatic and tumor-suppressive mechanism.

Acknowledgements
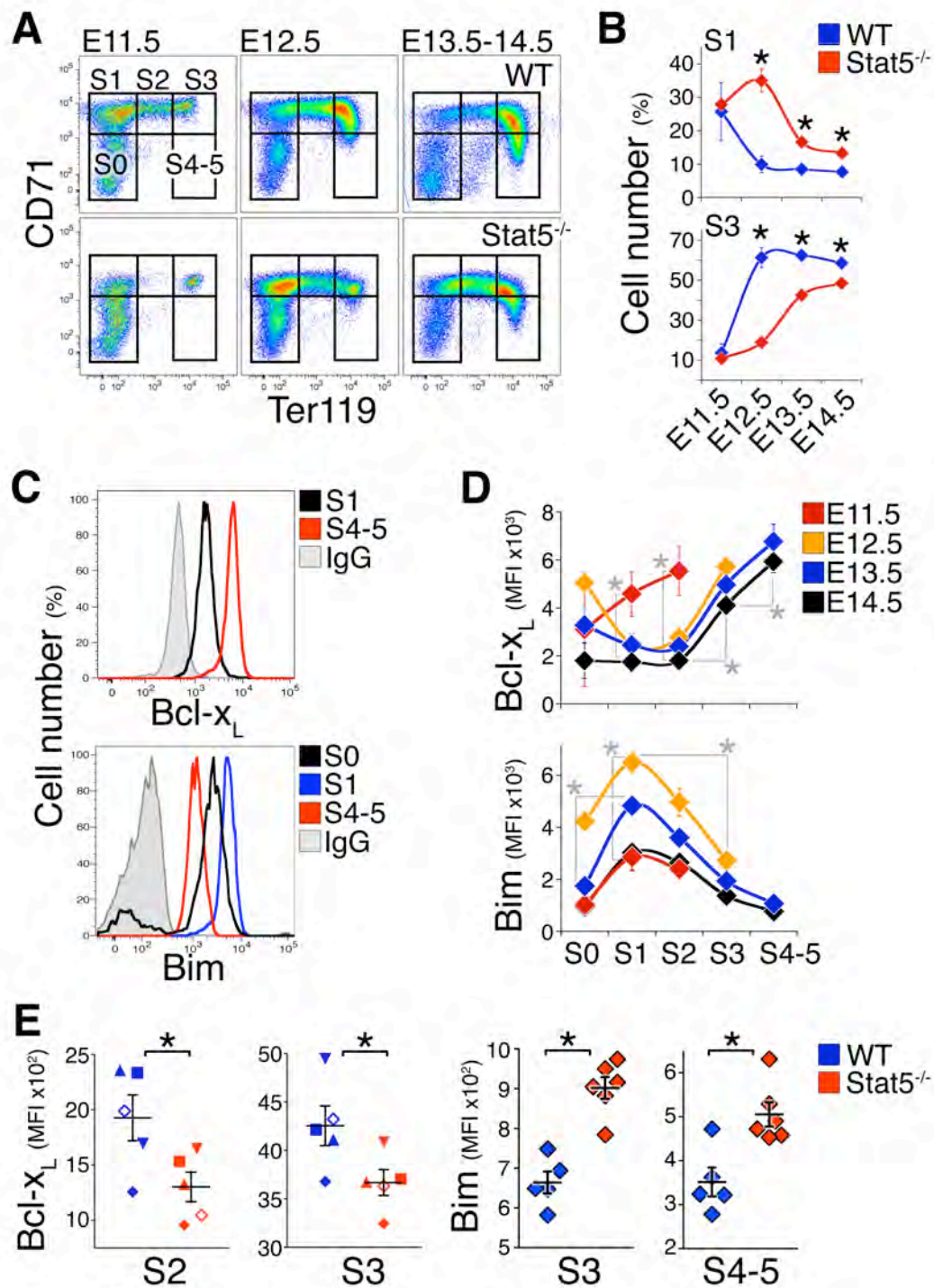
Figure 4.1

Figure 4.1   Delayed maturation and altered Bcl-x$_L$ and Bim expression in Stat5$^{-/-}$ fetal liver.

(A)   Representative CD71/Ter119 profiles of Stat5$^{-/-}$ fetal livers and wild-type littermates freshly isolated on consecutive embryonic developmental days (E11.5 to E14.5). S0 to S4/5 are increasingly differentiated erythroid progenitors and precursors subsets [46]. Dead cells were excluded using LIVE/DEAD viability dye. E11.5 S3 cells are yolk sac-derived, primitive lineage erythroid cells.

(B)   Summary statistics for analysis performed as in 'A', on 5 to 21 embryos per data point (mean ±SEM). Pooled from 3 independent experiments with multiple litters. Stars indicate statistically significant difference between wild-type and Stat5$^{-/-}$ subsets with the following p values: For S1, E12.5 *p=0.002, E13.5 *p=0.00001. E14.5 *p=0.014. For S3, E12.5 *p=0.005, E13.5 *p=0.00004. E14.5 *p=0.010 (two-tailed t-test, unequal variance).

(C)   Intracellular flow cytometry for Bcl-x$_L$ and Bim proteins, in the indicated fetal liver subsets. Representative histograms are shown. Freshly isolated wild-type E14.5 fetal liver cells were stained with CD71, Ter119 and the LIVE/DEAD viability dye as in 'A'. Cells were then fixed, permeabilized and stained intracellularly with: an anti-Bcl-x$_L$ antibody or non-specific Rabbit Serum; an anti-Bim antibody or Rabbit IgG isotype control.

(D)   Bcl-x$_L$ and Bim protein expression profiles, measured as in panel 'C', in fresh wild-type fetal liver cells at the indicated embryonic days, in each of the indicated differentiation subsets S0 to S4/5. Expression is measured as median fluorescence

intensity (MFI), from which non-specific background fluorescence, defined as the MFI of the corresponding subset when binding an isotype control antibody/non-specific serum, was subtracted. Data points are mean ±SEM.

For Bcl-x_L: n=5 to 14 wild-type embryos per data point, pooled from 3 independent experiments with multiple litters. Statistical significance values: S1, E11.5 *vs.* E14.5, *p<0.05 (two-tailed t-test, unequal variance). E14.5 S2 *vs.* S3, and E14.5 S3 *vs.* S4-5, *p<0.0002 (paired t-test).

For Bim: n=6 wild-type Balb/C embryos per data point. Statistical significance values: E13.5 S0 *vs.* E13.5 S1, *p<0.0001; E12.5 S1 *vs.* E12.5 S3, *p<0.0001; E11.5 S1 *vs.* E12.5 S1, *p<0.0001 (two-tailed t-test, unequal variance). Similar developmental pattern was observed in C57BL/6 and Balb/C backgrounds.

(E)   Lower Bcl-x_L and higher Bim protein expression in E14.5 Stat5$^{-/-}$ embryos compared with wild-type littermate controls, at the indicated differentiation subset.

For Bcl-x_L: n=11 to 21 embryos per genotype, with each symbol type representing median expression for one litter. Means ±SEM for the population are indicated. Statistical significance values: S2, *p=0.03. S3, *p=0.002 (paired t-test).

For Bim: data points are individual embryos. Mean ±SEM for the population is shown. Statistical significance values: S3 and S4-5, *p<0.01, two-tailed t-test, unequal variance. See also Figure 4.8D,E.

MK performed all experiments for this figure with help from AP.

Figure 4.2
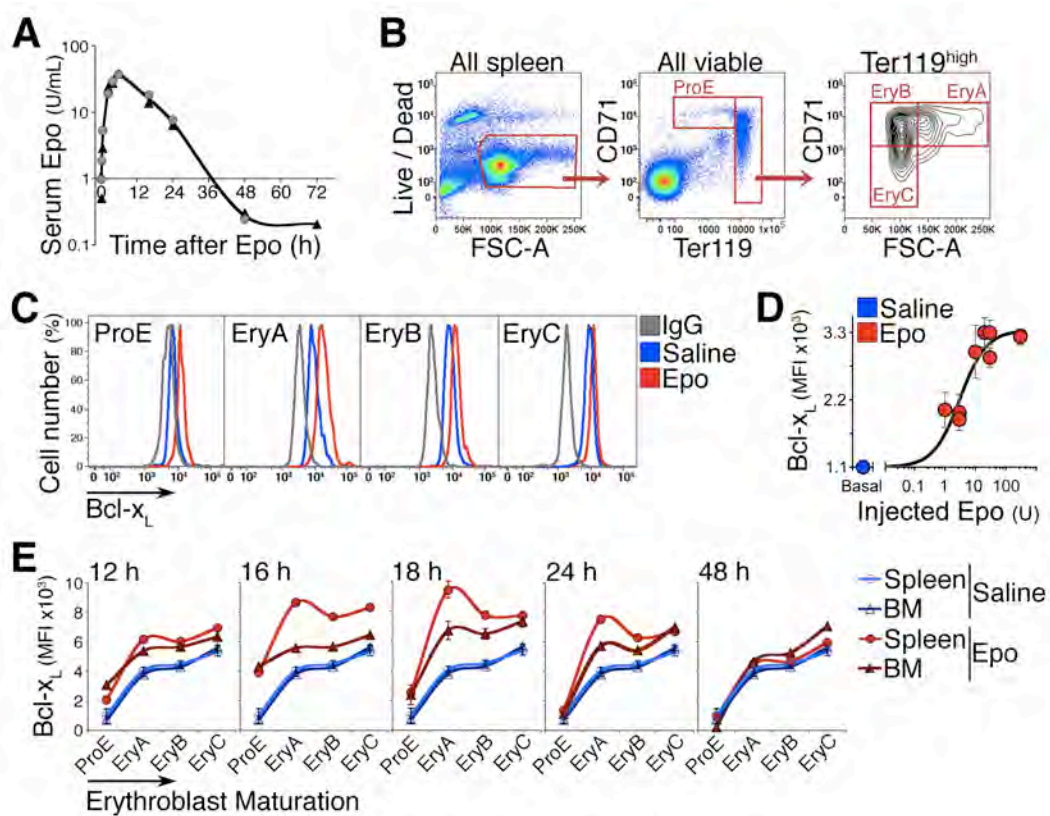
Figure 4.2   Bcl-x$_L$ induction   in   adult   early   erythroblasts   in   response   to   Epo injection.

(A)   Time course of plasma Epo, assayed by ELISA, following a subcutaneous injection of 300 U /25 g. Two mice (identified as either circles or triangles) were assayed per time point.

(B)   Gating strategy for freshly explanted ProE, EryA, EryB and EryC spleen erythroid subsets [42]. Live cells were selected, and subsets gated based on Ter119, CD71 expression and forward scatter (FSC).

(C)   Representative flow-cytometric histograms of intracellular Bcl-x$_L$ protein in the indicated spleen erythroblast subsets. Anti-Bcl-x$_L$ antiserum was used to stain erythroblasts from a saline-injected mouse (blue histograms), or an Epo-injected mouse (300 U /25 g, red histograms) in freshly explanted spleen at 18 hours post injection. An isotype control antibody was used to measure the non-specific binding in each subset (grey histograms).

(D)   Epo dose/ Bcl-x$_L$ response *in vivo* in spleen EryA. Wild-type Balb/C mice were injected subcutaneously with either saline (=basal, blue circle) or a single, increasing dose of Epo (1, 3, 10, 20, 30, or 300 U /25 g, red circles). Bcl-x$_L$ was measured by flow cytometry as in panel 'C' at 18 hours post-injection, with the non-specific fluorescence reading subtracted for each subset. Data from two independent experiments were pooled and normalized. Data points were fitted with a Hill curve. Each data point represents mean ±SEM of n=3 to 4 mice.

(E)   Bcl-x$_L$ expression measured as in panel 'C' in freshly explanted spleen, in each

erythroblast subset at each of the indicated time points following a single Epo injection (300 U /25 g). Each data point for Epo-injected mice is mean ±SEM of n=4 mice for t=16, 18, 24, 48 hours; and mean of 2 mice for t=12 hours. Blue curves are mean ±SEM of n=14 saline-injected mice pooled from all time points. The same blue curves are reproduced for comparison with Epo-injected mice at each time point). Statistical significance values: ProE at t=16h, in bone-marrow *p=0.005, in spleen *p=0.0006. EryA in spleen, *p=0.0009 at 16h, *p=0.0009 at 18h. EryA in bone-marrow, *p=0.013 at 16h, *p=0.015 at 18h. The induction of Bcl-x_L in splenic EryA was significantly higher than in bone-marrow EryA (*p=0.021). Two-tailed t-test with unequal variance used for all comparisons.

MK performed experiments for part (D) and analyzed the data. YL performed the rest of experiments presented in this figure.

Figure 4.3
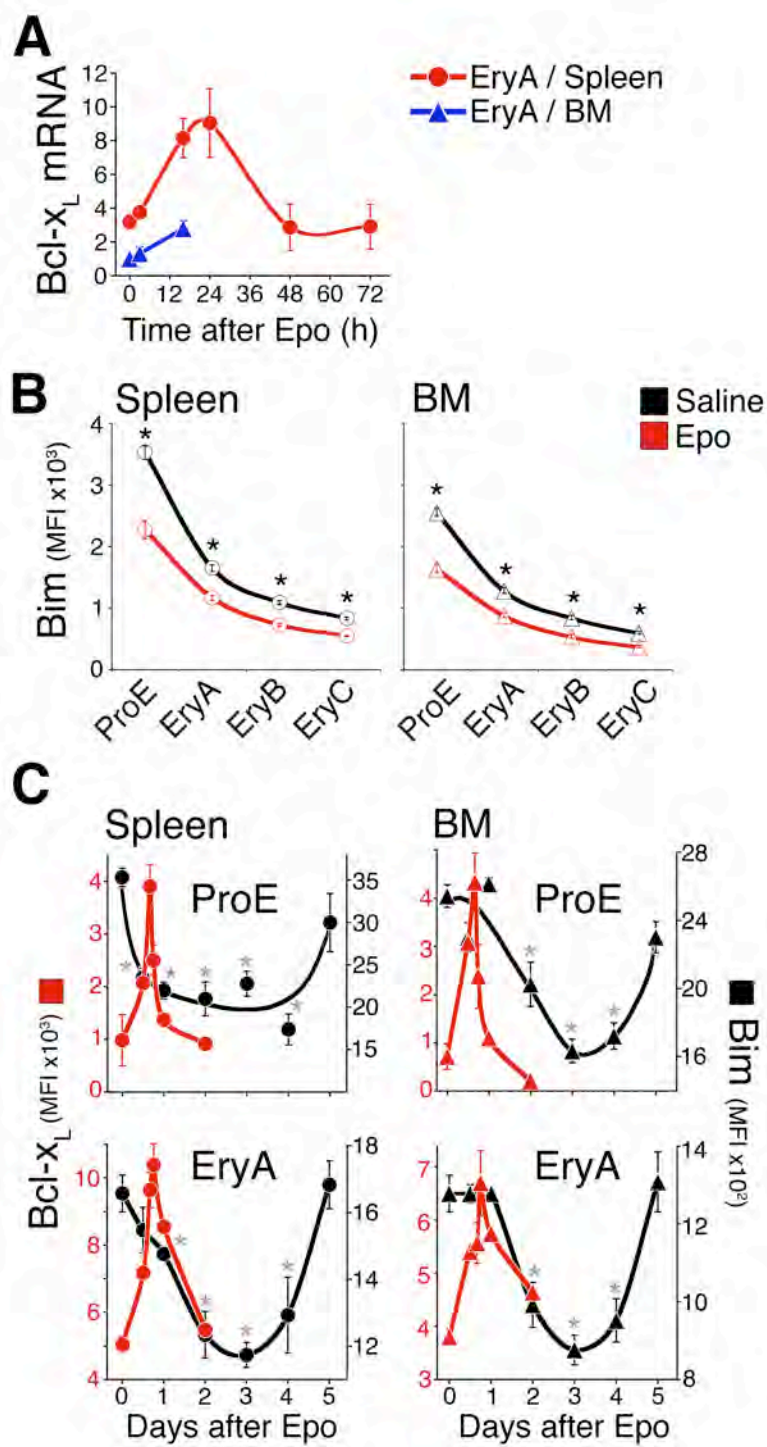
Figure 4.3   Transient Bcl-x$_L$ induction contrasts with slower Bim suppression in response to Epo injection.

(A)   Time course of Bcl-x$_L$ mRNA expression following a single Epo injection (300 U /25 g), in freshly isolated and sorted spleen and bone-marrow EryA. Quantitative real-time PCR, data points are mean ±SEM of 3 independent experiments. Data are expressed relative to the β-actin mRNA and normalized to the value in bone-marrow EryA in saline-injected mice.

(B)   Bim protein expression in adult erythroid differentiation subsets 3 days following a single injection of either Epo (red, 300 U /25 g) or saline (black). Bim was measured by flow cytometry in freshly explanted tissue, as illustrated in Figure 4.8A. Data are mean ±SEM of n=21 mice for saline injection, and n=10 mice for Epo injection. *$p<0.000005$ (two-tailed t-test, unequal variance) for differences between Epo-injected and saline-injected mice.

(C)   Time course of Bcl-x$_L$ upregulation (red symbols, plotted on the left, red-numbered y-axis) and Bim suppression (black symbols, plotted on the right-numbered y-axis) in spleen (circles) and bone-marrow (BM, triangles) in response to a single Epo injection (300 U /25 g) on day 0. Includes a subset of the data plotted in panel 'B' (for Bim) and Figure 4.2E (for Bcl-x$_L$). For Bim, 5 experiments were normalized together. Bim data are mean ±SEM of n=21 mice for day 0, and n=3 to 10 mice for days 1 to 5. Bim ProE curves (black lines) for spleen and bone-marrow were hand-drawn. Statistical analysis was performed by comparing Bim readings on day 0 with readings on the following days. Where indicated, spleen ProE: *$p<0.005$. Spleen EryA: *$p<0.025$. BM

ProE: *p<0.02; BM EryA: *p<0.01. For all statistical tests, two-tailed t-test with unequal variance was used.

YL performed experiments for part (A) and Bcl-x$_L$ experiments for part (C). MK performed all the Bim experiments with help from AP, and analyzed data presented in this figure.

Figure 4.4
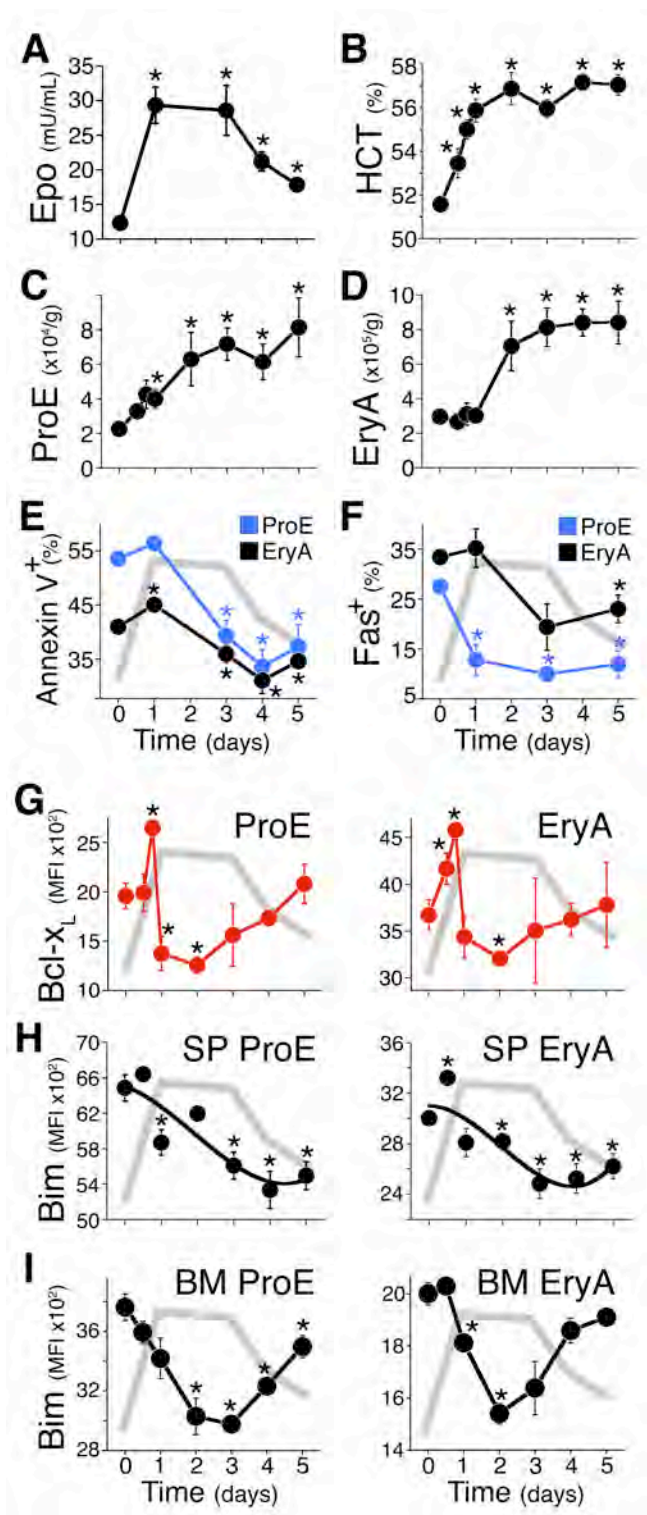
Figure 4.4   A reduced oxygen environment elicits a rapid, transient Bcl-x$_L$ induction and a slow, persistent Bim suppression.

(A – I) Mice were placed in a low oxygen chamber (11%) on day 0, for the numbers of days indicated.

(A)   Endogenous plasma Epo, assayed by ELISA. Data are mean ±SEM. Difference relative to day 0 (n=27 mice) were significant at the following levels: day 1 (n=6), *p=0.001; day 3 (n=6), *p=0.006; day 4 (n=12), *p<0.0001; day 5 (n=3), *p=0.0000005. This Epo time course is drawn as a grey line in panels E to I.

(B)   Daily hematocrit (HCT) measurements on blood collected immediately post-euthanasia. Data are mean ±SEM of n≥6 mice per time point. Differences from day 0 are significant at the following levels: 12h, *p=0.019; 18h to day 5, *p<0.0002.

(C-D) Absolute number of spleen ProE and EryA per gram body weight. Data pooled from 23 independent experiments. Each data point is mean ±SEM of n≥6 mice. Differences from day 0 (n=82 mice) are significant at the following levels: Spleen ProE day 1, *p=0.005; day 2, *p=0.047; days 3 to 5, *p≤0.005. Spleen EryA day 2, *p=0.034; days 3 to 5, *p≤0.001.

(E)   Annexin V binding in spleen ProE (blue) and EryA (black). Data points are mean ±SEM of 33 mice for day 0 and 3 to 7 mice for subsequent days, pooled from 2 to 5 independent experiments per day. Differences from day 0 are significant at the following values: Spleen ProE days 3 to 5, *p≤0.002. Spleen EryA day 1, *p=0.001; day 3, *p=0.03; day 4, *p=0.02; day 5, *p=0.001.

(F)   Fas-positive cell frequency in spleen ProE (blue) and EryA (black), measured by

flow cytometry in freshly explanted tissue. Data are mean ±SEM of n=26 mice, pooled from 4 experiments (day 0) or n=3 mice for subsequent days. Differences from day 0 are significant at the following values: Spleen ProE day 1, *p=0.024; day 3, *p<0.00001; day 5, *p=0.001. Spleen EryA day 5, *p=0.04.

(G)   Bcl-x_L protein expression in spleen ProE and EryA measured by flow cytometry in freshly explanted tissue. Data pooled from three independent experiments. Each data point is mean ±SEM of n≥3 mice. Differences from day 0 (n=17) are significant at the following levels: Spleen ProE 18h (n=3), *p<0.001; 24h (n=7), *p=0.019; day 2 (n=5), *p<0.0005. Spleen EryA 12h, *p=0.046; 18h, *p<0.0001; day 2, *p=0.02

(H-I)   Bim protein expression in spleen (H) and bone-marrow (I) ProE and EryA, measured by flow cytometry in freshly explanted tissue. Data are mean ±SEM of n≥3 mice pooled from two experiments. Differences from day 0 are significant at the following levels: Spleen ProE day 1, p=0.014; days 3-5, p<0.002. Spleen EryA day 0.5, p=0.0014; day 2, p=0.038; days 3-5, p<0.03. Bone-marrow ProE day 2, p=0.007; day 3, p<0.00001; day 4, p<0.001; day 5, p=0.04. Bone-marrow EryA day 1, p=0.002; day 2, p=0.0001; day 3, p=0.05.

For all statistical tests, two-tailed t-test with unequal variance was used.

MK performed all the experiments presented in this figure with help from AP, and analyzed all of the data.

Figure 4.5
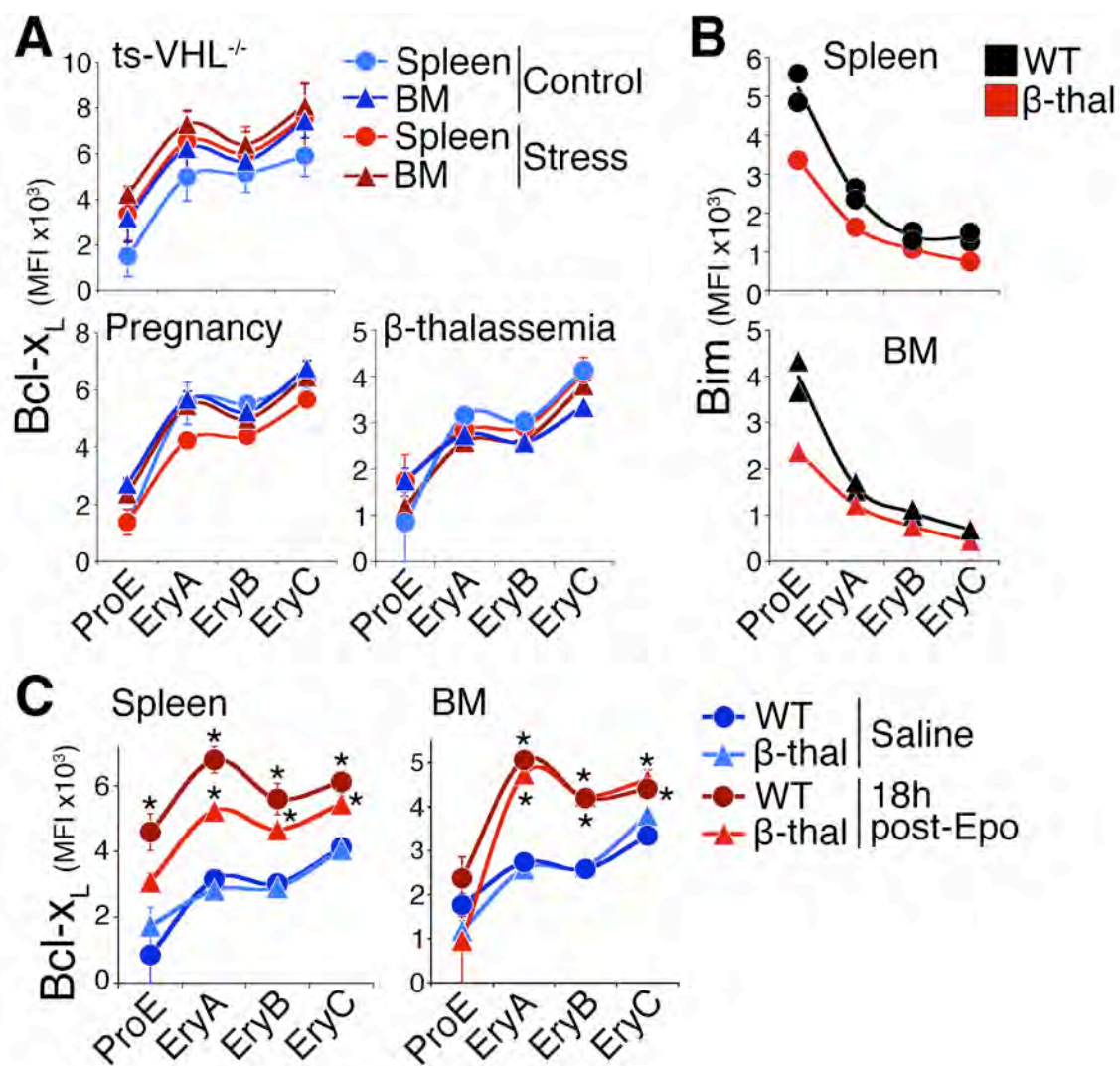
Figure 4.5   **The Bcl-x$_L$ response to chronic stress and to 'acute on chronic' stress.**

(A)   Bcl-x$_L$ expression in each of the three indicated mouse models of erythropoietic stress (red symbols) and matched controls (blue symbols), measured in freshly explanted tissue. Each data point is mean ±SEM of 2 to 4 mice. There were no statistically significant differences between chronic stress and control mice.

(B)   Representative experiment showing Bim expression in β-thalassemia mice in spleen (top) and bone-marrow (bottom). Two wild-type (black symbols) and one β-thalassemia mouse (red symbols) are shown.

(C)   The Bcl-x$_L$ response to an 'acute on chronic' stimulus. Bcl-x$_L$ expression in spleen and bone-marrow erythroblasts in β-thalassemia mice and matched controls, 18 hours following a single injection of either Epo (300 U /25 g, red symbols) or saline (blue symbols). Data points are mean ±SEM of n=3 to 4 mice. Representative of 4 independent experiments. Statistically significant differences in Bcl-x$_L$ between Epo and saline injections in each mouse model were seen in wild-type spleen ProE, *p=0.025; EryA, *p=0.0009; EryB, *p=0.01; EryC, *p=0.006; β-thalassemia spleen EryA, *p=0.0004; EryB, *p=0.004; EryC, *p=0.03; Wild-type BM EryA, EryB and EryC, *p≤0.0005; β-thalassemia BM EryA and EryB, *p<0.0005; EryC, *p=0.025. The increase in spleen EryA Bcl-x$_L$ was significantly higher (p=0.023) in wild-type spleen than in wild-type β-thalassemia mice. For all statistical tests, two-tailed t-test with unequal variance was used.

MK performed β-thalassemia experiment in part (A), and all of experiments in parts (B) and (C), with help from AP [part (C)]. YL performed the rest of experiments

shown in part (A). MK analyzed all the data in part (A) for β-thalassemia, and in parts (B) and (C).

Figure 4.6
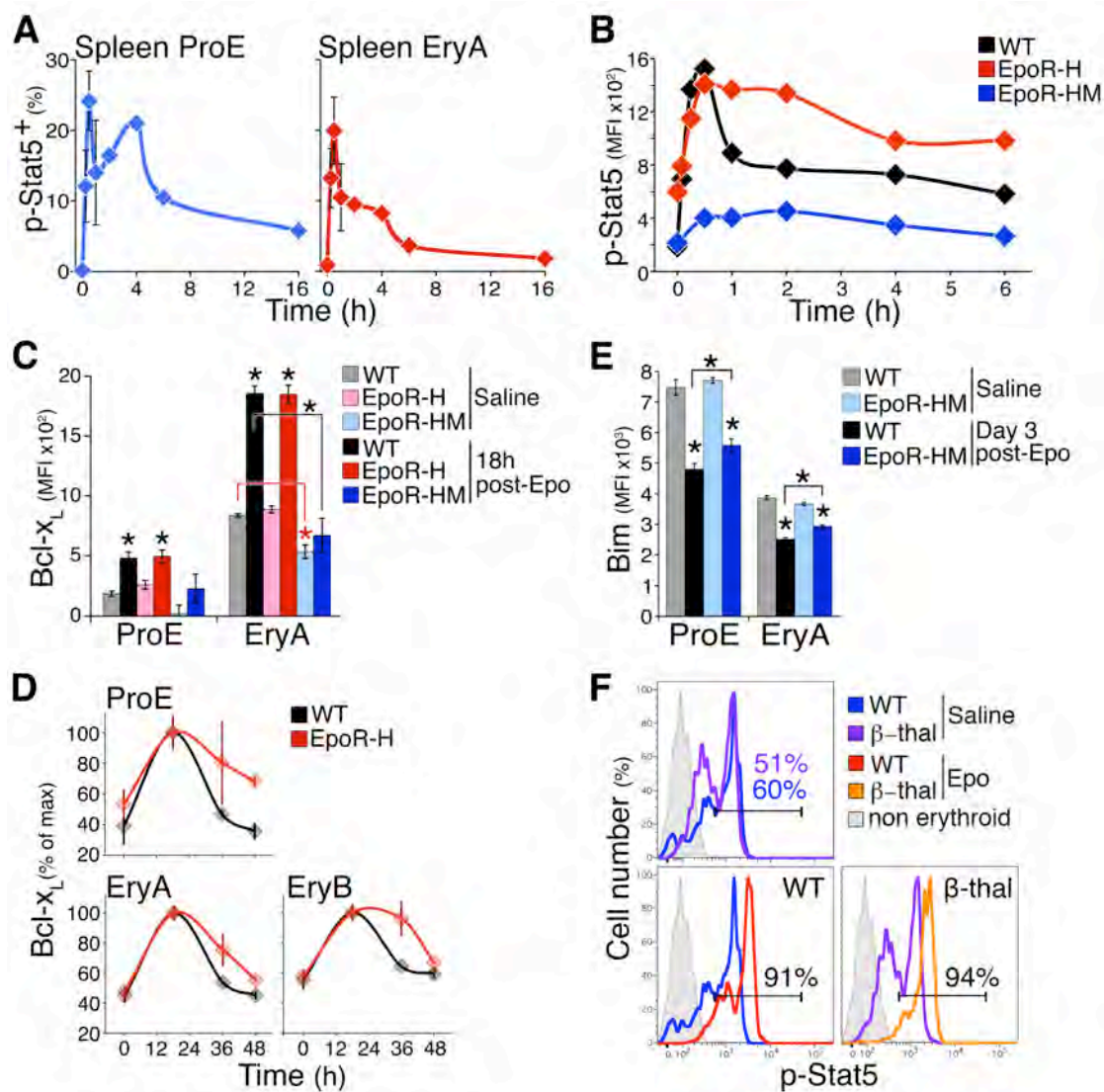
Figure 4.6   Adaptation in the Bcl-x$_L$ and p-Stat5 responses is dependent on the EpoR C-terminal cytoplasmic domain.

(A)   The p-Stat5 response in spleen ProE and EryA *in vivo*, measured in freshly explanted spleen at the indicated time points following a single Epo injection (300 U /25 g). Data are pooled from four independent experiments. Each time point is the mean ± SEM of data from 2 to 4 mice.

(B)   The p-Stat5 time course in response to Epo stimulation for the indicated periods. Freshly harvested fetal liver cells from EpoR-HM, EpoR-H and matched wild-type embryos at E13.5 were stimulated *in vitro* with 2 U/mL Epo. p-Stat5 in S1 cells is shown, expressed as median fluorescence intensity above background (isotype-control antibody). Representative of 3 similar experiments.

(C)   The Bcl-x$_L$ response in EpoR-H and EpoR-HM mice. Bcl-x$_L$ was measured 18 hours following a single injection of either Epo or saline, in freshly explanted spleen ProE and EryA of EpoR-H, EpoR-HM or wild-type controls. Data are mean ±SEM of n=3 to 5 mice per bar. Significant Bcl-x$_L$ increase from basal levels in spleen ProE and EryA was seen in Epo *vs.* saline injected wild-type (black) and EpoR-H (red) mice (stars without brackets: WT ProE *p=0.003; EpoR-H ProE *p=0.012; WT EryA *p=0.00004; EpoR-H EryA *p=0.0001), but not in EpoR-HM mice. Bcl-x$_L$ was reduced in basal state EpoR-HM spleen EryA (red star with red bracket, *p=0.027) compared with wild-type basal control. Bcl-x$_L$ induction in wild-type spleen EryA was significantly above that of EpoR-HM EryA (black stars with brackets, *p=0.007, two-tailed t-test with unequal variance).

(D)   Time course of the Bcl-x_L response in EpoR-H mice and in matched wild-type controls, following a single Epo injection (300 U /25 g). Measurements were made in freshly explanted spleen at the indicated time points. Bcl-x_L is significantly higher in EpoR-H at 36 and 48 hours ($p<0.005$, paired t-test on all subsets).

(E)   Bim protein in spleen ProE and EryA of wild-type and EpoR-HM mice on day 3 following a single Epo injection (300 U /25 g). Data are mean ±SEM of n=4 to 5 mice per bar. There was no significant difference in basal Bim between EpoR-HM and wild-type control mice. Bim was significantly suppressed following Epo injection (*$p<0.001$). Bim was suppressed by a significantly smaller extent in EpoR-HM ProE and EryA subsets (stars with brackets, *$p=0.03$ and *$p=0.001$, respectively, two-tailed t-test with unequal variance).

(F)   The p-Stat5 histograms *in vivo* at peak response (30 minutes) following a single injection of either Epo (300 U /25 g) or saline, in either β-thalassemia mice or in matched wild-type controls, measured in freshly explanted spleen ProE. The p-Stat5$^+$ gate was drawn based on the non-erythroid population in spleen (grey histograms).

EP developed and performed experiments, and analyzed the data shown in parts (A), (B) and (F). MK performed all of the experiments and data analysis in parts (C-E).

Figure 4.7
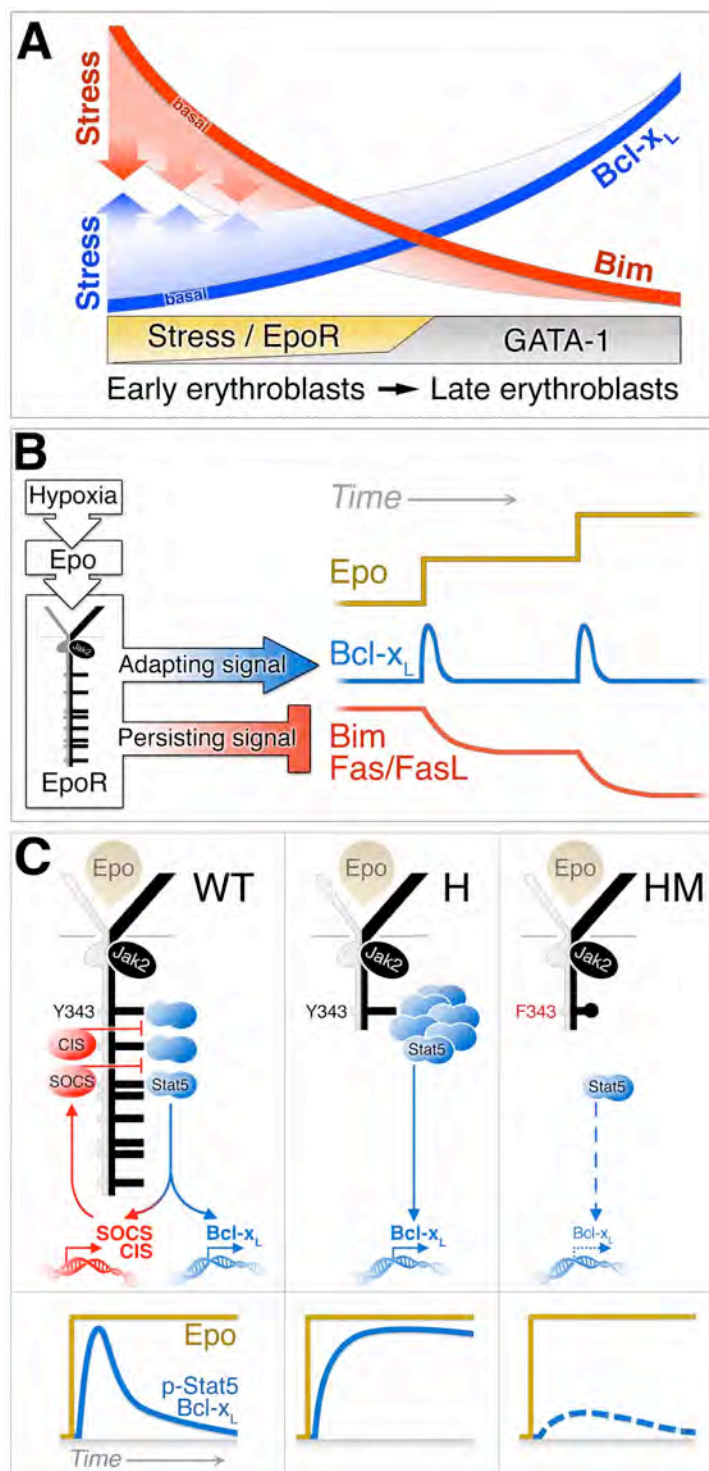
Figure 4.7   Regulation of Bcl-x$_L$ and Bim expression in erythropoiesis.

(A)   Model depicting expression of Bcl-x$_L$ and Bim in the late and early erythroblast compartments, in basal erythropoiesis (solid lines) and during stress (fading shaded area). GATA-1 induces Bcl-x$_L$ and suppresses Bim with differentiation, with maximal responses achieved in late erythroblasts. During stress, EpoR signaling operates principally in the early erythroblast compartment, accelerating both Bim suppression and Bcl-x$_L$ induction. Model does not quantitatively depict the actual data.

(B)   Contrasting dynamic stress responses of the Bcl-x$_L$, Bim and Fas pathways, both driven by the EpoR in the early erythroblast compartment. A sudden increase in stress drives a rapid, but transient adapting Bcl-x$_L$ response. This response is re-activated with a further change in the stress level, but is insensitive to the absolute level of stress. Bim and Fas suppression in response to stress is slower but persistent and reflects the level of stress.

(C)   Mechanism of adaptation in the Bcl-x$_L$ response. EpoR-HM activation of both p-Stat5 and the Bcl-x$_L$ is drastically attenuated, due to the absence of Stat5 phosphotyrosine docking sites on the EpoR-HM mutant receptor, in support of the role of p-Stat5 in the EpoR and stress-induced Bcl-x$_L$ induction. In wild-type mice, the EpoR distal cytoplasmic domain binds p-Stat5-activated negative regulators of Jak2 and Stat5 such as SOCS3, SOCS2 and CIS, limiting the duration of both the p-Stat5 and the Bcl-x$_L$ responses. In EpoR-H mice, absence of the distal EpoR domain results in a prolonged response and loss of adaptation.

MK designed and created all parts of this figure.

Figure 4.8
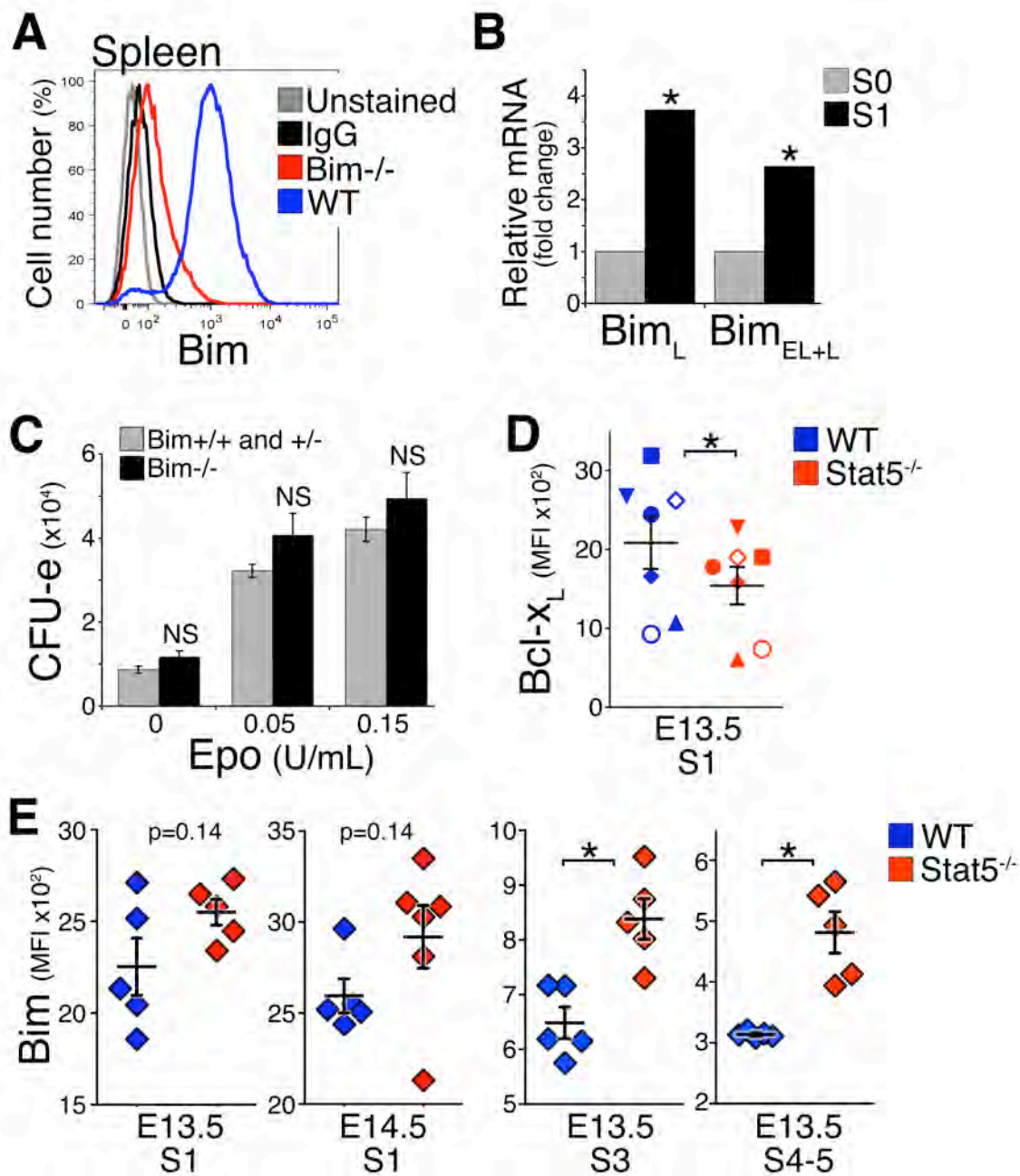
Figure 4.8   Bim and Bcl-x$_L$ in fetal liver erythropoiesis.

(A)   Bim protein measurement by intracellular flow cytometry. Freshly explanted spleen cells from wild-type (blue) and Bim$^{-/-}$ (red) mice were stained with the LIVE/DEAD viability dye, fixed, permeabilized, and stained with an anti-Bim antibody (Cell Signaling, #2819) or isotype control IgG, as described in materials and methods. Dead cells were excluded from analysis. Highly similar data were obtained when gating on erythroid subsets in spleens of wild-type and Bim$^{-/-}$ mice.

(B)   Quantitative real-time PCR for the Bim isoforms Bim$_{EL}$ and Bim$_L$ in sorted S0 and S1 subsets from freshly harvested wild-type fetal liver. Data were expressed as a ratio to β-actin mRNA in each sample and normalized to the levels measured in S0 cells. Differences between S0 and S1 are statistically significant, Bim$_{EL+L}$, *p=0.0003; Bim$_L$, *p=0.0000004 (two-tailed t-test, unequal variance).

(C)   CFU-e assay performed on wild-type and Bim$^{-/-}$ fetal livers. CFU-e colonies per whole fetal liver are shown for each genotype. Data are mean ±SEM of 6 individual fetal livers per genotype from the same E13.5 litter. Grey bars are a pool containing one Bim wild-type embryo and five Bim$^{+/-}$ embryos. No significant (NS) difference in CFU-e numbers between the genotypes was observed (p>0.05, two-tailed t-test, unequal variance). Similar results were obtained when data were expressed as CFU-e colonies per 1x10^6 plated cells. Representative of two similar experiments.

(D)   Lower Bcl-x$_L$ expression in Stat5$^{-/-}$ embryos compared with wild-type littermate controls, at the indicated embryonic day and differentiation subset. n=11 to 21 embryos per genotype, with each symbol type representing median expression for one litter.

Means ±SEM for the population are indicated. Statistical significance values: E13.5 S1, *p=0.012 (paired t-test).

(E)   Higher Bim protein expression in Stat5^{-/-} embryos compared with wild-type littermate controls: data points are individual embryos. Mean ±SEM for the population is shown. Statistical significance values: E13.5 S3 and S4-5, *p<0.01, two-tailed t-test, unequal variance.

MK performed experiments, analyzed and presented the data shown in parts (A) and (C-E). KH helped MK perform experiments in part (C), and also performed experiments for part (B).

Figure 4.9
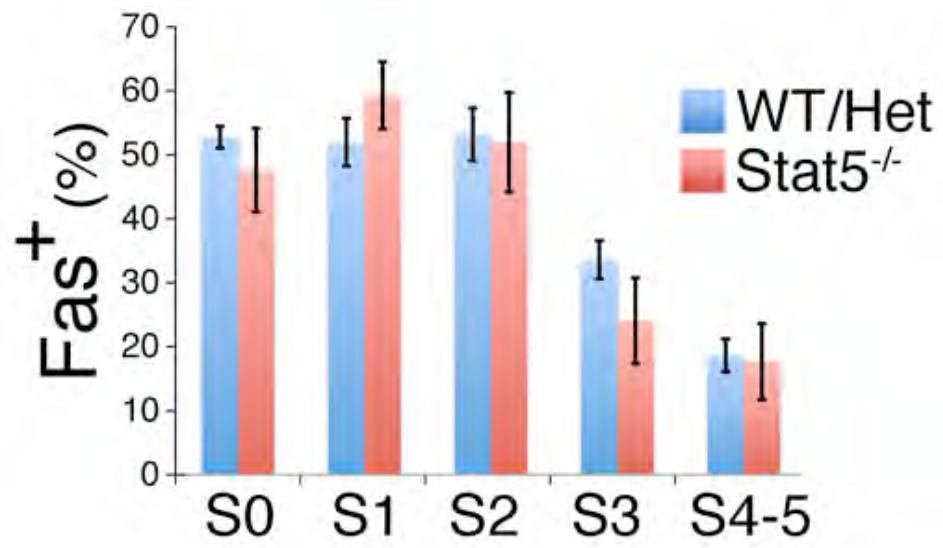
Figure 4.9   Fas expression in E14.5 fetal liver erythroblasts.

Cell-surface Fas was measured on freshly explanted fetal livers from wild-type or Stat5 heterozygous embryos (n=6) and from Stat5$^{-/-}$ embryos (n=3). No significant differences were detected between the genotypes (two-tailed t-test, unequal variance).

MK performed experiment and analyzed the data presented in this figure.

Figure 4.10
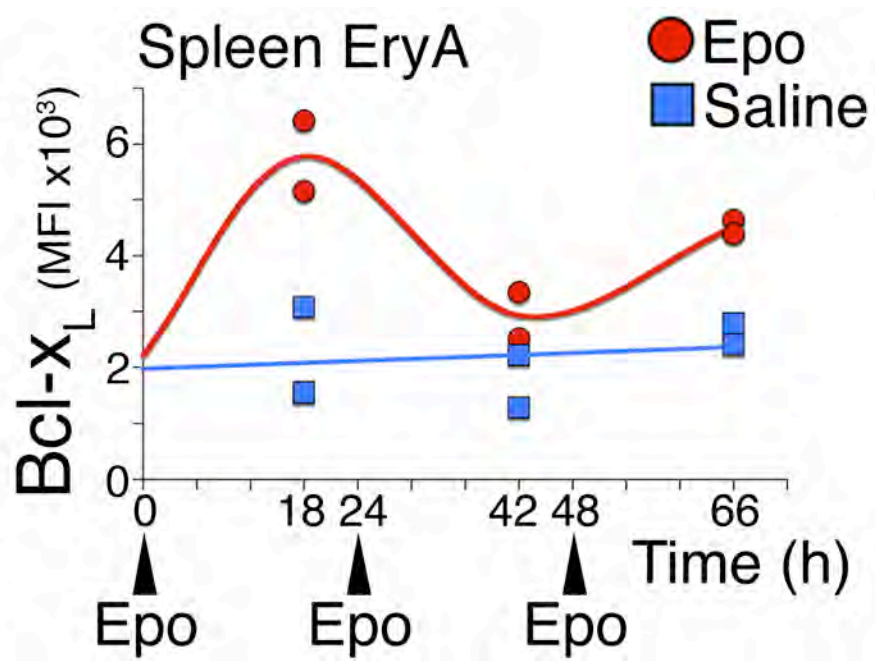
Figure 4.10   The Bcl-x$_L$ response to repeated Epo injections.

Bcl-x$_L$ expression in spleen EryA following consecutive Epo injections. Wild-type mice were injected at time points 0, 24 and 48 hours with either Epo (300 U /25 g, indicated with arrowheads) or with saline. Bcl-x$_L$ expression was assayed by flow cytometry in 2 mice for each treatment, 18 hours following each injection.

YL performed this experiment and analyzed the data.

Figure 4.11
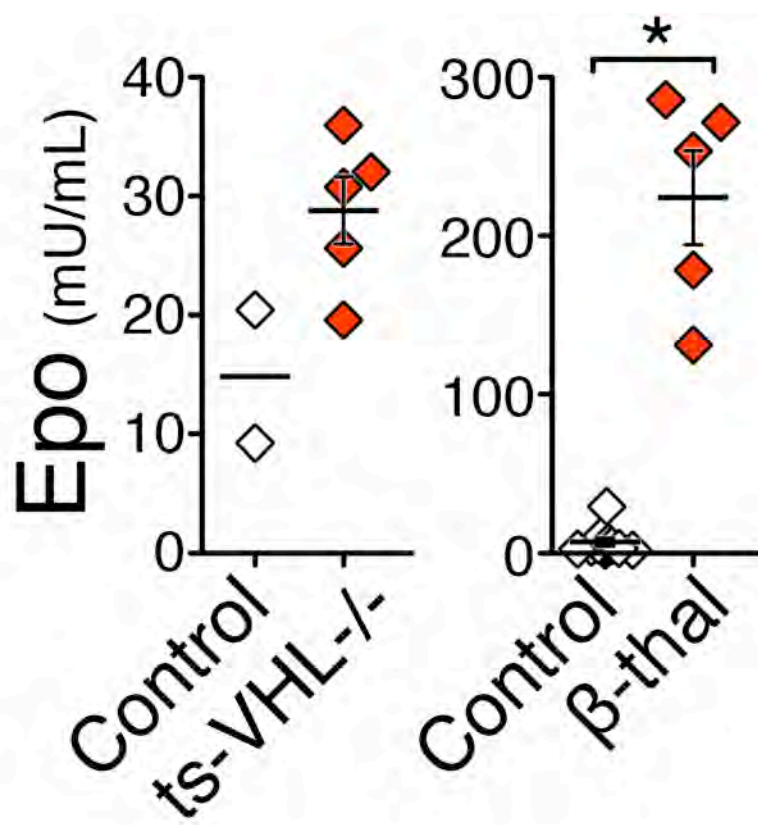
**Figure 4.11   Plasma Epo measurements in mice with β-thalassemia and in ts-VHL⁻
/⁻ mice.**

For each mouse model, two independent ELISAs, each with similar results, were
pooled together. Individual mouse data as well as mean ±SEM are shown. Epo increase
in β-thalassemia was significant at p=0.002 (two-tailed t-test, unequal variance).

MK performed all of the experiments and data analysis presented in this figure.

Figure 4.12
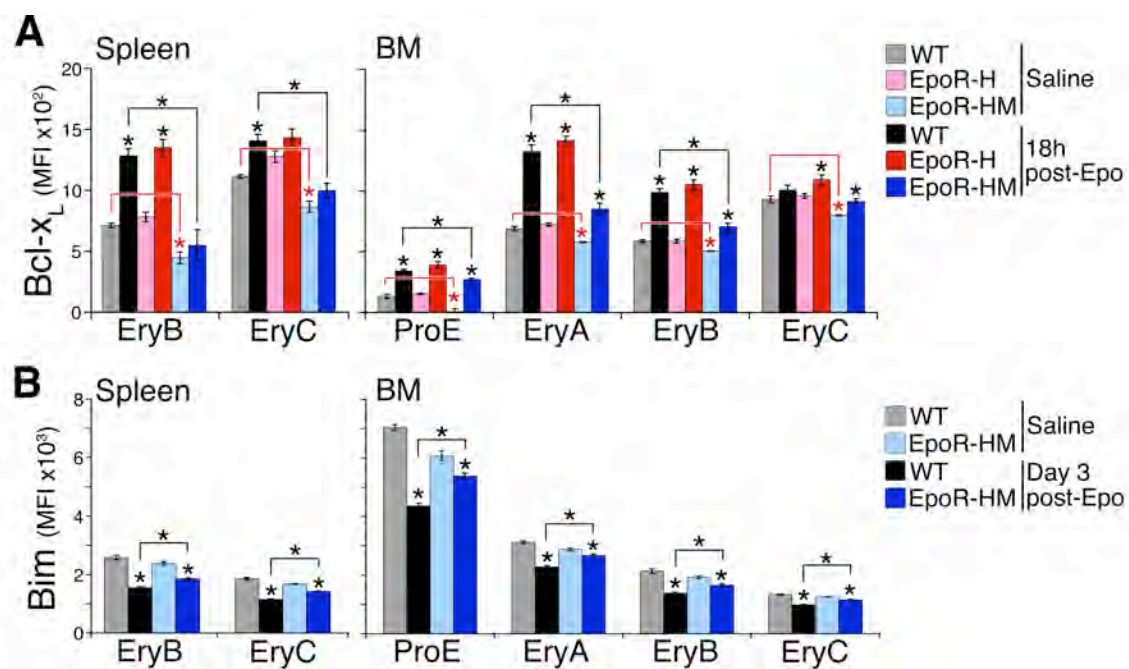
Figure 4.12   The Bcl-x$_L$ and Bim Epo responses in the EpoR-H and EpoR-HM mice.

Experiment and same mouse dataset as in Figure 4.6C and 4.6E.

(A)   Bcl-x$_L$ expression in spleen (left) and bone-marrow (right) in erythroid subsets, 18 hours post-Epo or saline injection in wild-type, EpoR-H, and EpoR-HM mice. Experiment and same mouse dataset as in Figure 4.6C.

Left panel: Black stars without brackets indicate significant Bcl-x$_L$ induction in spleen EryB and EryC subsets in Epo treated mice (*p<0.005). No significant Bcl-x$_L$ induction was observed in EpoR-HM spleens (light blue *vs.* dark blue bars). EpoR-HM mice failed to increase Bcl-x$_L$ to the level of EpoR-H or wild-type mice (black stars with brackets, *p<0.02). Basal Bcl-x$_L$ levels in EpoR-HM EryB and EryC were also lower than in basal wild-type mice (red stars with red brackets, *p<0.05).

Right panel: Bcl-x$_L$ induction in the bone-marrow erythroid subsets was observed for all three genotypes. Stars indicate significant differences. Wild-type Epo response *vs.* control: ProE, EryA and EryB, *p<0.0002. EpoR-H Epo response *vs.* control: ProE, EryA and EryB, *p<0.0001; EryC, *p=0.025. EpoR-HM Epo response *vs.* control: ProE, *p=0.003; EryA, EryB and EryC, *p<0.05. Magnitude of Bcl-x$_L$ induction in EpoR-HM subsets was lower compared with wild-type induction (black stars with brackets, *p<0.006). Basal Bcl-x$_L$ levels in EpoR-HM bone-marrow subsets were lower than in basal wild-type mice (red stars with red brackets, *p<0.02).

(B)   Bim expression in spleen (left) and bone-marrow (right) in erythroid subsets, 3 days following Epo or saline injection in wild-type, EpoR-H, and EpoR-HM mice.

Experiment and same mouse dataset as in Figure 4.6E. Data are mean ±SEM of n=4 to 5 mice per bar.

In both wild-type and EpoR-HM spleen EryB and EryC subsets, Bim was significantly suppressed below their respective basal levels with Epo (black stars, no brackets, *p<0.001). Similar findings were observed in the bone-marrow subsets (wild-type subsets: *p<0.0005; EpoR-HM subsets: *p<0.03). Magnitude of Bim suppression in EpoR-HM mice was lower than in the wild-type mice (black stars with brackets, *p<0.005). Some differences in basal Bim levels were observed between wild-type and EpoR-HM mice (gray bars *vs.* light blue bars, *not* indicated in plots: spleen EryB, p=NS; spleen EryC, *p=0.02; BM ProE, *p=0.004; BM EryA, *p=0.01; BM EryB, p=NS; BM EryC, *p=0.03).

For all statistical tests, two-tailed t-test with unequal variance was used.

MK performed all of the experiments and data analysis presented in this figure.

Chapter V Attributions and Copyright Information

The work in this chapter has been accepted for publication in Journal of Visual Experiments (JoVE) in a modified format.

Identification and analysis of mouse erythroid progenitors using the CD71/Ter119 Flow-cytometric assay

Miroslav Koulnis*, Ramona Pop*, Ermelinda Porpiglia*, Jeffrey R. Shearstone*, Daniel Hidalgo and Merav Socolovsky**.**

*contributed equally to this work.

Specific Authorship Contributions:

MK contributed to writing the adult tissue staining protocol (harvesting of adult spleen and bone marrow, staining cells with antibodies against surface CD71, Ter119 and Fas). MK contributed to filming of spleen cell isolation and blood drawing, and created Figures 5.1 and 5.2A. Figure 5.1 was used by JoVE editors to create parts of the film (Figure 5.1 represents original design work by MK). MK also tested CD44 staining discussed in this chapter, and contributed to writing 'Intracellular antigens' and 'Interpretations of changes in the frequency of erythroid subsets' sections of the discussion.

Disclosure of Conflicts of Interest:

None of the authors have any conflicts of interest to declare.

CHAPTER V

IDENTIFICATION AND ANALYSIS OF MOUSE ERYTHROID PROGENITORS USING THE CD71/TER119 FLOW-CYTOMETRIC ASSAY

SHORT ABSTRACT

A flow-cytometric method for identification and molecular analysis of differentiation-stage-specific murine erythroid progenitors and precursors, directly in freshly-harvested mouse bone marrow, spleen or fetal liver. The assay relies on cell-surface markers CD71, Ter119, and cell size.

INTRODUCTION

The study of erythropoiesis aims to understand how red cells are formed from earlier hematopoietic and erythroid progenitors. Specifically, the rate of red cell formation is regulated by the hormone erythropoietin (Epo), whose synthesis is triggered by tissue hypoxia. A threat to adequate tissue oxygenation results in a rapid increase in Epo, driving an increase in erythropoietic rate, a process known as the erythropoietic stress response. The resulting increase in the number of circulating red cells improves tissue oxygen delivery. An efficient erythropoietic stress response is therefore critical to the survival and recovery from physiological and pathological conditions such as high altitude, anemia, hemorrhage, chemotherapy or stem cell transplantation.

The mouse is a key model for the study of erythropoiesis and its stress response. Mouse definitive (adult-type) erythropoiesis takes place in the fetal liver between

embryonic days E11.5 and E15.5, in the neonatal spleen, and in adult spleen and bone marrow. Classical methods of identifying erythroid progenitors in tissue rely on the ability of these cells to give rise to red cell colonies when plated in Epo-containing semi-solid media. Their erythroid precursor progeny are identified based on morphological criteria. Neither of these classical methods allow access to large numbers of differentiation-stage-specific erythroid cells for molecular study. Here we present a flow-cytometric method of identifying and studying differentiation-stage-specific erythroid progenitors and precursors, directly in the context of freshly isolated mouse tissue (Figure 5.1). The assay relies on the cell-surface markers Ter119, CD71, and on the flow-cytometric 'forward-scatter' parameter, which is a function of cell size. The CD71/Ter119 assay can be used to study erythroid progenitors during their response to erythropoietic stress *in vivo*, for example, in anemic mice or mice housed in low oxygen conditions. It may also be used to study erythroid progenitors directly in the tissues of genetically modified adult mice or embryos, in order to assess the specific role of the modified molecular pathway in erythropoiesis.

PROTOCOL

1   Harvesting of tissues:

    1.1 Prepare tubes containing 2 to 5 mL cold staining buffer (phosphate-buffered saline (PBS) with added 0.2% BSA and 5mM glucose). Keep tubes on ice prior to tissue harvest.

1.2 Cull mice according to appropriate approved protocol (e.g. CO_2 inhalation followed by cervical dislocation).

1.3 Draw blood by cardiac puncture into EDTA or heparin blood-collection tubes for later analysis (e.g. hematocrit, reticulocyte count or CBC analysis).

1.4 Harvest the spleen and bones, placing tissues from each mouse in a separate tube, prepared in step 1. Easy access to spleen is from the left side. For the bone marrow, harvest one or both femurs. Keep tubes with harvested tissue on ice.

1.5 If desired, weigh the spleen. Mice undergoing an erythropoietic stress response are likely to show a significant increase in spleen weight.

2 Preparation of spleen cells:

2.1 Using a pre-moistened 3 mL syringe plunger, gently push the spleen, or part of the spleen (ideally, 0.1 gram or less, equivalent to approximately 10^8 cells) through a 40 µm sterile cell strainer (Fisherbrand catalog number 22363547 or other) placed on top of a 50 mL conical tube. Keep the tube on ice during this procedure. Wash the cells through the strainer with a total of 2 mL staining buffer.

2.2 Gently pipette the strained cell suspension to break up any small clumps. If necessary, re-strain the cells.

2.3 Wash the cells twice by centrifugation and resuspend in cold buffer. For centrifugation, spin for 3' to 5' at approximately 1400 RPM at 4°C.

2.4 Count the cells using a hemocytometer. Typical yields are 1-2 x 10^8 cells/spleen. For flow cytometry analysis, aliquote 1 to 2 x 10^6 cells per sample, either into

FACS staining tubes (BD Falcon polystyrene round-bottom tubes, 352008) or U-bottom 96 well plate (BD Falcon 353910). Sample staining volume is 200 μl, to a final cell concentration 0.5 to 1 x 10^7 cells/mL or 1-2 x 10^6 cells/ 200 μl sample.

3   Preparation of bone marrow cells:

3.1 Prepare 1 or 3 ml syringes with an attached 26G needle, pre-filled with cold staining buffer.

3.2 Remove muscles attached to the femur so as to visualize the bone clearly.

3.3 Using sharp surgical scissors, snip off both ends of the femur, as close as possible to the ends of the bone. This should reveal a small hole at each cut end, leading into the bone-marrow cavity, which runs through the length of the femur.

3.4 Using the pre-filled syringe in step 1, insert the needle through one of these holes, and gently flush the marrow out through the hole at the other end into a tube.

3.5 Dissociate the flushed cells by gentle pipetting, and strain through a 40 μm strainer as for the spleen above (see section **2.1**).

3.6 Wash cells twice by centrifugation in cold staining buffer.

3.7 Count the cells and resuspend as in section **2.4**. Typical yields are approximately 10^7 cells per femur.

4   Preparation of fetal liver cells:

4.1 To prepare timed-pregnant female mice, set up mice for mating in the evening; examine for vaginal plugs before 10 am the following day; the day on which the

vaginal plug is detected is considered day 0.5. Veterinary staff may be able to assist investigators who are unfamiliar with this technique to identify pregnant females.

4.2 Timed-pregnant female mice are culled on days E11.5 to 14.5 of pregnancy. The uterine horns are removed into a Petri-dish containing ice-cold culture medium or staining buffer.

4.3 Embryos are removed from each uterus and the fetal liver is dissected. A dissecting microscope is required for E12.5 embryos or younger.

4.4 Livers may be dissociated mechanically by pipetting in buffer, and are processed either individually in 96-well plates, or pooled together, depending on experimental requirements.

4.5 A fetal liver at E13.5 has ~10^7 cells. Cells are washed twice in staining buffer and resuspended at 1-2 x 10^6 cells/ 200 µl sample for flow-cytometric analysis.

5 Antibody staining for flow cytometry:

5.1 Prepare a primary antibody staining pre-mix to be used for all samples, except for control samples, containing the following:

- ChromePure Rabbit IgG (Jackson, 015-000-003), to a final concentration of 200 µg/mL. Check the stock concentration on the bottle (it can vary). This is used to block Fc receptors in mouse cells; alternative species that may be used for this are mouse IgG or rat IgG. Species choice is determined by the potential presence in the staining protocol of secondary antibodies directed

against primary rat/mouse/rabbit antibodies, in which case those species cannot be used as blocking antibodies. Alternatively, 5% rabbit serum may also be used in place of purified IgG. A further alternative is the use of monoclonal antibodies or Fab fragments directed at the mouse Fc receptors. The basic protocol below does not include any secondary antibodies and so IgG of any of the three species may be used.

- CD71-FITC, diluted 1:200 (stock 0.5 mg/mL, BD-Biosciences, 553266)

- Ter119-PE, diluted 1:200 (stock 0.2 mg/mL, BD-Biosciences, 553673)

- Any additional antibodies directed at surface epitopes of interest, e.g. antibodies directed at Fas or FasL (final concentration 5 µg/mL) (see [42,44]). Mix the antibody solution gently by inverting the tube 2-3 times.

5.2 Add 200 µl of the pre-mix to each cell sample and gently resuspend the cells.

5.3 Prepare control cell samples as follows:

- 'Unstained': these cells are left in staining buffer and provide the background autofluorescence of the cells.

- 'Single color' controls: one such control is required for each antibody/color used in the protocol. The cells in these controls are stained either with a directly conjugated primary antibody, or with both a primary antibody and a conjugated secondary antibody. These controls are used to correct for spectral overlap between channels.

- 'Fluorescence minus one' (FMO) controls: one such control is required for each antibody/color in the protocol: cells are stained with all the

colors/antibodies in the protocol except for the color/antibody for which this is the FMO control. The FMO control for a particular channel provides the true background for that channel. It may include non-specific antibody of the same isotype, and conjugated with the same fluorescence mark as the test antibody (isotype control).

5.4 Incubate samples and relevant controls in the primary antibody stain on ice for 45' to 1 hour in the dark (put aluminum foil cover on ice-bucket).

5.5 At the end of incubation, wash the cells by adding 3 mL of staining buffer to each sample tube and spin for 3' to 5' at approximately 1400 RPM at 4°C. If using 96 well plates, wash the cells three times in a volume of 200 µl.

5.6 If relevant, apply secondary antibody stain. Apply and wash as for the first antibody stain.

5.7 If relevant, a stain with Annexin V (apoptosis marker) is applied at the end of incubation, using a Hepes buffer as in the manufacturer's instructions. This stain is applied for 15 minutes at room-temperature, or for 1 hour on ice.

5.8 Cells are resuspended for flow cytometry analysis in staining solution containing a cell-impermeable DNA dye, to exclude dead cells. Several DNA dyes are available, including Propidium Iodide, 7-amino-actinomycin D (7AAD), or DAPI. The choice from amongst these depends on the available flow-cytometer channels, given the channels taken up for specific antibody staining, and channels available on the flow-cytometer. 7AAD is obtained from BD-Biosciences (559925) and used according to the manufacturer's instructions. For DAPI

staining, make a stock of 1 mg/mL in dimethylformamide (DMF) from powder (Roche, 236276), keep at -20°C, and dilute 1:10,000 to 1:15,000 in staining buffer.

6 **Flow-cytometric sorting:**

6.1 Cells are labeled with CD71, Ter119, and a viability dye as described for flow-cytometric analysis (section **5**). Cell concentration during labeling may be increased to 5 x 10^7/mL.

6.2 Antibody labeling for lineage-positive non-erythroid cells may be added with the primary antibody stain, if required, as follows:

Mix an equal volume of each of the following antibodies to make the lineage master mix:

FITC Rat Anti-Mouse CD41 MWReg30, BD Pharmingen 553848

FITC Rat Anti-Mouse CD45R/B220 RA3-6B2, BD Pharmingen 553087

FITC Hamster Anti-Mouse CD3e 145-2C11, BD Pharmingen 553061

FITC Rat Anti-Mouse CD11b/Mac-1 M1/70, BD Pharmingen 557396

FITC Rat Anti-Mouse Ly-6G and Ly-6C (Gr-1) RB6-8C5, BD Pharmingen 553126

Use the master mix at 1:80 (This is equivalent to 1:400 dilution of each individual antibody stocks, which are all 0.5 mg/mL).

6.3 Use low-pressure sorting conditions and wide nozzles. For the Aria (BD Biosciences) we use 100 µ nozzle, 20 psi pressure.

6.4 Collection buffer: PBS with added 20% Fetal Bovine Serum.

6.5 To check the purities of the sorted populations, re-run a small aliquot from each sample in a buffer that contains a viability dye (7AAD or similar).

REPRESENTATIVE RESULTS

CD71/Ter119 staining of adult bone marrow or spleen identifies a developmental sequence of four subsets, labeled ProE, EryA, EryB and EryC (Figure 5.2) [42]. Morphologically, these correspond to increasingly mature erythroblasts. Figure 5.2 illustrates the gating sequence at the data analysis stage, which discards very small event (including nuclei, red cells), aggregated cells and dead cells.

Expression of cell-surface proteins may be measured simultaneously for each of these subsets, by adding the relevant antibodies at the same time as Ter119 and CD71 staining. Figure 5.2 shows an example of cell-surface expression of the death receptor Fas [42]. This measurement was carried out in mice injected with Epo, or in control mice injected with saline. It is apparent that Epo suppresses Fas expression in the EryA population *in vivo* [42].

Expression of intracellular proteins or cell cycle status may also be measured for cells in each subset. Figure 5.3 illustrates representative cell cycle analysis of freshly harvested bone-marrow cells. These measurements require, in addition to cell-surface staining with CD71 and Ter119, the fixation and permeabilization of cells for intracellular labeling (see Discussion section).

In fetal liver, non-erythroid cells are first excluded by gating on 'Lin⁻' cells that are negative for CD41, Mac-1, Gr-1, B220 and CD3 (Figure 5.4). The remaining cells are sub-divided into 6 subsets, S0 to S5. The precise pattern of cells in fetal liver is dependent on embryonic age (see Discussion section). A representative cell cycle analysis of the S3 subset in E13.5 fetal liver is shown (Figure 5.5).

DISCUSSION

The flow-cytometric methodology allows simultaneous investigation of any cellular function that may be detected with a fluorescence-conjugated specific antibody or ligand, including cell-surface markers, protein expression, cell survival, cell signaling using phospho-specific antibodies [184], and cell cycle status. These measurements may be made in each of a number of differentiation-stage specific subsets, in the context of freshly isolated erythropoietic tissue. This method therefore allows assessment of functional and molecular changes at different levels of the erythropoietic system, in response to a wide range of erythropoietic stimuli or as a result of genetic mutations.

No antibody is without cross-reactivity, and cross-reactivity may be tissue-specific. It is therefore important to verify, even for previously tested antibodies, their specificity in the context of erythropoietic tissue, using either a null or a knock-down cell model.

Cells from specific erythroid subsets may be sorted for RNA or transcriptome analysis. Sort experiments should use low sorting pressures and wide nozzles, in order to minimize the shear stress on the cells. We recommend checking cell purity and viability

following each sorting experiment. Of note, in the case of multiparameter flow cytometry, the true background for each color is its 'FMO' control (see **5.3**), which includes, in addition to autofluorescence, the background due to spectral overlap from all other colors. At the analysis stage, a subset-specific 'FMO' control needs to be used.

Differentiation stage of erythroblasts within the flow-cytometrically defined subsets

The flow-cytometric ProE/EryA/EryB/EryC subsets are defined in terms of cell-surface marker expression and forward scatter. While it is likely that each of these subsets corresponds to approximately the same morphological erythroblast differentiation stage in a wide variety of mouse models, we recommend verifying this when examining a new mouse model. Cells from each of the flow-cytometrically-defined subsets should be sorted and cytospin preparations examined for morphological staging of erythroblasts.

Although the CD71/Ter119 subsets each contain erythroblasts of similar differentiation stage, there remains a degree of heterogeneity within each subset. In the first application of the CD71/Ter119 method, we divided Ter119$^+$ cells into regions I to IV based on their CD71 expression. The precise borders between these regions were determined arbitrarily [43]. We subsequently added cell size information to the analysis, in the form of the forward scatter parameter. This allowed us to divide Ter119^{high} cells into subsets by following natural population contours [42] (Figure 5.2). This approach resulted in populations of more uniform maturation and in more reproducible results, and has been recently adapted by other investigators [155,185,186]. The EryA subset may be subdivided further where desired [186]. One group suggested the use of CD44 in place of CD71 [47].

Although CD44 is less useful in resolving early erythroblast stages, it may resolve later erythroblast subsets with more precision. Both markers may therefore be used, or alternatively, their choice may depend on the specific subsets of interest.

An alternative strategy employs multispectral imaging using the ImageStream technology (Amnis Corporation, Seattle, WA) [48]. It allows the simultaneous and rapid acquisition of both morphological and flow-cytometric data on many thousands of cells. It is likely to become the 'gold standard' with respect to molecular analysis of stage-specific erythroblasts, since the morphological criteria by which differentiation stage is defined may be measured directly. However, at the present time this technology is less widely available than conventional flow cytometry, and suffers from two drawbacks: it does not allow cell sorting; and it is limited to a smaller number of flow-cytometric parameters.

Intracellular antigens

Detection of intracellular proteins or BrdU requires cell fixation and permeabilization. The precise fixation and permeabilization procedure depends on the intracellular antigen in question. We use the LIVE/DEAD Fixable Dead Cell Stain (Molecular Probes) during the fixation procedure, to distinguish viable from dead cells. Of note, permeabilization with detergents usually impacts the Ter119 signal, which is partially detergent soluble. We overcome this difficulty by using gentle detergents (such as the saponin-based 'perm/wash' buffer from BD Biosciences). We also stain for Ter119 both prior to, and following, the fixation & permeabilization procedure, in order to

optimize the Ter119 signal. Alternatively, it is possible to sort viable cells from each of the CD71/ Ter119 subsets first, and carry out fixation and permeabilization separately on purified cells from each subset (e.g. see the cell cycle analysis in fetal liver) [46].

Fetal liver CD71/Ter119 subsets

The CD71/Ter119 staining pattern in fetal liver is dependent on embryonic age [44] (Figure 5.4). We subdivide fetal liver cells into 6 subsets, S0 to S5 [46]. At the onset of definitive erythropoiesis in fetal liver on embryonic day 11 (E11), cells are concentrated in subsets S0 and S1 and are largely erythroid colony-forming cells (CFU-e). With embryonic development, CFU-e cells differentiate into proerythroblasts and maturing erythroblasts, and gradually populate subsets S2 to S5 (Figure 5.4).

Subsets S1 to S5 are composed almost entirely of erythroid cells of the definitive lineage. These subsets are absent in the EpoR$^{-/-}$ fetal liver. A small number of Ter119^{+} cells in fetal liver correspond to the primitive (yolk sac) erythroid lineage. These cells are apparent in EpoR$^{-/-}$ fetal liver, where no definitive lineage erythroblasts arise, but by E13.5 form less than 1% of Ter119^{+} cells in wild-type fetal liver [46].

The S0 subset is heterogeneous. At E13.5, 70% of S0 cells are erythroid cells at the CFU-e stage, just prior to the onset of EpoR dependence [46]. The remainder are earlier progenitors as well as cells of other hematopoietic lineages, principally megakaryocytes and macrophages; these cells may be sorted or gated out [46] (Figure 5.4).

Interpretation of changes in the frequency of erythroid subsets

Changes in the frequency of erythroid subsets should be interpreted with care. A change in frequency of cells in any given subset may be due to their altered apoptotic rate, altered transit time through that subset, or alternatively may be due to changes in the number of cells in other subsets. A common cause for increased frequency of early erythroblast subsets ProE and EryA is erythropoietic stress of multiple etiologies [42]. Similar findings have been noted in the 1960's by inspecting erythroblast morphologies during the stress response [154]. The precise reason for the increase in the relative frequency of earlier precursors during stress is not clear, but in part may be due to the improved survival of these precursors during stress [42].

Acknowledgements
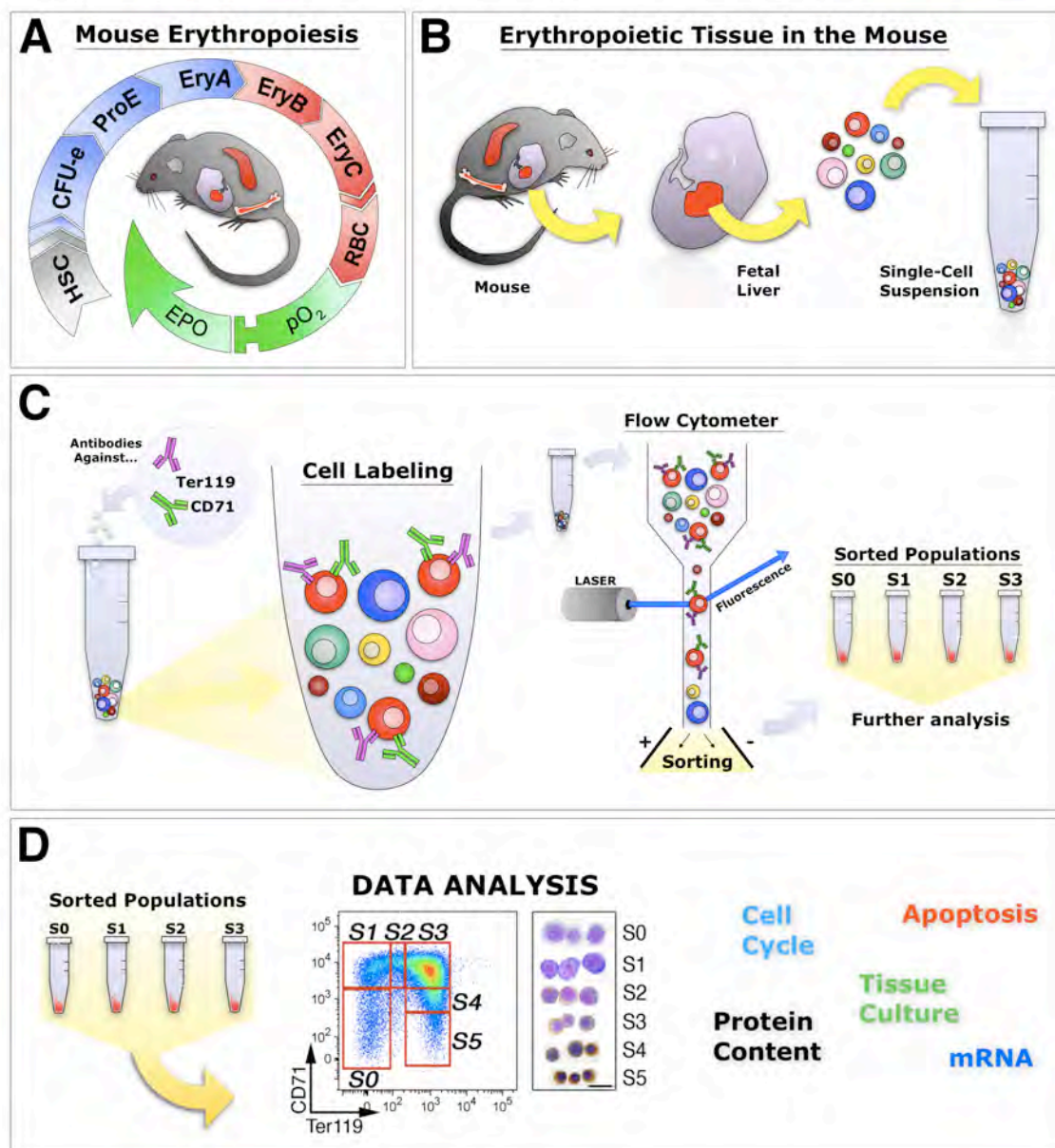
Figure 5.1

Figure 5.1   Experimental strategy to study erythropoiesis using flow cytometry.

(A)   The mouse is a key model for the study of erythropoiesis and its stress response. Mouse erythropoiesis occurs in the spleen, bone marrow, and in the fetal liver (middle). In these tissues, hematopoietic stem cells (HSC) are restricted to the erythroid lineage (blue and red stages), which in turn gives rise to red blood cells. Proper number of red cells maintains tissue oxygen (green) normal and negatively regulates Epo. Not enough red cells leads to tissue hypoxia. In turn, high Epo (green) increases erythropoiesis to correct the deficit.

(B)   To study erythroid cells, we first isolate total cells from hematopoietic tissues (e.g. fetal liver).

(C)   Freshly-isolated cells are labeled with fluorescent markers directed against erythroid, or any additional membrane or intracellular, antigens. Fluorescence data of the labeled sample are collected using flow-cytometer. Cells can be physically sorted using a cell sorter into separate tubes.

(D)   Sample data are then analyzed using FlowJo analysis for erythroid markers, apoptosis and cell cycle. Representative analysis of fetal liver is shown in the middle panel. Sorted populations can be cytospun onto microscope slides (cytospins shown), analyzed for their protein and mRNA content, or cultured for further analysis.

This figure was designed and created by MK [with the exception of FlowJo panel in the middle of part (D)].

Figure 5.2
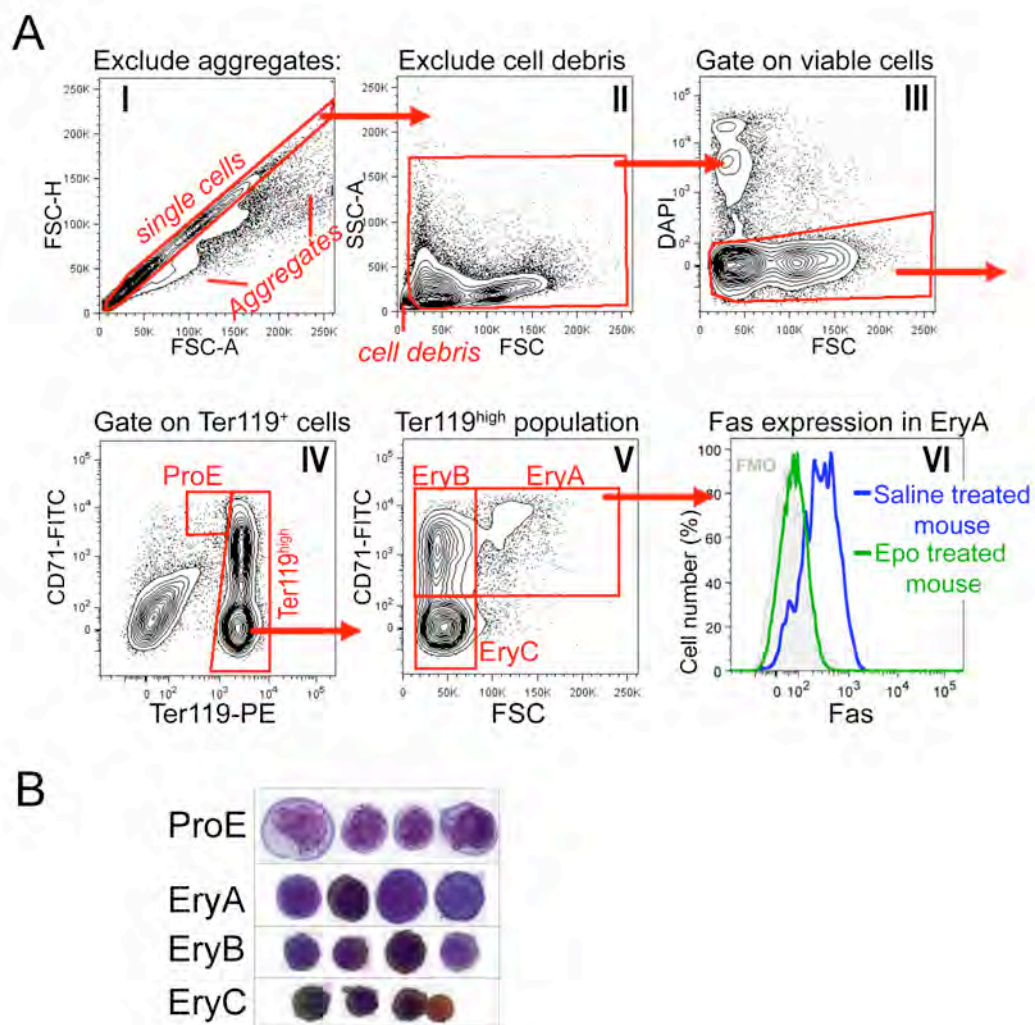
Figure 5.2 **The CD71/Ter119 erythroid subsets in mouse spleen.**

(A) Gating strategy: Spleen cells were processed and labeled with antibodies directed at CD71 and Ter119. This figure shows the analysis strategy following the data acquisition step. Dot-plot I shows all acquired events. The diagonal gate represents events that are likely to be single cells/events, excluding doublets or larger aggregates. Cells in this gate are further analyzed in dot-plot II. Here, very small events, likely nuclei or debris, are excluded. The gated cells are shown in dot-plot III, where DAPI-positive cells, that are likely membrane-permeable apoptotic cells, are excluded from further analysis. Dot-plot IV shows the resulting population of viable spleen cells. The ProE gate contains $CD71^{high}Ter119^{intermediate}$ cells. $Ter119^{high}$ cells are further analyzed in dot-plot V. Here $CD71^{high}$ cells are subdivided into less mature, large 'EryA' erythroblasts ($CD71^{high}Ter119^{high}FSC^{high}$) and smaller, more mature 'EryB' erythroblasts ($CD71^{high}Ter119^{high}FSC^{low}$). The most mature erythroblast subset is EryC ($CD71^{low}Ter119^{high}FSC^{low}$). Dot-plot VI shows cell-surface Fas expression, specifically in the EryA subset, in mice in the basal state (injected with saline), and mice injected with a single dose of Epo. Staining with Fas was carried out simultaneously with the CD71/Ter119 staining.

(B) Cytospin preparations of cells sorted from each of the indicated subsets. Cells were stained with Giemsa and with Diaminobenzidine, the latter generates a brown stain with hemoglobin. (Cytospin data were originally published in [42]).

MK performed the experiment and data analysis for part (A).

Figure 5.3
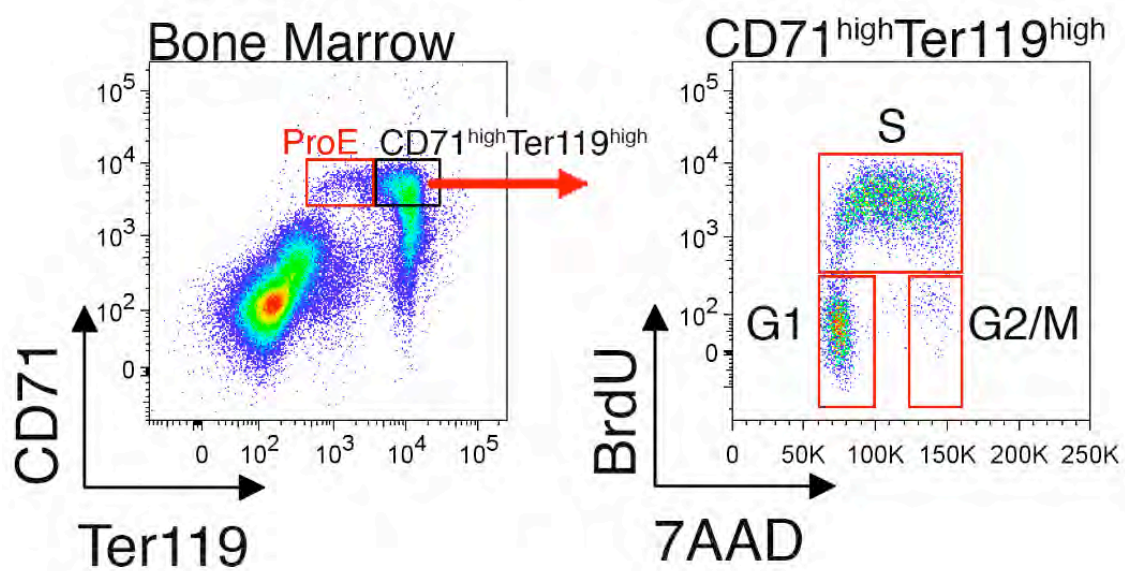
Figure 5.3   Cell cycle analysis of CD71^{high}Ter119^{high} erythroblasts in mouse bone marrow.

Mice were injected intraperitoneally with BrdU, and spleen and bone marrow were harvested 30 to 60 minutes later. Bone marrow cells were fixed and permeabilized, and in addition to being stained for CD71 and Ter119, were stained for BrdU incorporation into their replicating DNA with a monoclonal antibody directed at BrdU (fixation, permeabilization and BrdU-staining protocol was according to manufacturer's instruction). BrdU-positive cells are in S-phase of the cycle. Interphase cells are BrdU-negative and may be resolved into G1 or G2/M phases using the DNA dye 7AAD.

RP/JS/EP performed the experiment shown in this figure.

Figure 5.4
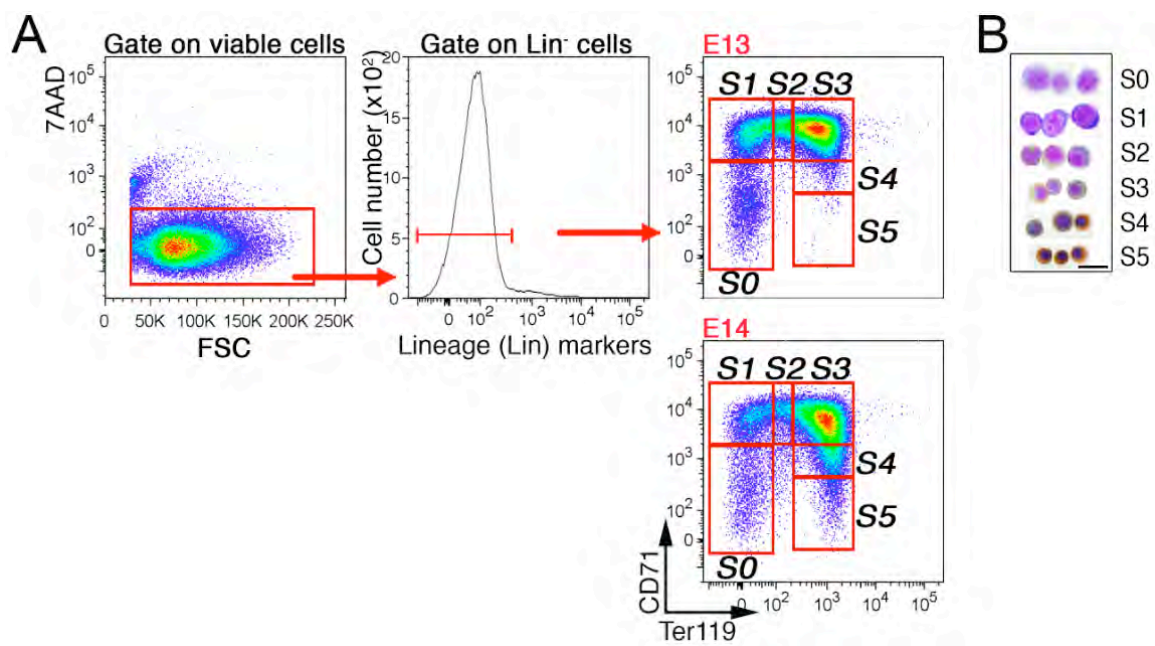
Figure 5.4   **CD71/Ter119 erythroid subsets in mouse fetal liver.**

(A)   Gating strategy: Fetal liver cells were labeled for CD71, Ter119, and a cocktail of FITC-labeled antibodies directed at non-erythroid lineage markers ('Lin'). Viable cells (7AAD-negative) were analyzed for Lin expression, and the Lin⁻ cells were further sub-divided into the S0 to S5 erythroid subsets. Younger, E13 fetal liver is composed of less mature erythroblasts, shown by the near absence of cells in the mature S4/S5 subsets.

(B)   Cytospin preparations of cells sorted from each of the indicated subsets. Cells were stained with Giemsa and with Diaminobenzidine, the latter generates a brown stain with hemoglobin. (Cytospin data were originally published in [46]).

RP and JS performed the experiments shown in this figure.

Figure 5.5
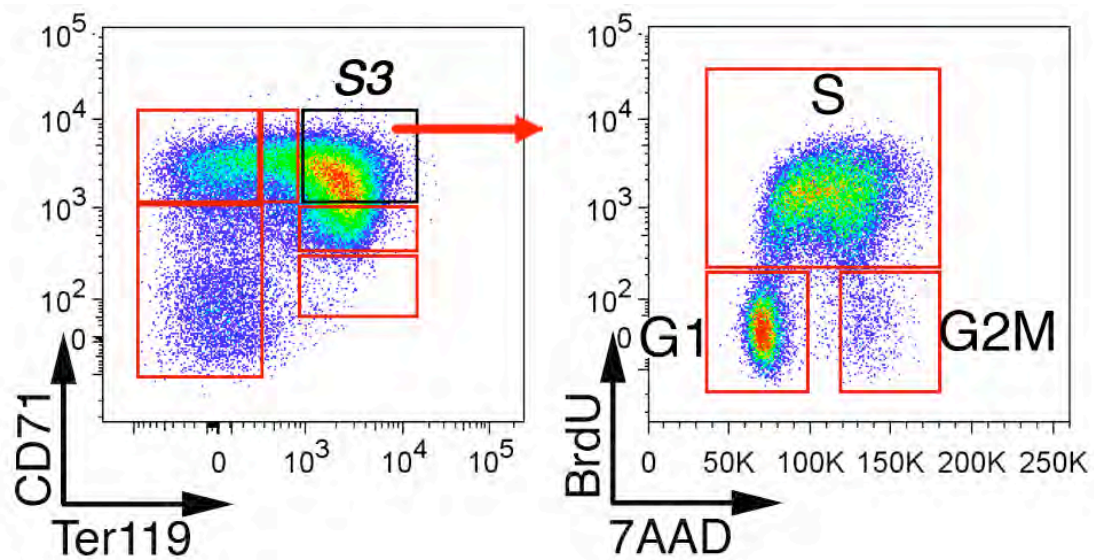
Figure 5.5   Cell cycle analysis of fetal liver erythroid subsets.

Pregnant mice were injected with BrdU, and fetal livers were harvested 30 to 60 minutes later, fixed, permeabilized and stained with antibodies against CD71, Ter119 and BrdU. Cell cycle status of S3 cells is shown.

RP/JS/EP performed the experiment shown in this figure.

Table 5.1 Specific reagents and equipment:

Name of the reagent	Company	Catalogue number
40 mm sterile cell strainer	Fisherbrand	22363547
Polystyrene round-bottom tubes for FACS staining	BD Falcon	352008
U-bottom 96 well plate	BD Falcon	353910
ChromePure Rabbit IgG	Jackson ImmunoResearch	015-000-003
CD71-FITC (stock 0.5 mg/mL)	BD-Biosciences	553266
Ter119-PE (stock 0.2 mg/mL)	BD-Biosciences	553673
7AAD	BD-Biosciences	559925
DAPI powder	Roche	236276
FITC Rat Anti-Mouse CD41 MWReg30	BD Pharmingen	553848
FITC Rat Anti-Mouse CD45R/B220 RA3-6B2	BD Pharmingen	553087
FITC Rat Anti-Mouse CD411b/Mac-1 M1/70	BD Pharmingen	557396
FITC Rat Anti-Mouse Ly-6G and Ly-6C (Gr-1) RB6-8C5	BD Pharmingen	553126
FITC Hamster Anti-Mouse CD3e 145-2C11	BD Pharmingen	553061
APC BrdU Flow kit	BD Pharmingen	557892
Annexin V-biotin	BD Pharmingen	556418

Chapter VI Attributions and Copyright information

DISCUSSION AND FUTURE DIRECTIONS

All sections of this chapter were written by me.

CHAPTER VI

DISCUSSION AND FUTURE DIRECTIONS

6.1   Relevance of my thesis work

Erythropoiesis is essential to life, and is characterized by a number of remarkable properties. Its key regulator, Epo, spans a large concentration range, upregulating erythropoietic rate as high as 10-fold to precisely match physiological need. Another property is its rapid response to stress where a large number of cells are quickly generated. Yet another essential property is the ability of erythropoiesis to maintain a stable red cell output with minimal deviations for very long periods of time. Even though these are clearly observable characteristics, the molecular mechanisms that create them remain 'hidden' from view. For example, the precise nature of the EpoR survival signal in erythroblasts is still unclear. Many pathways have been implicated based on studies in vitro, but few have been tested *in vivo*.

There are many important reasons to describe these mechanisms in more detail, and to discover new ones. From a clinical perspective, erythropoietic stress occurs in many human diseases. For example, Polycythemia Vera arises due to Jak2 mutations [27]. Anemia results from multiple causes, including ineffective erythropoiesis in myelodysplasia, where erythroblasts overexpress Fas and FasL [121]. Other causes of anemia include chronic disease, kidney disease and diabetes, cancer and chemotherapy, nutritional deficiencies and various autoimmune anemia syndromes; anemia is also associated with some infectious diseases, notably parvovirus, which specifically destroys

red cell progenitors. Other causes include the hemoglobinopathies and other genetic causes of anemia. To treat these complex disorders, we must fully understand how *in vivo,* EpoR signaling regulates various cellular functions. From a basic science perspective, erythropoiesis contains many of the elements fundamental to other studied cellular systems; it has a known cytokine and its receptor, progenitors expressing the receptor, and final output (red cells) which negatively regulate the cytokine. Knowing how these components act together to create a coherent response to hypoxia may be relevant to our understanding of analogous responses in other cytokine-dependent systems, such as granulopoiesis, thrombopoiesis, or the generation of neutrophils and lymphoid cells [187].

6.2   Innovative approach to study erythropoiesis *in vivo*

My thesis work tested the hypothesis that Epo regulates erythropoietic rate through progenitor survival. This hypothesis was based on studies in which several apoptotic regulators, including Fas/FasL, Bcl-x_L and Bim, were identified downstream of EpoR signaling *in vitro* [89,96,124]. How Epo regulates erythropoietic rate through these apoptotic pathways cannot be re-created *in vitro* with great certainty, and must therefore be tested using *in vivo* technology.

Previous *in vivo* approaches to address this question utilized mouse genetic models coupled with erythropoietic stress [52,188]. Most often, stress was induced by bleeding the animal, or by treating it with phenylhydrazine, a highly toxic compound to hematopoietic environment, in order to induce acute hemolytic anemia. To understand

the response to stress, previous *in vivo* studies examined 'peripheral' parameters. These classical methods included: determining the hematocrit, hemoglobin and reticulocyte count in peripheral blood; determining serum Epo; determining the radioactive iron uptake by the hematopoietic tissue as a reflection of erythropoietic rate; examining hematopoietic tissues histologically for a qualitative assessment of erythropoiesis [16]. Yet, erythroid progenitors could not be isolated for a direct biochemical analysis. To bypass this problem, various erythroid culture methods have been developed [189,78]. The *in vitro* culture is useful for studying erythroblast biochemistry without complications inherent to the *in vivo* models. However, progenitors are often grown in the absence of a supporting microenvironment and with altered cytokine levels. These conditions lead to potentially altered expression of cell-surface markers and transcriptional factors, and to the changes in the timing and nature of erythroid differentiation, all of which do not directly reflect the *in vivo* process.

To address these many issues, our laboratory developed a novel flow-cytometric approach (Chapter V) making my *in vivo* studies possible. I used this approach to identify maturation-specific erythroblast subsets that form a developmental sequence directly in the murine hematopoietic tissue. I was able to directly measure how erythroblasts at specific developmental stages change in frequency with time and stress level directly *in vivo*. Flow cytometry also quantitatively measures various cellular parameters (e.g. cell-cycle, apoptosis, cell-surface- and phospho- proteins) on a single-cell level. From this 'biochemical' perspective, I addressed how EpoR signaling regulates Fas/FasL, Bcl-x_L and Bim apoptotic proteins in specific erythroid subsets *in vivo*. From an 'organism-

level' perspective, I used flow-cytometric and classical measurement methods in various genetic models of erythropoietic stress to determine where, when and how in the stress response each of the three apoptotic pathways plays a role.

6.3   Novel findings

First, my analysis of erythropoiesis *in vivo* provides evidence in support of the hypothesis that erythroblast apoptosis determines erythropoietic rate. Second, my work describes an important new concept in the field of erythropoiesis, that survival pathways each have unique, specialized properties and functions in the erythropoietic response. Many of these properties could not have been predicted from the survival response of single cells *in vitro*.

In my work with Fas- and FasL-mutant mice (Chapter III), I found that Fas/FasL play an important autoregulatory role at the local tissue level, where they minimize random fluctuations in erythroblast frequency, stabilizing the size of the erythroblast pool in the steady state. In mice mutant for Fas or FasL, basal erythropoiesis was increased and, importantly, was more variable. Furthermore, the erythropoietic stress response to high Epo or low oxygen in mutant mice lagged significantly behind that of control mice. In keeping with the hypothesis originally described in Chapter I, Figure 1.4, these data suggest that Fas/FasL in wild-type spleen provide an apoptotic 'reserve' of cells. Although apparently wasteful in the basal state, this reserve allows mice to quickly rescue cells from apoptosis and recruit them to increase erythropoietic rate during stress.

I also compared and contrasted the *in vivo* behavior of two cell-intrinsic apoptotic regulators, Bcl-x_L and Bim (Chapter IV), previously unexamined in the stress response. I found Bcl-x_L responded only to acute, but not chronic, stress. My data suggest that Bcl-x_L is a key mediator of EpoR's anti-apoptotic signal very early in the stress response in ProE and EryA cells, before Bim and Fas are suppressed. Bcl-x_L adaptation to high Epo occurs at the level of Stat5 activation, and resets it for the next acute stress.

In addition, I 'resurrected' an old model of erythropoietic stress, the low atmospheric oxygen treatment (Figure 3.1C in Chapter III and Figure 4.4 in Chapter IV). This stress model provided me with a unique opportunity to test my hypothesis in a more physiological, albeit more complex, setting. In the process of testing this model, I found increased erythroblast apoptosis when mice were transferred back from hypoxia to a normal oxygen environment (Figure 3.1C). Therefore, regulation of apoptotic rates is important in both increasing and decreasing erythropoietic rate. Together, my overall findings suggest that *in vivo*, Epo regulates erythropoietic rate by modulating erythroblast apoptosis, and that various apoptotic regulators play distinct and unique roles in this process.

6.4   Interpretations and future directions

Erythropoiesis is a complex and dynamic process; my thesis work addressed only some of its aspects. Future experiments derived from this work will provide new and exciting discoveries relevant to the field of erythropoiesis and other areas of molecular biology.

New flow-cytometric identification of BFU-e and CFU-e progenitors.

It is currently unknown whether EpoR regulates the survival of earlier erythroid subsets, the BFU-e and the CFU-e, in adult mice. Unlike in the fetal liver, where CFU-e activity was identified in both the S0 and S1 populations based only on CD71 and Ter119 markers [46], we cannot easily identify BFU-e and CFU-e progenitors in the adult, where they are very rare. Previous studies used negative exclusion criteria to define CFU-e in the bone marrow as CD71^{high}cKit$^+$Ter119^{low} (and Endoglin$^+$) [190,191]. A similar approach was used to define stress BFU-e as CD71^{med}cKit$^+$Ter119^{low} (population I) and CFU-e as CD71^{hi}cKit$^+$Ter119^{med} (population II) [54]. Overall, CD71, Ter119 and cKit may not provide the most precise method of staging erythroid progenitors in the adult. Therefore, new markers are needed to improve the specific identification of BFU-e and CFU-e subsets in the fetal liver as well as in adult basal and stress erythropoiesis. Based on *in vitro* methods, EpoR is thought to be induced between the BFU-e and CFU-e stages, with CFU-e expressing maximal levels [2]. Currently, there are no reliable antibodies for flow-cytometric use against the murine EpoR. The overall cell-surface expression of this receptor is very low, even in the CFU-e subset. In the future, a reliable EpoR antibody may allow us to better resolve early erythroid subsets and to determine EpoR expression in other cell lineages and tumors.

Transit time through erythroid differentiation stages in basal state and in stress.

My work focused on understanding how erythroblasts within a given subset, as defined by two cell surface markers and cell size, during stress differ in their survival

properties from cells in the equivalent subset in the basal state *in vivo*. It takes roughly 3 to 4 days for CFU-e progenitors to reach the late EryC stage. Thus, a given erythroid subset on day 3 of the Epo response likely does not contain the same cohort of cells found there at time-point 0. Furthermore, the rate at which cells transition from one subset to the next may be altered during stress response. Literature suggests that acute stress accelerates erythroid maturation, with bigger cells appearing in the blood early on. It was previously suggested that in response to stress, there is a 'skipped' cell division that allows polychromatic cells to become reticulocytes that are larger and contain more hemoglobin [153,154]. Therefore, apart from effects upon erythroblast survival, these data point to additional Epo roles in cell cycle and differentiation.

The continuous input of progenitors from earlier differentiation stages may affect our measurements of apoptotic regulators in early erythroblasts. Thus, future experiments should determine the transition time of progenitors from one subset to the next in the basal state and during stress. To do this, an *in vivo* labeling system will need to be developed and tested (*in vivo* cell labeling with BrdU/CFSE, adoptive transfer of labeled progenitors or progenitors expressing Bcl-x_L-GFP fusion protein, inducible transgenic mouse models).

How does the continuous input from earlier erythroid compartments into the ProE pool affect our interpretation of observed Bcl-x_L adaptation to high Epo?

Our data show that Epo is still high when ProE and EryA suddenly become refractory in their Bcl-x_L response to Epo stimulation between 18 and 24 hours (Chapter

IV, Figures 4.2, 4.4 and 4.10). Reduction of Bcl-x_L signal between 18 and 24 hours in the ProE population could result from: (a) a switch from positive to negative regulation of Stat5 signaling directly in those cells and the subsequent degradation of Bcl-x_L protein, or (b) an input of cells with low Bcl-x_L from an earlier subset of possibly an altered lineage.

Our results with EpoR-H mice (where Stat5 and Bcl-x_L persist high for longer, as shown in Figure 4.6), and our laboratory's preliminary data with SOCS3 knock-down in cultured fetal liver erythroid progenitors, both show persistent Stat5 activation when the negative regulation of EpoR signaling is disrupted. These data support our model according to which, Epo-sensitive progenitors themselves become refractory to Epo stimulation. However, we cannot exclude the possibility that some CFU-e, also refractory to Epo stimulation, may transition into the ProE subset by 24 hours. To address if the refractory period in the Bcl-x_L response occurs in the same progenitors *in vivo*, labeled cells will be examined throughout the differentiation after multiple Epo injections. If the refractory period occurs in the same, labeled cells, a second Epo injection at 18 to 24 hours should not induce, or maintain, Bcl-x_L mRNA or protein in these cells (as in Figure 4.10).

The short time-frame of Bcl-x_L response (Figure 4.3) makes it unlikely that the input of very early, low-frequency progenitors (BMP4^R/stress BFU-e [17]) with low Bcl-x_L is responsible for the Bcl-x_L reduction in the ProE and EryA. To address whether these very early progenitors play a role in the Bcl-x_L adaptation mechanism, *flexed-tail* mutant mouse defective in BMP4^R progenitors that give rise to stress BFU-e [53], could be utilized.

If Bcl-x_L adaptation in ProE and EryA in Epo-injected mutant mice is preserved, then progenitors prior to the CFU-e stage are likely not involved.

At which differentiation stage does the suppression of Fas and Bim begin?

During stress, Epo persists above basal level for at least 36 hours (Figure 4.2A). In contrast to Bcl-x_L upregulation, Fas and Bim suppression takes longer to be achieved (Figures 4.3 and 4.4) [42]. Cell labeling experiments are necessary to address whether Fas and Bim suppression begins in very early CFU-e progenitors or only in the ProE and EryA subsets.

Alternatively, Epo indirectly participates in the generation of 'stress BFU-e' [17,53,54] that lower Fas and Bim developmentally (via GATA-1), or via activation of other receptors (e.g. cKit or Glucocorticoid Receptor). To test this, *flexed-tail* mutant mice can be injected with Epo to see if Fas and Bim suppression on day 3 is absent due to the defect in very early, stress-responsive progenitors. Furthermore, if stress BFU-e can be purified, their Fas and Bim response to Epo in culture, or *in vivo* via adoptive mouse transfer, may also be studied.

How does EpoR signaling lead to Fas down-regulation?

The mechanism of Fas/FasL down-regulation by Epo in EpoR-expressing cells remains unstudied. Therefore, future experiments could determine whether Epo suppresses Fas by decreasing Fas mRNA stability, or by suppressing its transcription. This could be done by sorting and culturing erythroblasts (ProE/EryA or S1-2) with or

without transcriptional inhibitors and monitoring Fas mRNA by quantitative real-time PCR. EpoR activates multiple signaling pathways including Stat5, Stat1, PI3K/AKT and MAPK. While Stat5 does not appear to suppress Fas (Figure 4.9), Stat1 [192] and PI3K/AKT [83,193,194], but not ERK [155], pathways may regulate Fas transcription. These regulators could also be tested *in vitro* by depletion with shRNA, or by retroviral transduction of erythroblasts with dominant-negative and constitutively-active mutant molecules. Micro-RNAs may also regulate the expression of Fas and FasL, and could be tested.

Fas and FasL can exist in two main forms, membrane-bound and soluble: sFas results from alternative splicing [195], while sFasL results from cleavage of membrane bound FasL by metalloproteases [196]. Therefore, future experiments, using metalloprotease inhibitors in spleen EryA cultures or *in vivo*, could address whether metalloproteases (e.g. MMP-8 and ADAM10) function as Fas or FasL sheddases and whether sheddase action is required for erythroblast Fas and FasL down-regulation. Alternative splice variants of Fas will be detected by quantitative real-time PCR, while soluble Fas or FasL will be monitored by an ELISA method.

The role of Bim in stress erythropoiesis in vivo.

My work established that Bim expression declines with erythroid differentiation, and is further suppressed by erythropoietic stress. However, Bim$^{-/-}$ fetal livers contained normal CFU-e numbers (Figure 4.8C), which suggests that Bim is not the only pro-apoptotic factor in early erythroblasts. Furthermore, the magnitude of Bim suppression

was not as high as for Fas suppression or Bcl-x_L upregulation (Figure 4.3C). It has not been determined whether Bim$^{-/-}$ mice have an enhanced response to erythropoietic stress. Adult Bim$^{-/-}$ mice appear to suffer from an autoimmune disorder complicating the study of their erythropoietic stress response [89]. To bypass this issue, experimental strategy similar to Fas-mutant mice (Chapter III) could be used: Bim$^{-/-}$ mice could be bred onto Rag1$^{-/-}$ background to prevent an autoimmune syndrome, and their basal and stress erythropoiesis could be examined. Multiple apoptotic regulators could also be examined to ensure that the phenotype is not masked by compensatory upregulation of apoptosis via other pathways. For example, Trail-R2 receptor, expressed on human erythroid cells [197], could be one such molecule that needs to be tested in mouse erythroblasts. Furthermore, Bim$^{-/-}$Rag1$^{-/-}$ mice can be crossed with Fas-mutant mice, providing a new model where two negative regulators of erythropoiesis are removed.

Significance

Much work remains to be done in order to fully understand how EpoR regulates erythropoietic rate, as well as how these findings may be relevant to studying other systems and diseases. For example, my work on the adapting nature of Stat5-Bcl-x_L response downstream of EpoR *in vivo* has potential implications for myeloproliferative diseases. Elevated levels of Bcl-x_L were found in Polycythemia Vera and other myeloproliferative syndromes, where they are thought to contribute to cytokine independence of progenitors. Mutations in Jak2 are an established cause of persistent Stat5 activation and elevation of Bcl-x_L. Our work suggests that failure of the

mechanisms of adaptation of the Stat5 and Bcl-x$_L$ response may also contribute to these syndromes [27,169,182,183].

REFERENCES

1.   Wu H, Liu X, Jaenisch R, Lodish HF. Generation of committed erythroid BFU-E and CFU-E progenitors does not require erythropoietin or the erythropoietin receptor. Cell. 1995;83:59-67.

2.   Koury MJ, Bondurant MC. The molecular mechanism of erythropoietin action. Eur J Biochem. 1992;210:649-663.

3.   Shoemaker CB, Mitsock LD. Murine erythropoietin gene: cloning, expression, and human gene homology. Mol Cell Biol. 1986;6:849-858.

4.   Jelkmann W. Molecular biology of erythropoietin. Intern Med. 2004;43:649-659.

5.   Stockmann C, Fandrey J. Hypoxia-induced erythropoietin production: a paradigm for oxygen-regulated gene expression. Clin Exp Pharmacol Physiol. 2006;33:968-979.

6.   Brahimi-Horn MC, Pouyssegur J. HIF at a glance. J Cell Sci. 2009;122:1055-1057.

7.   Haase VH. Hypoxic regulation of erythropoiesis and iron metabolism. Am J Physiol Renal Physiol. 2010;299:F1-13.

8.   Gruber M, Hu CJ, Johnson RS, Brown EJ, Keith B, Simon MC. Acute postnatal ablation of Hif-2alpha results in anemia. Proc Natl Acad Sci U S A. 2007;104:2301-2306.

9.   Haase VH, Glickman JN, Socolovsky M, Jaenisch R. Vascular tumors in livers with targeted inactivation of the von Hippel-Lindau tumor suppressor. PNAS. 2001;98:1583-1588.

10.   Rankin EB, Tomaszewski JE, Haase VH. Renal cyst development in mice with conditional inactivation of the von Hippel-Lindau tumor suppressor. Cancer Res. 2006;66:2576-2583.

11.   Erslev AJ, Caro J. Physiologic and molecular biology of erythropoietin. Med Oncol Tumor Pharmacother. 1986;3:159-164.

12.   Eckardt KU, Boutellier U, Kurtz A, Schopen M, Koller EA, Bauer C. Rate of erythropoietin formation in humans in response to acute hypobaric hypoxia. J Appl Physiol. 1989;66:1785-1788.

13.   Abbrecht PH, Littell JK. Plasma erythropoietin in men and mice during acclimatization to different altitudes. J Appl Physiol. 1972;32:54-58.

14.   Risso A, Turello M, Biffoni F, Antonutto G. Red blood cell senescence and neocytolysis in humans after high altitude acclimatization. Blood Cells Mol Dis. 2007;38:83-92.

15.   Broudy VC, Lin NL, Priestely GV, Nocka K, Wolf NS. Interaction of Stem Cell Factor and its receptor c-kit mediates lodgement and acute expansion of hematopoietic cells in the murine spleen. blood. 1996;88:75-81.

16.   Ou LC, Kim DW, Layton MJ, Smith RP. Splenic erythropoiesis in polycythemic response of the rat to high-altitude exposure. J Appl Physiol. 1980;48:857-861.

17.   Paulson RF, Shi L, Wu DC. Stress erythropoiesis: new signals and new stress progenitor cells. Curr Opin Hematol. 2011.

18.   Kline DD, Peng YJ, Manalo DJ, Semenza GL, Prabhakar NR. Defective carotid body function and impaired ventilatory responses to chronic hypoxia in mice partially

deficient for hypoxia-inducible factor 1 alpha. Proc Natl Acad Sci U S A. 2002;99:821-826.

19.   Schmidt W. Effects of intermittent exposure to high altitude on blood volume and erythropoietic activity. High Alt Med Biol. 2002;3:167-176.

20.   West, Schoene, Milledge. High Altitude Medicine and Physiology (ed 4). London: Hodder Arnold; 2007.

21.   Bauer A, Tronche F, Wessely O, et al. The glucocorticoid receptor is required for stress erythropoiesis. Genes Dev. 1999;13:2996-3002.

22.   Chasis JA, Mohandas N. Erythroblastic islands: niches for erythropoiesis. Blood. 2008;112:470-478.

23.   Socolovsky M. Molecular insights into stress erythropoiesis. Curr Opin Hematol. 2007;14:215-224.

24.   Ebert BL, Bunn HF. Regulation of the erythropoietin gene. Blood. 1999;94:1864-1877.

25.   Rice L, Alfrey CP. The negative regulation of red cell mass by neocytolysis: physiologic and pathophysiologic manifestations. Cell Physiol Biochem. 2005;15:245-250.

26.   Alfrey CP, Rice L, Udden MM, Driscoll TB. Neocytolysis: physiological down-regulator of red-cell mass. Lancet. 1997;349:1389-1390.

27.   James C, Ugo V, Le Couedic JP, et al. A unique clonal JAK2 mutation leading to constitutive signalling causes polycythaemia vera. Nature. 2005;434:1144-1148.

28.   Divoky V, Liu Z, Ryan TM, Prchal JF, Townes TM, Prchal JT. Mouse model of congenital polycythemia: Homologous replacement of murine gene by mutant human erythropoietin receptor gene. Proc Natl Acad Sci U S A. 2001;98:986-991.

29.   Percy MJ, Furlow PW, Lucas GS, et al. A gain-of-function mutation in the HIF2A gene in familial erythrocytosis. N Engl J Med. 2008;358:162-168.

30.   Ang SO, Chen H, Hirota K, et al. Disruption of oxygen homeostasis underlies congenital Chuvash polycythemia. Nat Genet. 2002;32:614-621.

31.   Iwasaki H, Akashi K. Myeloid lineage commitment from the hematopoietic stem cell. Immunity. 2007;26:726-740.

32.   Cantor AB, Orkin SH. Transcriptional regulation of erythropoiesis: an affair involving multiple partners. Oncogene. 2002;21:3368-3376.

33.   Iscove NN, Sieber F. Erythroid progenitors in mouse bone marrow detected by macroscopic colony formation in culture. Exp Hematol. 1975;3:32-43.

34.   Axelrad AA, McLeod DL, Shreeve MM, Heath DS. Properties of cells that produce erythrocytic colonies in vitro. In: Robinson WA, ed. Hemopoiesis in culture. Washington: U.S. Government Printing Office; 1974.

35.   Stephenson JR, Axelrad AA, McLeod DL, Shreeve MM. Induction of colonies of hemoglobin-synthesizing cells by erythropoietin in vitro. Proc Natl Acad Sci USA. 1971;68:1542-1546.

36.   Koury MJ, Bondurant MC. Maintenance by erythropoietin of viability and maturation of murine erythroid precursor cells. J Cell Physiol. 1988;137:65-74.

37.   Bessis M. [Erythroblastic island, functional unity of bone marrow]. Rev Hematol. 1958;13:8-11.

38.	Levy JE, Jin O, Fujiwara Y, Kuo F, Andrews NC. Transferrin receptor is necessary for development of erythrocytes and the nervous system. Nat Genet. 1999;21:396-399.

39.	Ponka P, Nam-lok C. Identification of an erythroid active element in the transferrin receptor gene. J Biol Chem. 2000;275:24185-24190.

40.	Kina T, Ikuta K, Takayama E, et al. The monoclonal antibody TER-119 recognizes a molecule associated with glycophorin A and specifically marks the late stages of murine erythroid lineage. Br J Haematol. 2000;109:280-287.

41.	Koulnis M, Pop R, Porpiglia E, Shearstone JR, Hidalgo D, Socolovsky M. Identification and analysis of mouse erythroid progenitors using the CD71/Ter119 Flow-cytometric assay. JoVE. 2011.

42.	Liu Y, Pop R, Sadegh C, Brugnara C, Haase VH, Socolovsky M. Suppression of Fas-FasL coexpression by erythropoietin mediates erythroblast expansion during the erythropoietic stress response in vivo. Blood. 2006;108:123-133.

43.	Socolovsky M, Nam H, Fleming MD, Haase VH, Brugnara C, Lodish HF. Ineffective erythropoiesis in Stat5a(-/-)5b(-/-) mice due to decreased survival of early erythroblasts. Blood. 2001;98:3261-3273.

44.	Socolovsky M, Murrell M, Liu Y, Pop R, Porpiglia E, Levchenko A. Negative Autoregulation by FAS Mediates Robust Fetal Erythropoiesis. PLoS Biol. 2007;5:e252.

45.	Zhang J, Socolovsky M, Gross AW, Lodish HF. Role of Ras signaling in erythroid differentiation of mouse fetal liver cells: functional analysis by a flow cytometry-based novel culture system. Blood. 2003;102:3938-3946.

46.	Pop R, Shearstone JR, Shen Q, et al. A key commitment step in erythropoiesis is synchronized with the cell cycle clock through mutual inhibition between PU.1 and S-phase progression. PLoS Biol. 2010;8.

47.	Chen K, Liu J, Heck S, Chasis JA, An X, Mohandas N. Resolving the distinct stages in erythroid differentiation based on dynamic changes in membrane protein expression during erythropoiesis. Proc Natl Acad Sci U S A. 2009;106:17413-17418.

48.	McGrath KE, Bushnell TP, Palis J. Multispectral imaging of hematopoietic cells: where flow meets morphology. J Immunol Methods. 2008;336:91-97.

49.	Wickrema A, Bondurant MC, Krantz SB. Abundance and stability of erythropoietin receptor mRNA in mouse erythroid progenitor cells. Blood. 1991;78:2269-2275.

50.	Broudy VC, Lin N, Brice M, Nakamoto B, Papayannopoulou T. Erythropoietin receptor characteristics on primary human erythroid cells. Blood. 1991;77:2583-2590.

51.	Peschle C, Magli MC, Cillo C, et al. Kinetics of erythroid and myeloid stem cells in post-hypoxia polycythaemia. British Journal of Hematology. 1977;37:345-352.

52.	Hara H, Ogawa M. Erthropoietic precursors in mice with phenylhydrazine-induced anemia. Am J Hematol. 1976;1:453-458.

53.	Lenox LE, Perry JM, Paulson RF. BMP4 and Madh5 regulate the erythroid response to acute anemia. Blood. 2005;105:2741-2748.

54.	Harandi OF, Hedge S, Wu DC, McKeone D, Paulson RF. Murine erythroid short-term radioprotection requires a BMP4-dependent, self-renewing population of stress erythroid progenitors. J Clin Invest. 2010;120:4507-4519.

55.   Luck L, Zeng L, Hiti AL, Weinberg KI, Malik P. Human CD34(+) and CD34(+)CD38(-) hematopoietic progenitors in sickle cell disease differ phenotypically and functionally from normal and suggest distinct subpopulations that generate F cells. Exp Hematol. 2004;32:483-493.

56.   D'Andrea AD, Lodish HF, Wong GG. Expression cloning of the murine erythropoietin receptor. Cell. 1989;57:277-285.

57.   Livnah O, Stura EA, Middleton SA, Johnson DL, Jolliffe LK, Wilson IA. Crystallographic evidence for preformed dimers of erythropoietin receptor before ligand activation. Science. 1999;283:987-990.

58.   Miyamoto T, Iwasaki H, Reizis B, et al. Myeloid or lymphoid promiscuity as a critical step in hematopoietic lineage commitment. Dev Cell. 2002;3:137-147.

59.   Forsberg EC, Serwold T, Kogan S, Weissman IL, Passegue E. New evidence supporting megakaryocyte-erythrocyte potential of flk2/flt3+ multipotent hematopoietic progenitors. Cell. 2006;126:415-426.

60.   Huang LJ-s, Constantinescu SN, Lodish HF. The N-terminal domain of Janus Kinase 2 is required for Golgi processing and cell surface expression of erythropoietin receptor. Molecular Cell. 2001;8:1327-1338.

61.   Remy I, Wilson IA, Michnick SW. Erythropoietin receptor activation by a ligand-induced conformation change. Science. 1999;283:990-993.

62.   Neubauer H, Cumano A, Muller M, Wu H, Huffstadt U, Pfeffer K. Jak2 deficiency defines an essential developmental checkpoint in definitive hematopoiesis. Cell. 1998;93:397-409.

63.   Kralovics R, Passamonti F, Buser AS, et al. A gain-of-function mutation of JAK2 in myeloproliferative disorders. N Engl J Med. 2005;352:1779-1790.

64.   Watowich SS. The Erythropoietin Receptor: Molecular Structure and Hematopoietic Signaling Pathways. J Investig Med. 2011.

65.   Richmond TD, Chohan M, Barber DL. Turning cells red: signal transduction mediated by erythropoietin. Trends Cell Biol. 2005;15:146-155.

66.   Constantinescu SN, Ghaffari S, Lodish HF. The Erythropoietin Receptor: Structure, Activation and Intracellular Signal Transduction. Trends Endocrinol Metab. 1999;10:18-23.

67.   Menon MP, Karur V, Bogacheva O, Bogachev O, Cuetara B, Wojchowski DM. Signals for stress erythropoiesis are integrated via an erythropoietin receptor-phosphotyrosine-343-Stat5 axis. J Clin Invest. 2006;116:683-694.

68.   Watowich SS, Xie X, Klingmuller U, et al. Erythropoietin receptor mutations associated with familial erythrocytosis cause hypersensitivity to erythropoietin in the heterozygous state. Blood. 1999;94:2530-2532.

69.   Socolovsky M, Fallon AEJ, Lodish HF. The prolactin receptor rescues EpoR -/- erythroid progenitors and replaces EpoR in a synergistic interaction with c-kit. Blood. 1998;92:1491-1496.

70.   Socolovsky M, Lodish HF, Daley GQ. Control of hematopoietic differentiation: lack of specificity in signaling by cytokine receptors. Proc Natl Acad Sci USA. 1998;95:6573-6575.

71.   Testa U. Apoptotic mechanisms in the control of erythropoiesis. Leukemia. 2004;18:1176-1199.

72.   Kelley LL, Koury MJ, Bondurant MC, Koury ST, Sawyer ST, Wickrema A. Survival or death of individual proerythroblasts results from differing erythropoietin sensitivities: a mechanism for controlling rates of erythrocyte production. Blood. 1993;82:2340-2352.

73.   Koury MJ, Bondurant MC. Erythropoietin retards DNA breakdown and prevents programmed death in erythroid progenitor cells. Science. 1990;248:378-381.

74.   Jegalian AG, Acurio A, Dranoff G, Wu H. Erythropoietin receptor haploinsufficiency and in vivo interplay with granulocyte-macrophage colony-stimulating factor and interleukin 3. Blood. 2002;99:2603-2605.

75.   Zang H, Sato K, Nakajima H, McKay C, Ney PA, Ihle JN. The distal region and receptor tyrosines of the Epo receptor are non-essential for in vivo erythropoiesis. Embo J. 2001;20:3156-3166.

76.   Socolovsky M, Fallon AEJ, Wang S, Brugnara C, Lodish HF. Fetal anemia and apoptosis of red cell progenitors in Stat5a$^{-/-}$5b$^{-/-}$ mice: a direct role for Stat5 in bcl-X$_L$ induction. Cell. 1999;98:181-191.

77.   Cui Y, Riedlinger G, Miyoshi K, et al. Inactivation of Stat5 in mouse mammary epithelium during pregnancy reveals distinct functions in cell proliferation, survival, and differentiation. Mol Cell Biol. 2004;24:8037-8047.

78.   Dolznig H, Grebien F, Deiner EM, et al. Erythroid progenitor renewal versus differentiation: genetic evidence for cell autonomous, essential functions of EpoR, Stat5 and the GR. Oncogene. 2006;25:2890-2900.

79.   Zhu BM, McLaughlin SK, Na R, et al. Hematopoietic-specific Stat5-null mice display microcytic hypochromic anemia associated with reduced transferrin receptor gene expression. Blood. 2008;112:2071-2080.

80.   Kerenyi MA, Grebien F, Gehart H, et al. Stat5 regulates cellular iron uptake of erythroid cells via IRP-2 and TfR-1. Blood. 2008;112:3878-3888.

81.   Bouscary D, Pene F, Claessens YE, et al. Critical role for PI 3-kinase in the control of erythropoietin-induced erythroid progenitor proliferation. Blood. 2003;101:3436-3443.

82.   Haseyama Y, Sawada K, Oda A, et al. Phosphatidylinositol 3-kinase is involved in the protection of primary cultured human erythroid precursor cells from apoptosis. Blood. 1999;94:1568-1577.

83.   Kashii Y, Uchida M, Kirito K, et al. A member of Forkhead family transcription factor, FKHRL1, is one of the downstream molecules of phosphatidylinositol 3-kinase-Akt activation pathway in erythropoietin signal transduction. Blood. 2000;96:941-949.

84.   Halupa A, Bailey ML, Huang K, Iscove NN, Levy DE, Barber DL. A novel role for STAT1 in regulating murine erythropoiesis: deletion of STAT1 results in overall reduction of erythroid progenitors and alters their distribution. Blood. 2005;105:552-561.

85.   Kelley LL, Koury MJ, Bondurant MC, Koury ST, Sawyer ST, Wickrema A. Survival or death of individual proerythroblasts results from differing erythropoietin sensitivities: a mechanism for controlled rates of erythrocyte production. Blood. 1993;82:2340-2352.

86.   Nijhof W, de Haan G, Pietens J, Dontje B. Mechanistic options of erythropoietin-stimulated erythropoiesis. Exp Hematol. 1995;23:369-375.

87.   Landschulz KT, Boyer SH, Noyes AN, Rogers OC, Frelin LP. Onset of erythropoietin response in murine erythroid colony-forming units: assignment to early S-phase in a specific cell generation. Blood. 1992;79:2749-2758.

88.   Schweers RL, Zhang J, Randall MS, et al. NIX is required for programmed mitochondrial clearance during reticulocyte maturation. Proc Natl Acad Sci U S A. 2007;104:19500-19505.

89.   Abutin RM, Chen J, Lung TK, Lloyd JA, Sawyer ST, Harada H. Erythropoietin-induced phosphorylation/degradation of BIM contributes to survival of erythroid cells. Exp Hematol. 2009;37:151-158.

90.   Sathyanarayana P, Dev A, Fang J, et al. EPO receptor circuits for primary erythroblast survival. Blood. 2008;111:5390-5399.

91.   De Maria R, Zeuner A, Eramo A, et al. Negative regulation of erythropoiesis by caspase-mediated cleavage of GATA-1 [see comments]. Nature. 1999;401:489-493.

92.   De Maria R, Testa U, Luchetti L, et al. Apoptotic role of Fas/Fas ligand system in the regulation of erythropoiesis. Blood. 1999;93:796-803.

93.   Shibayama H, Takai E, Matsumura I, et al. Identification of a cytokine-induced antiapoptotic molecule anamorsin essential for definitive hematopoiesis. J Exp Med. 2004;199:581-592.

94.   Elmore S. Apoptosis: a review of programmed cell death. Toxicol Pathol. 2007;35:495-516.

95.   Cory S, Adams JM. The Bcl2 family: regulators of the cellular life-or-death switch. Nat Rev Cancer. 2002;2:647-656.

96.   Silva M, Grillot D, Benito A, Richard C, Nunez G, Fernandez-Luna JL. Erythropoietin can promote erythroid progenitor survival by repressing apoptosis through Bcl-XL and Bcl-2. Blood. 1996;88:1576-1582.

97.   Gregoli PA, Bondurant MC. The roles of bcl-X and apopain in the control of erythropoiesis by erythropoietin. Blood. 1997;90:630-640.

98.   Dolznig H, Habermann B, Stangl K, et al. Apoptosis protection by the Epo target Bcl-X(L) allows factor-independent differentiation of primary erythroblasts. Curr Biol. 2002;12:1076-1085.

99.   Rhodes MM, Kopsombut P, Bondurant MC, Price JO, Koury MJ. Bcl-xL prevents apoptosis of late-stage erythroblasts but does not mediate the anti-apoptotic effect of erythropoietin. Blood. 2005.

100.   Motoyama N, Wang F, Roth KA, et al. Massive cell death of immature hematopoietic cells and neurons in Bcl-X-deficient mice. Science. 1995;267:1506-1510.

101.   Gregory T, Yu C, Ma A, Orkin SH, Blobel GA, Weiss MJ. GATA-1 and Erythropoietin cooperate to promote erythroid cell survival by regulating bcl-x_L expression. Blood. 1999;94:87-96.

102.   Wojchowski DM, Sathyanarayana P, Dev A. Erythropoietin receptor response circuits. Curr Opin Hematol. 2010;17:169-176.

103. Aispuru GR, Aguirre MV, Aquino-Esperanza JA, Lettieri CN, Juaristi JA, Brandan NC. Erythroid expansion and survival in response to acute anemia stress: the role of EPO receptor, GATA-1, Bcl-xL and caspase-3. Cell Biol Int. 2008;32:966-978.

104. Bouillet P, Purton JF, Godfrey DI, et al. BH3-only Bcl-2 family member Bim is required for apoptosis of autoreactive thymocytes. Nature. 2002;415:922-926.

105. O'Connor L, Strasser A, O'Reilly LA, et al. Bim: a novel member of the Bcl-2 family that promotes apoptosis. EMBO J. 1998;17:384-395.

106. Maeda T, Ito K, Merghoub T, et al. LRF is an essential downstream target of GATA1 in erythroid development and regulates BIM-dependent apoptosis. Dev Cell. 2009;17:527-540.

107. Dijkers PF, Medema RH, Lammers JW, Koenderman L, Coffer PJ. Expression of the pro-apoptotic Bcl-2 family member Bim is regulated by the forkhead transcription factor FKHR-L1. Curr Biol. 2000;10:1201-1204.

108. Strasser A. The role of BH3-only proteins in the immune system. Nat Rev Immunol. 2005;5:189-200.

109. Ley R, Ewings KE, Hadfield K, Cook SJ. Regulatory phosphorylation of Bim: sorting out the ERK from the JNK. Cell Death Differ. 2005;12:1008-1014.

110. Puthalakath H, Huang DC, O'Reilly LA, King SM, Strasser A. The proapoptotic activity of the Bcl-2 family member Bim is regulated by interaction with the dynein motor complex. Mol Cell. 1999;3:287-296.

111. Curtin JF, Cotter TG. Live and let die: regulatory mechanisms in Fas-mediated apoptosis. Cell Signal. 2003;15:983-992.

112. Nagata S, Golstein P. The Fas death factor. Science. 1995;267:1449-1456.

113. Wajant H. The Fas signaling pathway: more than a paradigm. Science. 2002;296:1635-1636.

114. Adachi M, Suematsu S, Kondo T, et al. Targeted mutation in the Fas gene causes hyperplasia in peripheral lymphoid organs and liver. Nat Genet. 1995;11:294-300.

115. Pinkoski MJ, Brunner T, Green DR, Lin T. Fas and Fas ligand in gut and liver. Am J Physiol Gastrointest Liver Physiol. 2000;278:G354-366.

116. Desbarats J, Newell MK. Fas engagement accelerates liver regeneration after partial hepatectomy. Nat Med. 2000;6:920-923.

117. Silvestris F, Cafforio P, Tucci M, Dammacco F. Negative regulation of erythroblast maturation by Fas-L(+)/TRAIL(+) highly malignant plasma cells: a major pathogenetic mechanism of anemia in multiple myeloma. Blood. 2002;99:1305-1313.

118. Silvestris F, Tucci M, Cafforio P, Dammacco F. Fas-L up-regulation by highly malignant myeloma plasma cells: role in the pathogenesis of anemia and disease progression. Blood. 2001;97:1155-1164.

119. Gersuk GM, Beckham C, Loken MR, et al. A role for tumour necrosis factor-alpha, Fas and Fas-Ligand in marrow failure associated with myelodysplastic syndrome. Br J Haematol. 1998;103:176-188.

120. Gersuk GM, Lee JW, Beckham CA, Anderson J, Deeg HJ. Fas (CD95) receptor and Fas-ligand expression in bone marrow cells from patients with myelodysplastic syndrome. Blood. 1996;88:1122-1123.

121.   Claessens YE, Park S, Dubart-Kupperschmitt A, et al. Rescue of early stage myelodysplastic syndrome-deriving erythroid precursors by the ectopic expression of a dominant negative form of FADD. Blood. 2005.

122.   Dror Y, Freedman MH. Shwachman-Diamond syndrome marrow cells show abnormally increased apoptosis mediated through the Fas pathway. Blood. 2001;97:3011-3016.

123.   Oda A, Nishio M, Sawada K. Stem cell factor regulation of Fas-mediated apoptosis of human erythroid precursor cells. J Hematother Stem Cell Res. 2001;10:595-600.

124.   Dai CH, Price JO, Brunner T, Krantz SB. Fas ligand is present in human erythroid colony-forming cells and interacts with Fas induced by interferon gamma to produce erythroid cell apoptosis. Blood. 1998;91:1235-1242.

125.   Nagata S, Suda T. Fas and Fas ligand: lpr and gld mutations. Immunol Today. 1995;16:39-43.

126.   Jelkmann W. Erythropoietin: structure, control of production, and function. Physiol Rev. 1992;72:449-489.

127.   Semenza GL. Involvement of oxygen-sensing pathways in physiologic and pathologic erythropoiesis. Blood. 2009;114:2015-2019.

128.   von Lindern M, Schmidt U, Beug H. Control of erythropoiesis by erythropoietin and stem cell factor: a novel role for Bruton's tyrosine kinase. Cell Cycle. 2004;3:876-879.

129.   von Lindern M, Zauner W, Mellitzer G, et al. The glucocorticoid receptor cooperates with the erythropoietin receptor and c-Kit to enhance and sustain proliferation of erythroid progenitors in vitro. Blood. 1999;94:550-559.

130.   Palis J. Ontogeny of erythropoiesis. Curr Opin Hematol. 2008;15:155-161.

131.   Fawcett DW, Jensh RP. Hemopoiesis. In: Fawcett DW, Jensh RP, eds. Bloom & Fawcett: Concise Histology. NY, NY: Chapman & Hall; 1997:84-93.

132.   Gregory CJ, McCulloch EA, Till JE. Transient erythropoietic spleen colonies: effects of erythropoietin in normal and genetically anemic W/Wv mice. J Cell Physiol. 1975;86:1-8.

133.   Papayannopoulou T, Finch CA. On the in vivo action of erythropoietin: a quantitative analysis. J Clin Invest. 1972;51:1179-1185.

134.   Koury MJ, Sawyer ST, Brandt SJ. New insights into erythropoiesis. Curr Opin Hematol. 2002;9:93-100.

135.   Silva M, Benito A, Sanz C, et al. Erythropoietin can induce expression of bcl-xL through Stat5 in erythropoietin-dependent progenitor cell lines. J Biol Chem. 1999;274:25855-25861.

136.   Wood AD, Chen E, Donaldson IJ, et al. ID1 promotes expansion and survival of primary erythroid cells and is a target of JAK2V617F-STAT5 signaling. Blood. 2009;114:1820-1830.

137.   Longmore GD. A unique role for Stat5 in recovery from acute anemia. J Clin Invest. 2006;116:626-628.

138.   Alderson MR, Tough TW, Davis-Smith T, et al. Fas ligand mediates activation-induced cell death in human T lymphocytes. J Exp Med. 1995;181:71-77.

139.   Ju ST, Panka DJ, Cui H, et al. Fas(CD95)/FasL interactions required for programmed cell death after T-cell activation. Nature. 1995;373:444-448.

140.   Brunner T, Mogil RJ, LaFace D, et al. Cell-autonomous Fas (CD95)/Fas-ligand interaction mediates activation-induced apoptosis in T-cell hybridomas. Nature. 1995;373:441-444.

141.   Thieffry D, Huerta AM, Perez-Rueda E, Collado-Vides J. From specific gene regulation to genomic networks: a global analysis of transcriptional regulation in Escherichia coli. Bioessays. 1998;20:433-440.

142.   Alon U. Network motifs: theory and experimental approaches. Nat Rev Genet. 2007;8:450-461.

143.   Savageau MA. Comparison of classical and autogenous systems of regulation in inducible operons. Nature. 1974;252:546-549.

144.   Rosenfeld N, Elowitz MB, Alon U. Negative autoregulation speeds the response times of transcription networks. J Mol Biol. 2002;323:785-793.

145.   Ramsdell F, Seaman MS, Miller RE, Tough TW, Alderson MR, Lynch DH. gld/gld mice are unable to express a functional ligand for Fas. Eur J Immunol. 1994;24:928-933.

146.   Kawai T, Adachi O, Ogawa T, Takeda K, Akira S. Unresponsiveness of MyD88-deficient mice to endotoxin. Immunity. 1999;11:115-122.

147.   Nguyen T, Russell J. The regulation of FasL expression during activation-induced cell death (AICD). Immunology. 2001;103:426-434.

148.   David Bessman J. Reticulocytes. In: Kenneth Walker H, Dallas Hall W, Willis Hurst J, eds. Clinical Methods: The History, Physical and Laboratory Examinations (ed 3). Boston: Butterworths; 1990:735-738.

149.   Bader-Meunier B, Rieux-Laucat F, Croisille L, et al. Dyserythropoiesis associated with a fas-deficient condition in childhood. Br J Haematol. 2000;108:300-304.

150.   Mombaerts P, Iacomini J, Johnson RS, Herrup K, Tonegawa S, Papaioannou VE. RAG-1-deficient mice have no mature B and T lymphocytes. Cell. 1992;68:869-877.

151.   Russell ES, Bernstein SE. Blood and Blood Formation. In: Green EL, ed. Biology of the Laboratory Mouse. New York: McGraw-Hill Book Company; 1966:351-372.

152.   Stamatoyannopoulos G, Veith R, Galanello R, Papayannopoulou T. Hb F production in stressed erythropoiesis: observations and kinetic models. Ann N Y Acad Sci. 1985;445:188-197.

153.   Seno S, Miyahara M, Asakura H, Ochi O, Matsuoka K, Toyama T. Macrocytosis Resulting from Early Denucleation of Erythroid Precursors. Blood. 1964;24:582-593.

154.   Borsook H, Lingrel JB, Scaro JL, Millette RL. Synthesis of haemoglobin in relation to the maturation of erythroid cells. Nature. 1962;196:347-350.

155.   Guihard S, Clay D, Cocault L, et al. The MAPK ERK1 is a negative regulator of the adult steady-state splenic erythropoiesis. Blood. 2010;115:3686-3694.

156.   Schneider E, Moreau G, Arnould A, et al. Increased fetal and extramedullary hematopoiesis in Fas-deficient C57BL/6-lpr/lpr mice. Blood. 1999;94:2613-2621.

157.   McAdams HH, Arkin A. It's a noisy business! Genetic regulation at the nanomolar scale. Trends Genet. 1999;15:65-69.

158.   Stelling J, Sauer U, Szallasi Z, Doyle FJ, 3rd, Doyle J. Robustness of cellular functions. Cell. 2004;118:675-685.

159.   Bratsun D, Volfson D, Tsimring LS, Hasty J. Delay-induced stochastic oscillations in gene regulation. Proc Natl Acad Sci U S A. 2005;102:14593-14598.

160.   Becskei A, Serrano L. Engineering stability in gene networks by autoregulation. Nature. 2000;405:590-593.

161.   Camas FM, Blazquez J, Poyatos JF. Autogenous and nonautogenous control of response in a genetic network. Proc Natl Acad Sci U S A. 2006;103:12718-12723.

162.   Erslev AJ, Caro J. Erythropoietin titers in response to anemia or hypoxia. Blood Cells. 1987;13:207-216.

163.   Lodish HF, Ghaffari S, Socolovsky M, Tong W, Zhang J. Intracellular signaling by the erythropoietin receptor. In: Elliott SG, Foote M, Molineux G, eds. Erythropoietins, Erythropoietic Factors, and Erythropoiesis: Molecular, Cellular, Preclinical, and Clinical Biology (ed 2nd). Basel: Birkhäuser; 2009:155-174.

164.   Peslak SA, Wenger J, Bemis JC, et al. Sublethal radiation injury uncovers a functional transition during erythroid maturation. Exp Hematol;39:434-445.

165.   Wagner KU, Claudio E, Rucker EB, 3rd, et al. Conditional deletion of the Bcl-x gene from erythroid cells results in hemolytic anemia and profound splenomegaly. Development. 2000;127:4949-4958.

166.   Motoyama N, Kimura T, Takahashi T, Watanabe T, Nakano T. bcl-x prevents apoptotic cell death of both primitive and definitive erythrocytes at the end of maturation. J Exp Med. 1999;189:1691-1698.

167.   Teglund S, McKay C, Schuetz E, et al. Stat5a and Stat5b proteins have essential and nonessential, or redundant, roles in cytokine responses. Cell. 1998;93:841-850.

168.   Garcon L, Rivat C, James C, et al. Constitutive activation of STAT5 and Bcl-xL overexpression can induce endogenous erythroid colony formation in human primary cells. Blood. 2006;108:1551-1554.

169.   Silva M, Richard C, Benito A, Sanz C, Olalla I, Fernandez-Luna JL. Expression of Bcl-x in erythroid precursors from patients with polycythemia vera [see comments]. N Engl J Med. 1998;338:564-571.

170.   Green DR. Life, death, BH3 profiles, and the salmon mousse. Cancer Cell. 2007;12:97-99.

171.   Kuribara R, Honda H, Matsui H, et al. Roles of Bim in apoptosis of normal and Bcr-Abl-expressing hematopoietic progenitors. Mol Cell Biol. 2004;24:6172-6183.

172.   Shinjyo T, Kuribara R, Inukai T, et al. Downregulation of Bim, a proapoptotic relative of Bcl-2, is a pivotal step in cytokine-initiated survival signaling in murine hematopoietic progenitors. Mol Cell Biol. 2001;21:854-864.

173.   Pugh LG. Blood Volume and Haemoglobin Concentration at Altitudes above 18,000 Ft. (5500 M). J Physiol. 1964;170:344-354.

174.   Yang B, Kirby S, Lewis J, Detloff PJ, Maeda N, Smithies O. A mouse model for beta 0-thalassemia. Proc Natl Acad Sci U S A. 1995;92:11608-11612.

175.   Tyson JJ, Chen KC, Novak B. Sniffers, buzzers, toggles and blinkers: dynamics of regulatory and signaling pathways in the cell. Curr Opin Cell Biol. 2003;15:221-231.

176.   Yi TM, Huang Y, Simon MI, Doyle J. Robust perfect adaptation in bacterial chemotaxis through integral feedback control. Proc Natl Acad Sci U S A. 2000;97:4649-4653.

177.   Kuhara A, Inada H, Katsura I, Mori I. Negative regulation and gain control of sensory neurons by the C. elegans calcineurin TAX-6. Neuron. 2002;33:751-763.

178.   Wormald S, Hilton DJ. Inhibitors of cytokine signal transduction. J Biol Chem. 2004;279:821-824.

179.   Klingmuller U, Bergelson S, Hsiao JG, Lodish HF. Multiple tyrosine residues in the cytosolic domain of the erythropoietin receptor promote activation of STAT5. Proc Natl Acad Sci U S A. 1996;93:8324-8328.

180.   Hsieh PP, Olsen RJ, O'Malley DP, et al. The role of Janus Kinase 2 V617F mutation in extramedullary hematopoiesis of the spleen in neoplastic myeloid disorders. Mod Pathol. 2007;20:929-935.

181.   Diaz T, Navarro A, Ferrer G, et al. Lestaurtinib inhibition of the Jak/STAT signaling pathway in hodgkin lymphoma inhibits proliferation and induces apoptosis. PLoS One;6:e18856.

182.   Capello D, Deambrogi C, Rossi D, et al. Epigenetic inactivation of suppressors of cytokine signalling in Philadelphia-negative chronic myeloproliferative disorders. Br J Haematol. 2008;141:504-511.

183.   Fernandez-Mercado M, Cebrian V, Euba B, et al. Methylation status of SOCS1 and SOCS3 in BCR-ABL negative and JAK2V617F negative chronic myeloproliferative neoplasms. Leuk Res. 2008;32:1638-1640.

184.   Krutzik PO, Hale MB, Nolan GP. Characterization of the murine immunological signaling network with phosphospecific flow cytometry. J Immunol. 2005;175:2366-2373.

185.   Yu X, Kong Y, Dore LC, et al. An erythroid chaperone that facilitates folding of alpha-globin subunits for hemoglobin synthesis. J Clin Invest. 2007;117:1856-1865.

186.   Chen ML, Logan TD, Hochberg ML, et al. Erythroid dysplasia, megaloblastic anemia, and impaired lymphopoiesis arising from mitochondrial dysfunction. Blood. 2009;114:4045-4053.

187.   Haurie C, Dale DC, Mackey MC. Cyclical neutropenia and other periodic hematological disorders: a review of mechanisms and mathematical models. Blood. 1998;92:2629-2640.

188.   Coleman DL, Russell ES, Levin EY. Enzymatic studies of the hemopoietic defect in flexed mice. Genetics. 1969;61:631-642.

189.   Sawyer ST, Koury MJ, Bondurant MC. Large-scale procurement of erythropoietin-responsive erythroid cells: assay for biological activity of erythropoietin. Methods Enzymol. 1987;147:340-352.

190.   Terszowski G, Waskow C, Conradt P, et al. Prospective isolation and global gene expression analysis of the erythrocyte colony-forming unit (CFU-E). Blood. 2005;105:1937-1945.

191.   Pronk CJ, Rossi DJ, Mansson R, et al. Elucidation of the phenotypic, functional, and molecular topography of a myeloerythroid progenitor cell hierarchy. Cell Stem Cell. 2007;1:428-442.

192.   Battle TE, Frank DA. The role of STATs in apoptosis. Curr Mol Med. 2002;2:381-392.

193.   Brunet A, Bonni A, Zigmond MJ, et al. Akt promotes cell survival by phosphorylating and inhibiting a Forkhead transcription factor. Cell. 1999;96:857-868.

194.   Ghaffari S, Jagani Z, Kitidis C, Lodish HF, Khosravi-Far R. Cytokines and BCR-ABL mediate suppression of TRAIL-induced apoptosis through inhibition of forkhead FOXO3a transcription factor. Proc Natl Acad Sci U S A. 2003;100:6523-6528.

195.   Cascino I, Papoff G, Eramo A, Ruberti G. Soluble Fas/Apo-1 splicing variants and apoptosis. Front Biosci. 1996;1:d12-18.

196.   Tanaka M, Itai T, Adachi M, Nagata S. Downregulation of Fas ligand by shedding. Nat Med. 1998;4:31-36.

197.   Secchiero P, Melloni E, Heikinheimo M, et al. TRAIL regulates normal erythroid maturation through an ERK-dependent pathway. Blood. 2004;103:517-522.